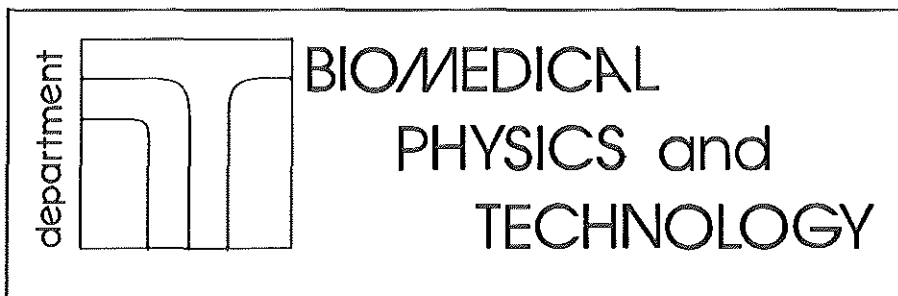


Biomechanical aspects of the intervertebral disc

Analysis of annular wall strain due to intradiscal pressure and spinal deformations

ERASMUS UNIVERSITY ROTTERDAM



Publication of this thesis has been supported by *Stichting Anna-Fonds*.

Door de watersnood van februari 1995 is de ISBN-registratie in het water gevallen.

° Luc van de Poel 1995

No part of this book may be reproduced in any form by print, photocopy, microfilm or any other means without written permission from the author.

Cover: Ruud van Workum

Printing: Copy Print 2000, Enschede

Biomechanical aspects of the intervertebral disc
Analysis of annular wall strain due to intradiscal pressure and spinal deformations

Biomechanische aspecten van de tussenwervelschijf
Analyse van de rek in de annuluswand ten gevolge van de intradiscale druk en
vervormingen van de wervelkolom

Proefschrift

ter verkrijging van de graad van doctor

aan de Erasmus Universiteit Rotterdam

op gezag van de rector magnificus

Prof.dr. P.W.C. Akkermans M.A.

en volgens besluit van het College voor Promoties.

De openbare verdediging zal plaatsvinden op

woensdag 29 maart 1995 om 13.45 uur

door

Lucas Petrus Franciscus van de Poel

geboren te Schipluiden

Promotiecommissie

Promotor: Prof.dr.ir. C.J. Snijders
Co-promotor: Dr.ir. W.A. van Duyl
Overige leden: Prof.dr.ir. H.J. Grootenboer
Prof.dr. H.J. Stam
Prof.dr. C.J.J. Avezaat

Voor wie dit lezen wil

Contents

Introduction	1
Nomenclature	7
1 Intradiscal pressure under complex loading conditions	11
2 Compression properties of the intervertebral disc	41
2-I Confined compression of the isolated nucleus	42
2-II Compression of the isolated disc	50
2-III Analytical model of the intervertebral disc	62
3 3-D Video registration of the strain in the annular wall	83
General conclusions	99
Appendices	105
References	119
Summary	129
Samenvatting	137
Nawoord	145
Curriculum vitae	146

Introduction

Introduction

The intervertebral disc is an important load bearing structure, transmitting approximately 85-90% of the axial load exerted on the spine ^{Nachemson '63 Nachemson '79}. In daily life situations (when a weight is held in the hands, especially in a stooped posture) the tension of the back-muscles contributes the major part of axial load on the spine. This tension is high, especially in stooped postures, because the moment of force needed to maintain the body posture and to be able to carry a weight in the hands is realized in the back by a small lever arm. Of lesser importance for the total axial load are the weight of the body above disc level and the lifted weight. The axial load on the disc can exceed 2000 N in working conditions ^{Nachemson '81}. It has been proven that the intervertebral disc is capable of carrying loads of more than 5000 N without indication of damage ^{Eise '66}. Which characteristics of the disc enable it to resist such high loads, while retaining enough flexibility to allow rotations in three directions? An explanation may be found in the structure of the disc. This structure has been described by many authors ^{Beattie '31 Rabichong '78}.

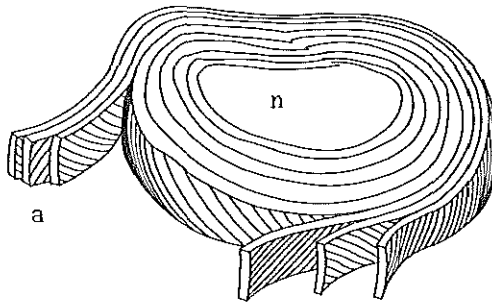


Figure I-1. Schematic representation of the intervertebral disc (according to Keessen '88).

The intervertebral disc consists mainly of three substances: glycosaminoglycans, collagen and hyaline cartilage. The nucleus pulposus, a structure concentrated in the center of the disc (n in Figure I-1), is a three-dimensional network of fine collagen fibers in a gel matrix of glycosaminoglycans and behaves fluid-like (Chapters 1 and 2). The nucleus is surrounded by the annulus fibrosus, which consists of bundles of coarse collagen fibers running in parallel layers obliquely from one vertebral end-plate to the other (a in Figure I-1). From the center of the nucleus towards the annular wall, the amount of nuclear matrix material decreases

Urban '81 Ohshima '89. Dense hyaline cartilage is predominant in the cartilage endplates, separating the nuclear tissue from the vertebral bodies.

The water content of the intervertebral disc is 70-80 %, while the water content of the nucleus is 80-90 %. The water content is divided in a free fraction and a fraction bounded to collagen and glycosaminoglycans Urban '85.

Under conditions of axial loading, the normal nucleus pulposus has a homogeneous distribution of pressure. (Chapter 1, Nachemson '60). In man, values of intradiscal pressure up to 3.6 Mpa have been measured Nachemson '70. Nachemson (1960) reported that the pressure in the nucleus is roughly 1.5 times the axial force on the disc divided by the cross-sectional area of the disc Nachemson '60. This excess needs clarifying.

With increasing deformation the stiffness of the intervertebral disc increases progressively Virgin '51 Brown '57. The resistance of the disc to deformation is generally attributed to osmosis, imbibition and fiber elasticity. When two compartments with solutions at different concentrations are separated by a membrane that is impermeable to the solutes there will be a flow of solvent from the compartment with lowest concentration to the compartment with the highest concentration. The pressure which can balance this flow is called the osmotic pressure Hendry '58. Imbibition is a process of binding and capturing of water molecules to a negative fixed charge Urban '81 of acidic groups (carboxyl and/or sulphate) of glycosaminoglycan-molecules (in cartilage chondroitin- 80% and keratan-sulphate 20%). The acidic groups in their turn are attached to a protein core, therefore these molecules are also referred to as proteoglycans. Both processes osmosis and imbibition will be referred to as swelling because both tend to increase the volume of the disc. The elastic properties of the intervertebral disc are due to solid tissue and predominantly of the elastic fibers in the annular wall. The collagen fibers in the outer layers of the annulus fibrosus are comparable to tendon fibers (tendon collagen, type-1). These fibers have a higher Young-modulus (higher stiffness) than the more central layers of collagen fibers (articular cartilage collagen, type-2). Deformation of the annular wall causes strain and stress in the fibers as well as intradiscal pressure. Thus the axial load is transmitted from one endplate to the other Sonnerup '82. The mechanical properties of each part of the disc are determined by the elasticity and swelling properties but to a different extent. In the annulus fibrosus the elastic properties of collagen type-1 are dominant Galante '67 while the nucleus is dominated by swelling phenomena. In the endplate collagen type-2 is dominant.

Water is an important intradiscal load transmitting component. Loss of water must therefore be prevented or compensated ^{Virgin '51 Brown '57}. Keller et al. ^{Keller '90} investigated the mechanical properties of the intervertebral disc under physiological conditions. He found that these mechanical properties change significantly in case of decreased respiration and after death. This suggests that *in-vivo* active processes, such as the production of proteoglycans ^{Bayliss '86 Schneiderman '86 Bayliss '88} have an important role in the mechanical behavior of the disc. In the isolated disc (that is without external load and with the ligaments and posterior elements removed) *in-vitro*, the intradiscal pressure is approximately 0.1 MPa ^{Nachemson '75}. Urban ^{Urban '85} and others ^{Obshima '89} showed that this initial pressure of the unloaded and isolated disc is caused by swelling. They found that even under the load of body weight and muscle tension the disc retains water. Water can be lost during periods of load, but is regained in more relaxed states by swelling. The low hydraulic permeability of the disc ^{Brown '57} restricts the expulsion of water in cases of high but short lasting pressures.

Despite the remarkable loadbearing qualities of the intervertebral disc, damage may develop under a normal lifespan, somehow related to loading, in particular in certain working situations. From epidemiological ^{Kelsey '84 Burdorf '91} studies is concluded that a repeated combination of physiological axial loads and axial, frontal and sagittal-plane rotations can cause disc prolapse. These epidemiological studies ^{Kelsey '84 Burdorf '91} report that, compared to single motions, combined motions of bending and twisting in particular increase the risk of damage to the annular wall. The aetiology of annular wall damage with its ultimate representation as a hernia nucleus pulposus is the subject of many studies. Because of the economical relevance of low back pain ^{Troup '84} (most patients are in the prime of their economical life) ergonomists want to know the biomechanical situations that promote the development of annular wall damage in order to develop safety margins and ergonomical guide-lines.

In order to explain the pathophysiology of the intervertebral disc, many scientists attempted to produce disc prolapse in specimens of human lumbar spine. However, neither axial compression ^{Eie '66} nor axial ^{Farfan '70 Nachemson '79 Adams '80 Adams '81} or sagittal-plane rotations ^{Korecka '77 Adams '80 Adams '82} caused annular failure under physiological ^{Adams '86} loads and rotations. Under extreme axial loads ^{Eie '66} end-plate failure preceded annular damage, whereas rotations ^{Farfan '70 Adams '82} cause damage only when exceeding the physiological limits. Annular rupture did occur after repetitive axial plane rotations ^{Farfan '70 Adams '82}, however not on the location seen in

man. Gordon et al. ^{Gordon '91} succeeded in generating disc prolapse *in-vitro* in intact human FSU's by applying a repeated load, consisting of a combination of compression, axial rotation and flexion, applied at a frequency of 1.5 Hz during 3 to 13 hours. Thus the combination of axial and sagittal-plane rotations under axial load, repeated many times, can produce annular failure similar to the lesions found in man.

In an analytical study Shirazi et al. ^{Shirazi '89(2)} predicted a significant local increase of stress in the annular wall under such combined loading conditions. This theoretical consideration predicted failure of the annular wall in the locations where it was experimentally found by Gordon et al. ^{Gordon '91}. So the locally increased stress in the annular wall, caused by combined rotations, seems to be the eventual cause of failure of the annular wall. Since higher stress in the annular fibers may increase the internal friction between the layers of fibers, the occurrence of damage in the predicted locations after repeated loading can be ascribed to higher wear in those parts of the annular wall as was suggested by Snijders ^{Snijders '69 Snijders '70}. However no experimental studies have been published, that verify the theoretically predicted increased stress in specific parts of the annular wall under those loading conditions which are predisposing to the specific annular wall damage, as was concluded from epidemiological studies. This stimulated us to do an *in-vitro* study in which human lumbar Functional Spinal Units (FSU's) are subjected to well defined loads and deformations.

Nomenclature

Nomenclature

Parameter	description	unit
β	= angle	rad
ϵ	= fiber strain	%
Θ	= fiber angle	rad
σ_e	= fiber stress	$\text{N}\cdot\text{m}^{-2}$
σ_a	= axial component of annular wall stress	$\text{N}\cdot\text{m}^{-2}$
σ_r	= radial component of annular wall stress	$\text{N}\cdot\text{m}^{-2}$
σ_w	= annular wall stress	$\text{N}\cdot\text{m}^{-2}$
τ	= relaxation time constant of fiber	s
a	= relative visco-elasticity of fiber	-
A	= cross-sectional area of the endplate	m^2
b	= bulging	m
c	= length of bulging curvature	m
C	= concentration	$\text{kg}\cdot\text{kg}^{-1}$
d	= thickness of the fiber layer	m
$D(t)$	= decrease of height of the tissue plug	m
Dx	= membrane thickness	m
F	= force	N
F_e	= axial applied external force	N
F_w	= total annular wall force	N
G	= amount of glycosaminoglycans	kg
h	= height of disc	m
H	= elastic compression modulus	$\text{N}\cdot\text{m}^{-2}$
$h(t)$	= decreasing relative plug height	%
$H(t)$	= Heaviside's function	-
h_0	= initial height	m
J	= fluid flow	$\text{m}^3\cdot\text{s}^{-1}$
K	= permeability modulus	$\text{m}^4\cdot\text{N}^{-1}\cdot\text{s}^{-1}$
K/Dx	= permeability	$\text{m}^3\cdot\text{N}^{-1}\cdot\text{s}^{-1}$
K_d	= total disc hydrodynamic permeability	$\text{m}^5\cdot\text{N}^{-1}\cdot\text{s}^{-1}$
l	= fiber length	m
p	= fiber pitch	m
P	= pressure	Pa

P_0	= initial pressure	Pa
P_h	= hydrodynamic pressure	Pa
P_s	= swelling pressure	Pa
Q	= volume flow density	$\text{m}\cdot\text{s}^{-1}$
r	= radius of endplate	m
r_b	= radius of bulging curvature	m
S	= sieving coefficient	-
t	= time	s
ν	= visco-elastic step-response of fiber	%
V_d	= total disc volume	m^3
V_w	= disc water volume	m^3

CHAPTER 1

Intradiscal Pressure Under Complex Loading Conditions

An in-vitro study

Intradiscal Pressure Under Complex Loading Conditions An in-vitro study

Introduction

The measurement of the intradiscal pressure plays an important role in the research of the low-back. Intervertebral disc pressures can be measured in man, with certain restrictions, and in *in-vitro* experiments. In search of parameters to describe the safe load on the human vertebral column, the intervertebral disc pressure is widely taken as a measure for the stress in the annulus fibrosus ^{Nachemson '60 Korecka '77 Nixon '86}. In most publications the nucleus pulposus is ascribed a hydrostatical kind of behavior ^{Nachemson '60 Korecka '77 Nixon '86}, which means that an increase in pressure, caused by a load on the vertebral column, is distributed immediately and homogeneously to the annulus fibrosus. This implies that the intradiscal pressure is related to the over-all axial load ^{Nachemson '81} applied to a Functional Spinal Unit (FSU) and to the stress in the annulus fibrosus ^{Nachemson '81}. However, Urban ^{Urban '81 Urban '85} et al. described the behavior of the intervertebral disc as pseudo-visco-elastic. According to their model, in contrast to the hydrostatic model, transient intradiscal pressure differences can exist for some time, but will eventually equilibrate, due to fluid shifts ^{Kramer '77 Kramer '80 Kramer '85}. Initial gradients in intradiscal pressure may be caused by a deformation, like the deformation that causes heterogenous stress in the annular wall as it was theoretically predicted by Shirazi et al. ^{Shirazi '89(2)}. Based on the pseudo-visco-elastic model we expect that local variations of stress in the annulus fibrosus will be reflected in transient, locally increased pressure. In order to investigate the possibility of pressure gradients in the intervertebral disc and subsequently the loading conditions that might cause such gradients, we recorded the pressure in the nucleus pulposus at two locations simultaneously.

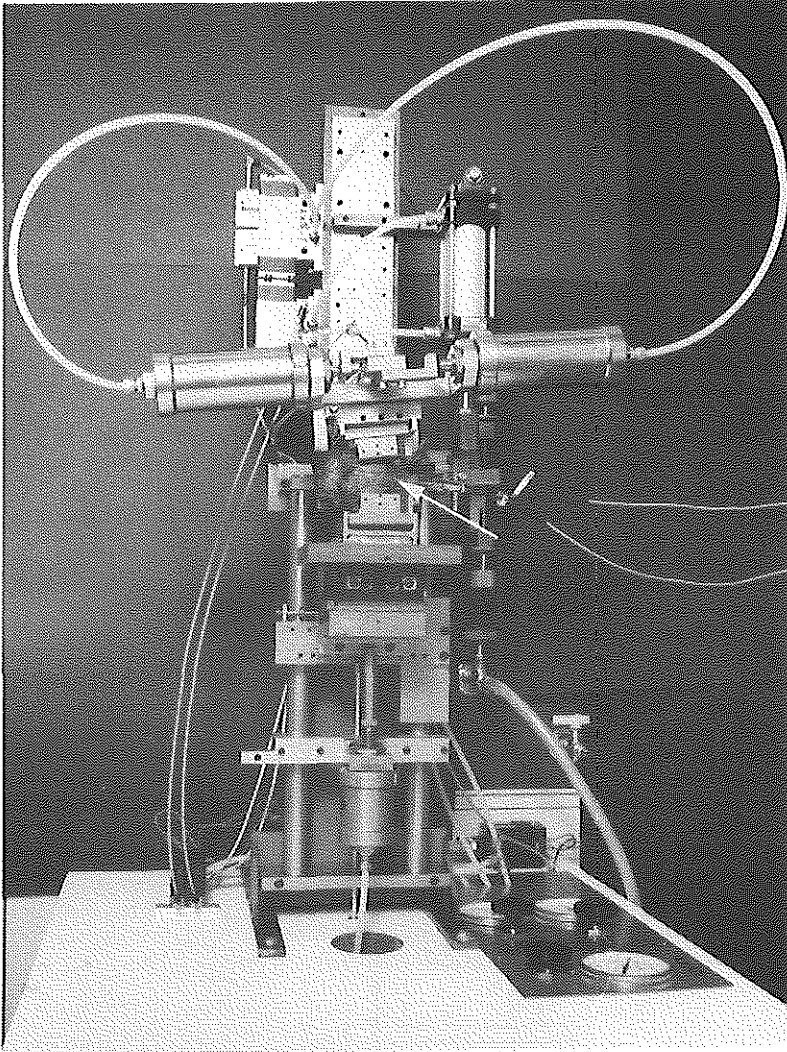


Figure 1-1. Loading apparatus with a specimen (arrow).

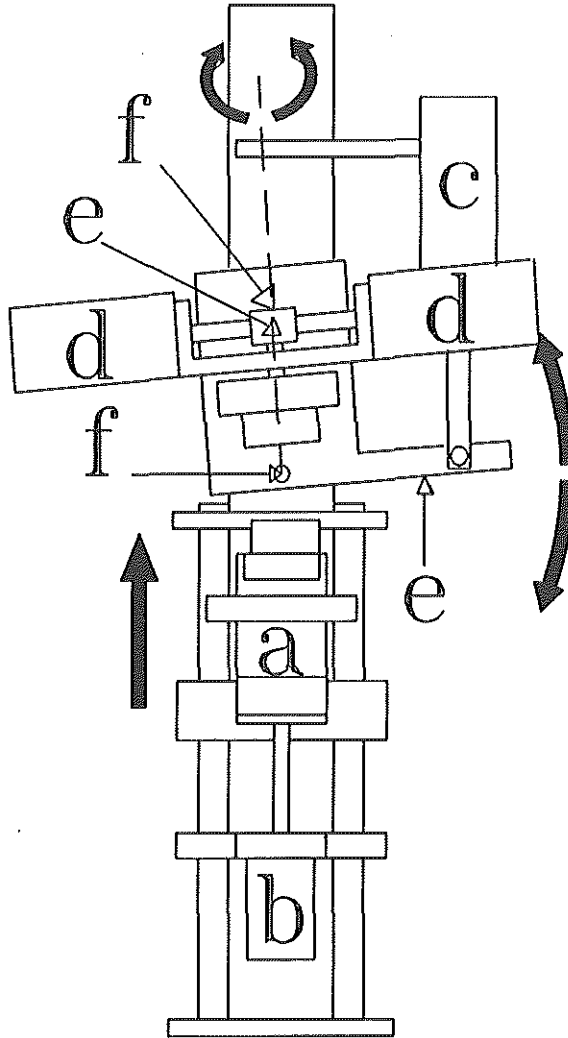


Figure 1-2. Loading apparatus, a) Gliding platforms b) Pneumatic cylinder c) Bidirectional pneumatic cylinder d) Pneumatic cylinder e) Lever arm f) Potentiometer.

Loading apparatus

Gertzbein ^{Gertzbein '84}, Shirazi ^{Shirazi '86 Shirazi '86(2)} and others have shown that in *in-vitro* experiments on FSU's the use of fixed rotation axes has to be avoided. Shear-forces are transmitted by other structures than the disc ^{Adams '80 Adams '81 Dunlop '84} and may be altered into a rotating momentum. Our loading apparatus, shown in figure 1-1, was constructed to apply loads to a FSU with free rotation axes via two, ball-bearing guided, gliding platforms (Figure 1-2 a). On these gliding platforms a platform is mounted to which the lower vertebra of the FSU is fixed. This assembly can be displaced by means of a pneumatic cylinder, b in figure 1-2, in order to load the specimen along its vertical axis. The upper vertebra is fixed to the upper platform, which can move in the sagittal plane, achieving flexion and extension, by means of a vertical bidirectional pneumatic cylinder, c in figure 1-2. By means of the horizontal cylinders d in figure 1-2 the upper platform can be rotated around its vertical axis and thus torsion of the FSU can be applied.

By means of computer-controlled pneumatics, specimens can be loaded during specified intervals in a pre-defined sequence of deformations: transversal rotation (flexion-extension), axial rotation (torsion) and axial translation (compression). Rotations can be applied with a predetermined moment of force or a predetermined rotation-angle. Rotation angles are measured with turn-potentiometers; f in figure 1-2. Exerted moment of force is derived from the forces recorded in both lever arms e in figure 1-2, by means of strain-gauge force-transducers mounted on the levers. A controlled axial load is applied by means of pneumatic pressure. A pressure-transducer (Watson Smith type 69 P/E 536935 OO 0-10 bar 0-10 Volt) was used to determine the applied force.

Rotation angles were calibrated using a goniometer. Errors and non-linearity are less than ± 0.1 degree. The strain-gauge force-transducers, used to measure moments of force, were calibrated with weights. The moments of force can be measured with an error of less than ± 0.02 Nm. According to the specifications the pressure transducer, used to measure applied axial load, has an error of less than ± 15 kPa. This means that the error in the applied axial load is less than ± 3.5 N.

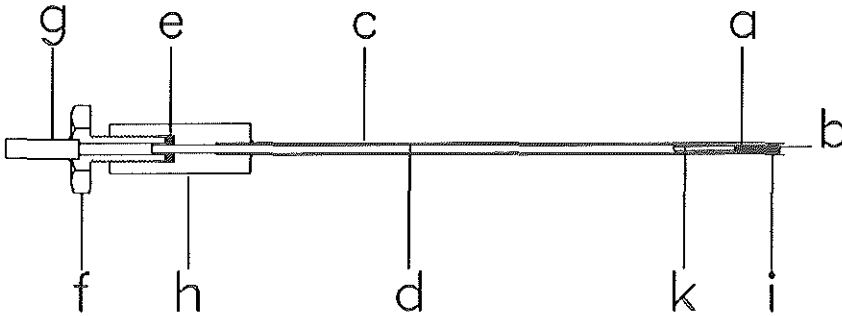


Figure 1-3. Sensing needle, a) transducer b) Parileen coating c) needle d) tube e) O-ring f) locking bolt g) wire guidance h) holder i) Silicone k) sensor ventilation.

Pressure transducers used in the nucleus pulposus; effect of displacements.

Intradiscal pressures are recorded with two strain-gauge based "Ultra Miniature Pressure Transducers" (Entran International, type Miniature, Model EPI-127-20 G, 13 kPa to 2 MPa)(Figure 1-3 a) The transducers were coated with Parileen (Figure 1-3 b) to protect them against moisture. The transducers are mounted with silicon glue (Sylgard A&B) into a stainless steel, hollow needle with inner diameter 1.4 mm, and outer diameter 1.6 mm (Figure 1-3 c). The transducer is supported by a stainless steel tube (inner diameter 0.9 mm, outer diameter 1.3 mm) (Figure 1-3 d). This supporting tube (Figure 1-3 d) is locked to the needle (Figure 1-3 c) by means of an O-ring, e in figure 1-3, and locking bolt f in figure 1-3. The sensing tip is retracted 1 mm into the needle to avoid forces from dry-tissue near the tip and to prevent damage to the transducer.

To place the sensor needles into the nucleus, inserting needles are used (outer diameter 2.1 mm) to cannulate them. The transducers were calibrated by comparing them with a pressure transducer of Transamerica Instruments (type BHL-4400-00, 0-6 MPa, temperature shift: $\pm 0.03\%$ FS/ $^{\circ}$ C (FS=6 MPa), non-linearity and hysteresis: $\pm 0.25\%$), both placed in a calibration chamber. Calibration of the sensor needles is done prior to each measurement to account for temperature shift and drifting. The error of the IDP-sensors was less than $\pm 1\%$ Full Scale (FS=2 MPa), and pressure changes at 30 Hz were followed for more than 95%.

The size of the IDP-needle inevitably disturbs the structure of the tissue in its

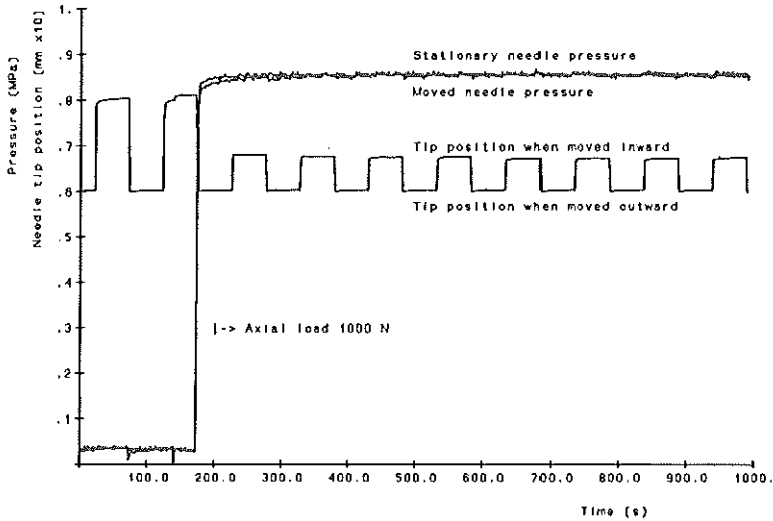


Figure 1-4. Example of a pressure test recording.

close vicinity, which means that the measured pressure may differ from the pressure that would exist at that location without the sensor. This difference may be bigger when the environment consists of stiffer material. In that case a small displacement of the tip of the sensor may show a significant variation of the pressure. This was tested by a small block-wise displacement of one needle, while the other needle situated 10 mm apart from the former, was kept at rest. In order to move the needle it was connected to an electromagnetic vibrator (Type: Ling 200) controlled by a block-wave generator. The position of the tip of the needle, relative to an arbitrary point along its axis, was measured by means of an electromagnetic displacement sensor (Type: Sangamo DF 50 STD, accuracy ± 0.025 mm).

Pressure- and displacement data were collected at a sampling rate of 10 Hz and fed into a personal computer. In figure 1-4 the recordings are shown. Block-wise movements of 0.8 mm were applied at a frequency of 0.01 Hz. After a period of 180 s the external load was increased from 0 to 1000 N.

As demonstrated by these recordings, the displacement of the needle hardly exercises any effect on the measured pressure, neither by the moved sensor nor by the sensor at rest. Hence the disturbance of the tissue by the needles can be

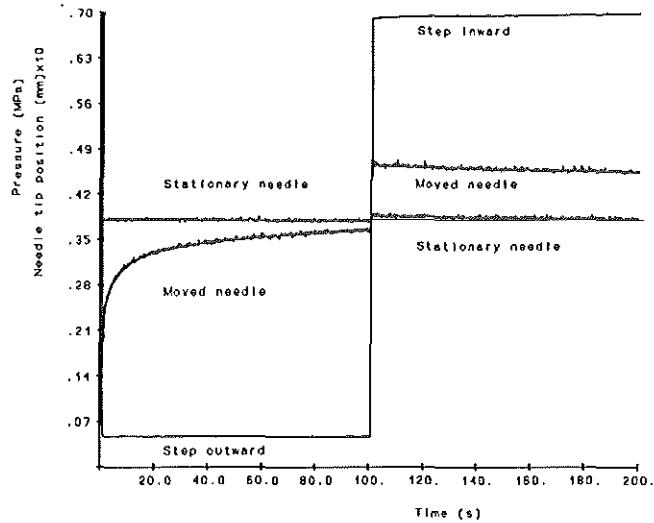


Figure 1-5. Fitted results of a pressure test. Pressures (in MPa) of a needle moved outward and inward and a stationary needle, needle tip position in mm x 10, step amplitude 3.27 mm. Axial load 500 N.

ignored. Furthermore we conclude that the pressure recording is not sensitive to movements, which might be inevitable during deformations of the specimen.

Figure 1-5 shows the response in recorded pressure when the sensor is displaced stepwise outward and inward over a total distance of 3.3 mm. In this case the external load applied to the FSU was 500 N. The outward displacement causes an almost simultaneous decrease in pressure measured by the displaced sensor, while no change in pressure is measured by the other sensor. The pressure of the displaced sensor gradually increases in the recorded period of 100 s almost to the value before displacement. We can explain this response in pressure by the void that is created behind the retracted tip of the sensor and which has to be refilled with water from the surrounding structure. The time this refilling takes is determined by the permeability for water of the surrounding structure. When the tip of the sensor is displaced inward, as is also shown in figure 1-5, there is a fast pressure increase, which subsequently decays again. The pressure change after the displacement inward appears to be slower than after the outward displacement. Probably, this is an indication of locally impaired permeability as a consequence

of the deformation of local tissue by pushing the tip of the sensor into the nucleus.

While the moved sensor shows a significant change in pressure which decays rather slowly, the pressure measured by the other sensor at a distance of approximately 10 mm does not change. These measurements demonstrate that during the rather long period of 100 seconds a gradient in pressure can exist. In case the nucleus would have behaved hydrostatically, such a pressure gradient would have been practically impossible. Apparently the tissue matrix in the nucleus has pores that limit the permeability for water, causing a delay in the equilibration of the pressure in case of an initial heterogenous distribution of pressure in the nucleus. Because of these poro-elastic properties of the nucleus, we may expect initial pressure gradients within the nucleus caused by certain motions of the FSU, which are associated with asymmetric deformation of the intervertebral disc.

Time dependent pressure changes are also accounted for by the visco-elastic properties of the annular wall, as described by Galante ^{Galante '67}. Therefore, to distinguish the effect of visco-elastic relaxation of the annular wall from pressure equilibration within the nucleus, pressure should be recorded at at least one other location as well.

The results of the pressure-needle tests (Figures 1-4 and 1-5) show that the nucleus has distinct pseudo-visco-elastic properties as described by Urban et al ^{Urban '81 Urban '85}.

To prevent artifacts in the pressure caused by the IDP-sensors, the tip of the inserting needle, used for cannulation, needs to be sharp (a-traumatic needle) so that tissue damage or deformation will be minimal.

Furthermore during loading of the FSU, movements of the needles should be prevented, since we have found that movements of more than 1 mm may cause significant changes in pressure.

Loading tests

Our protocol is based on pilot studies and data taken from literature ^{Parfen '70 Kulak '75 Kulak '76 Panjabi '77 Adams '82 Adams '86}.

We applied the rotations stepwise in order to evoke transient pressure responses that can be simply described by an exponential model. The angle of rotation is

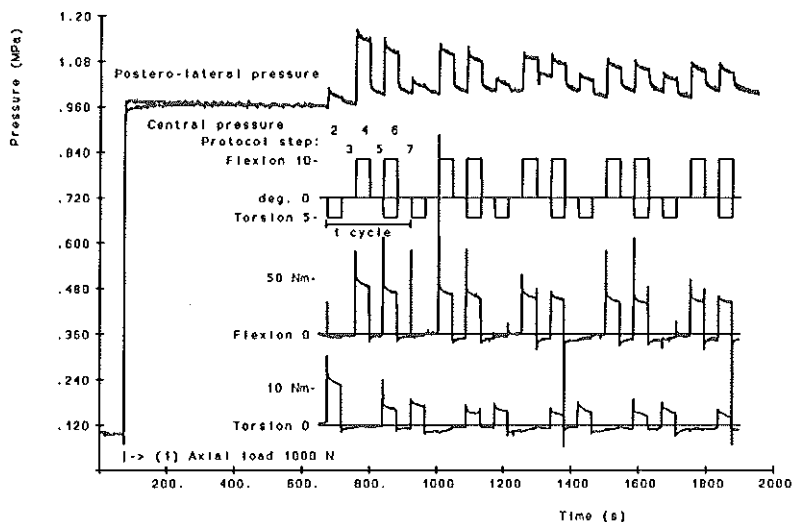


Figure 1-6. Example of a loading-test recording. Recordings of intradiscal pressures, rotations and moments of force.

predetermined. The resistance to rotation posed by the FSU is measured as the torque developed during the applied deformation.

The protocol comprises the following sequence of loadings of the FSU:

- 1: Application of axial load (i.e. compression), which is maintained during the experiment.
- 2: Application of stepwise axial rotation (i.e. torsion), maintained during 40 seconds.
- 3: Recuperation during 40 seconds, while axial load (1) is maintained.
- 4: Application of stepwise transverse rotation (i.e. flexion or extension), maintained during 40 seconds.
- 5: Recuperation during 40 seconds, while axial load (1) is maintained.
- 6: Application of stepwise axial rotation (2) and stepwise transverse rotation (4) simultaneously, maintained during 40 seconds.
- 7: Recuperation during 40 seconds, while axial load (1) is maintained.

The sequence is continued by repeating the loading conditions 2 to 7. Thus 5 loading cycles, consisting of conditions 2 to 7 are applied to one specimen. In figure 1-6 an example of the result of such a loading experiment is shown. The numbers marked to the recording of the applied deformations correspond to the defined loading conditions.

Based on epidemiological literature ^{Valkenburg '80 Kelsey '84 Burdorf '91} we suspected that, during the loading of discs in normal-life, combined rotations at small angles may already endanger the annular wall. This opinion is supported by the results of Shirazi ^{Shirazi '84 Shirazi '86 Shirazi '86(2) Shirazi '87 Shirazi '88 Shirazi '89 Shirazi '89(2)}, who calculated for example a doubled maximum tensile strain in combined rotations with 1° torsion and 1.7° lateral bending compared to flexion alone. Therefore we applied rotations over a small angle, namely 1.1° axial rotation and 3.2° rotation or less in the sagittal plane. For similar reasons we applied a low axial load (500 N), i.e., approximately 1.5 times the weight of the body above the FSU level corresponding *in-vivo* to standing at ease ^{Nachemson '81}.

Three specimens (series 5 to 14) were subjected to larger rotations, in some cases even more than the rotations reported to cause annular or other damage when exceeded ^{Roaf '60 Parfan '70 Adams '80} (axial rotation > 3° , flexion > 9°). The axial load was raised to 1000 N. Such an axial load corresponds to bending forward 40° while standing ^{Nachemson '81}. The sequence of loading conditions was effectuated by a personal computer which controlled the pneumatic valves of the testing apparatus and simultaneously collected the data via a 12 bit ADC (Labmaster) at a sampling rate of 5 Hz.

Analysis of recorded data

Figure 1-7 shows an example of a pressure recording registrated after a stepwise deformation of a FSU (nr 5 in table 1-1), namely 10.3° flexion combined with 5.3° torsion, i.e. number 6 of the protocol.

The currents running through the electronic pressure valves when changing the loading conditions, caused substantial temporary artifacts in the recorded data. Therefore the value of the first sample of digitized data is ignored.

The data from each interval of the loading protocol were first fitted to a linear function ($x \cdot t + y$) with correction for the first data point.

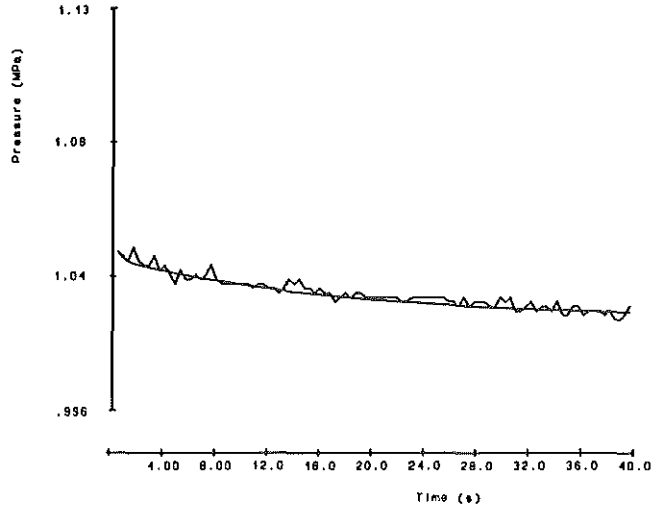


Figure 1-7. Fit on postero-lateral pressure (MPa).

Curves that were fit to a linear function with an accuracy that did not fall below 2.5 times the bit step size, which is the magnitude of the random noise of the recordings, were classified as not linear.

Then this non-linear change in pressure, registered after each type of stepwise deformation, is described by the following bi-exponential model:

$$g(t) = C_1 \cdot e^{-t/T_1} + C_2 \cdot e^{-t/T_2} + C_3 \quad (1)$$

where

- t = time, (s)
- C_1 = coefficient of the fast exponential (% of C_3)
- T_1 = time constant of the fast exponential (s)
- C_2 = coefficient of the slow exponential (% of C_3)
- T_2 = time constant of the slow exponential (s)
- C_3 = final pressure, (MPa)

In this expression C_3 corresponds to the theoretical value of the pressure to be reached after long (infinite) equilibration time.

The mathematical model was fitted to experimental pressure data by using a least-square-fitting procedure, with a correction for the first data point.

The fitting procedure was stopped when 95 % of the data differed no more than 6 times the bit step size from our fitted curve, which corresponds to 9 kPa or 0.3 % of the maximum pressure (3 MPa) (i.e. the accuracy of the pressure sensors when ignoring drift).

For statistical evaluation we used only the parameters obtained in cases of a successful fit of the multi-exponential model (with the exception of Table 1-2, for reasons that are discussed later).

Since our fits were performed on data sampled over periods of 40 seconds, fitting results with a time constant of more than (an arbitrary) 60 seconds are not considered in the statistical analysis as these curves can be represented by a number of solutions for the bi-exponential model ^{Van Duyl '83}. When using two exponential terms in a fitting procedure, it is possible that both terms are assigned the same time constant but have in effect opposing directions (i.e. they counterbalance each other). In that case the result would be a straight line or the curve could be described with a single exponential term and the two exponential terms are meaningless. To avoid this situation all fits that have exponential terms with an opposite sign should have a second time constant of at least 3 times the first one.

In figure 1-7 an example is given of a curve fitted to experimental data. By fitting the same model to all the pressure recordings the separate recordings are characterized by 5 parameters (C_1 , C_2 , C_3 , T_1 and T_2). These values are used to search for differences in pressure response according to statistical criteria.

A total of 554 out of 840 fitted pressure curves met the requirements discussed above and were used for statistical analysis.

The registered data with respect to the applied moments of force were fitted and analyzed likewise.

We are interested in differences between the pressures recorded at the two locations. Therefore the pressure measured with the sensor situated in the posterolateral part of the nucleus is divided by the pressure in the central part of the nucleus.

To get an indication of the importance of possible pressure differences, this quotient is subtracted with 1 and the result is multiplied with 100 %. Now the postero-lateral recorded pressure is expressed as equal to (=zero) or percents above (positive) or under (negative) the central recorded pressure, which renders

the relative pressure difference at the postero-lateral location (This procedure, $(A/B - 1) * 100 \%$, is equal to $(A-B)/B * 100 \%$ and was used because it facilitates the fitting procedure.). Because of the limited accuracy of the pressure transducers, pressure differences of less than approximately 4 % are to be ignored.

In accordance with the pressure recordings at the posterolateral and central locations that show pressure relaxation due to the relaxation of external structures such as the annular wall, we expect to find pressure equilibration between the two sensors caused by pressure relaxation within the nucleus. Therefore the relative postero-lateral pressure difference is fitted and analyzed using a bi-exponential function like $g(t)$ and subjected to the same exclusion criteria as we used for the pressure and moment of force recordings. The fit-accuracy however is no longer expressed in bit steps, but in percents of the reference pressure at the central location (Table 1-2).

The fitting procedure was stopped if 95 % of the data differed no more than 2 % from the fitted curve. As any pressure difference is of importance for this table we included the results of linear fits and of accurate fits to the bi-exponential function with T_2 greater than 60 seconds or T_2 less than T_1 . In those cases the pressure difference at $t=40$ is calculated from the fitted parameters and expressed in C_3 , the change in pressure difference between $t=0$ and $t=40$ that is not caused by the first exponential (C_1 and T_1) is calculated and expressed in C_2 .

Specimen

Five intact human FSU's (Functional Spinal Unit's) were used. Each FSU comprised two vertebral bodies with the intervertebral disc inbetween, with intact arcs and intervertebral joints, and all related ligaments. The FSU's were obtained within 24 hours post-mortem and subsequently stored at $-20 \text{ }^\circ\text{C}$ until use. According to Nachemson^{Nachemson '60} and Pelker^{Pelker '84} this preservation does not cause significant change in biomechanical properties. The surface of the cut off, upper part of each FSU was macroscopically inspected and classified according to Galante's^{Galante '67} degeneration scale, Table 1-1.

Prior to use, the specimen were thawed in an isotonic solution and mounted in steel cups with screws and cold-curing resin (Kulzer: Technovit 2060) (Figure 1-8). During measurements the FSU is continuously moistened by an isotonic solution dispenser.

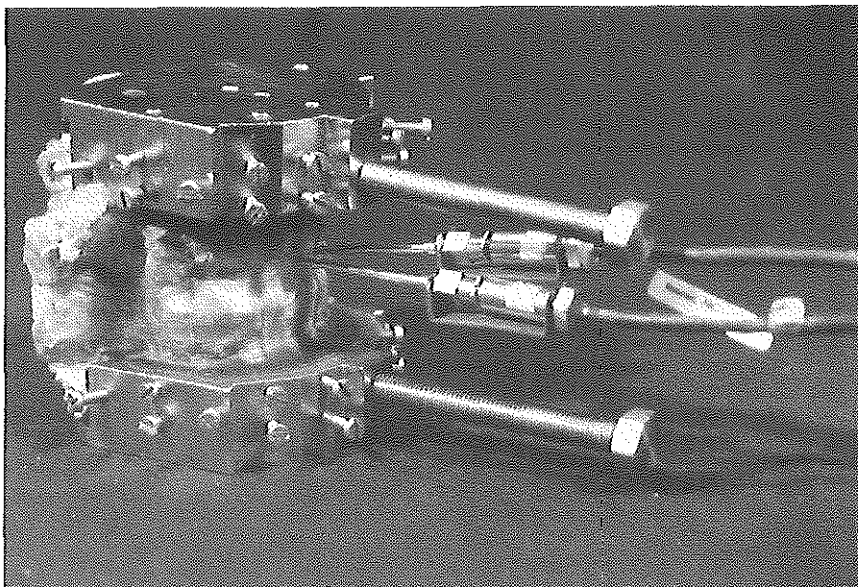


Figure 1-8. Specimen mounted and fixated in steel cups.

Table 1-1. FSU Biological Data

ID No	age	sex	length (m)	weight (kg)	FSU- level	Used in series:	degeneration
S90249L2L3	51	♂	178	60	L2-L3	1, 2, 3, 4	2 (L1-L2)
S89212L2L3	71	♂	170	64	L2-L3	5, 6, 7	2 (L1-L2)
S89212L4L5	71	♂	170	64	L2-L3	pressure tests	3 (L1-L2)
S89259L4L5	58	♂	180	70	L4-L5	8, 9, 10	3 (L3-L4)
S89259L2L3	58	♂	180	70	L2-L3	11, 12, 13, 14	3 (L1-L2)

Measurements, according to the previously described protocol, have been performed on five intact human FSU's (Functional Spinal Unit's). In Table 1-1 each series of 5 identical sequences of loading conditions has got a number 1 - 14. After the experiments each FSU was split, and the splitted surface was inspected and classified again, Table 1-1.

Results

Table 1-2. Median of parameters fitted on the procentual pressure difference at the posterolateral location compared to the central location, in series 1-14, medians of C_1 , C_2 and C_3 exceeding $\pm 5\%$ are in bold, medians of C_1 , C_2 and C_3 exceeding $\pm 10\%$ are in bold and underlined

Series	1	2	3	4	5	6	7	8	9	10	11	12	13	14
Postero-lateral needle-tip location:	left	left	left	left	left	left	left	right	right	right	left	left	left	left
Torsion	1.1°	-1.1°	1.1°	-1.0°	5.3°	-5.1°	-5.1°	3.1°	-3.1°	-3.1°	5.3°	-5.2°	3.0°	-3.0°
C_1 (%)	0	0	-1	0	0	0	0	0	0	0	0	0	<u>18</u>	0
C_2 (%)	-1	0	0	0	-1	1	1	-1	-1	-2	1	0	-3	-3
C_3 (%)	-4	-2	-2	0	-1	3	3	-1	-6	-6	2	1	<u>10</u>	<u>14</u>
Recuperation														
C_1 (%)	0	0	0	0	0	0	0	0	0	2	0	0	0	0
C_2 (%)	0	0	1	-1	0	0	0	1	1	5	1	0	-1	-1
C_3 (%)	-3	-2	-1	-2	-1	1	1	-7	-2	8	2	1	<u>12</u>	<u>16</u>
Bending	3.2°	-2.9°	2.2°	2.2°	10.3°	-7.1°	-7.2°	10.1°	-8.6°	-8.8°	10.2°	-4.9°	7.2°	-5.9°
C_1 (%)	0	-1	0	0	0	0	0	-1	8	-4	0	0	0	-2
C_2 (%)	0	-3	0	0	0	0	-1	-7	6	-4	1	1	-3	-3
C_3 (%)	-2	0	-2	-1	-2	-1	-1	<u>-56</u>	<u>73</u>	<u>54</u>	2	1	-4	<u>-11</u>
Recuperation														
C_1 (%)	0	0	0	0	0	2	2	1	0	3	0	0	0	0
C_2 (%)	-1	1	0	0	0	3	3	4	-1	5	1	-1	-2	-2
C_3 (%)	-4	-2	-2	-2	-1	2	2	-2	-5	5	2	1	<u>10</u>	<u>14</u>
Bending	3.2°	-2.9°	2.2°	2.2°	10.3°	-7.1°	-7.2°	10.1°	-8.6°	-8.8°	10.2°	-4.9°	7.2°	-5.9°
Torsion	1.1°	-1.1°	1.1°	-1.0°	5.3°	-5.1°	-5.1°	3.1°	-3.1°	-3.1°	5.3°	-5.2°	3.0°	-3.0°
C_1 (%)	0	-2	0	0	0	3	0	-5	<u>-12</u>	<u>-11</u>	0	0	-1	-2
C_2 (%)	-1	-2	-1	0	0	0	-1	-5	0	-2	0	1	-3	-3
C_3 (%)	-3	2	-3	0	-2	0	0	<u>-46</u>	<u>45.0</u>	<u>41</u>	2	1	-3	-9
Recuperation														
C_1 (%)	0	0	0	0	0	1	<u>10</u>	2	0	1	0	0	0	0
C_2 (%)	-1	0	0	0	0	4	2	4	-1	5	0	-1	-3	-2
C_3 (%)	-4	-2	-2	-1	-1	3	4	-3	-5	6	2	1	<u>10</u>	<u>15</u>

The parameters C_1 , C_2 and C_3 , describing the relative pressure difference at the posterolateral location are tabulated in table 1-2.

Since each number in table 1-2 represents no more than 5 loading cycles the median of the fitted parameters is used instead of the mean. (The median of a small group of numbers is less susceptible to extremes than the mean would be.)

Significant differences are indicated in the table in bold figures (pressure difference $> 5\%$) or in bold and underlined (pressure difference $> 10\%$).

Table 1-3 shows the mean values of the fast (T_1) and slow (T_2) time constants of the model $g(t)$.

Table 1-3. Comparison of fast and slow time constants T_1 and T_2 of pressure registrations at the central location with those of pressure registrations at the postero-lateral location, using a Kruskal-Wallis 1-way ANOVA at the 0.05 confidence level

Series	Central T_1 (s) Mean	Central T_2 (s) Mean	Cases	Postero- lateral T_1 (s) Mean	Postero- lateral T_2 (s) Mean	Cases	P-value for T_1	P-value for T_2
1	.4	17.0	11	.4	20.8	7	N.S.	N.S.
2	.4	19.0	7	.4	15.9	10	N.S.	N.S.
3	.4	17.0	11	.4	22.1	24	N.S.	N.S.
4	.4	17.0	10	.4	24.3	17	N.S.	N.S.
5	.6	19.2	26	.6	17.3	24	N.S.	N.S.
6	.8	16.2	25	.4	17.9	27	N.S.	N.S.
7	.9	15.4	16	.4	16.3	20	N.S.	N.S.
8	1.1	15.2	22	1.5	25.1	21	N.S.	.02
9	.5	20.3	26	.8	15.1	17	N.S.	.03
10	1.1	18.1	25	.7	15.3	22	N.S.	.02
11	.6	17.7	29	.7	21.7	27	N.S.	.05
12	.9	20.0	26	.8	20.2	26	N.S.	N.S.
13	.6	18.0	17	1.5	29.2	16	.00	.00
14	.6	20.0	23	.9	30.5	22	.00	.00

The model was fitted to the recorded pressure for each interval (out of 6 intervals) of the loading sequence and its repetitions (5 repetitions) in series 1 to 14. Table 1-3 compares the central time constants T_1 and T_2 with the posterolateral ones. Since T_1 and T_2 were not distributed normally, a nonparametric Kruskal-Wallis one-way analysis of variance was performed to test this relation (Table 1-3).

In series 1 to 7 and 12 there is no significant difference at the 0.05 confidence level between central and posterolateral time constants. This indicates that in those series pressure relaxation is similar at both locations of the sensors.

Table 1-4. Comparison of fast and slow time constants T_1 and T_2 of pressure registrations at the central location with those of sagittal plane (flexion/extension) moment of force registrations, using a Kruskal-Wallis 1-way ANOVA at the 0.05 confidence level

Series	Central T_1 (s) Mean	Central T_2 (s) Mean	Cases	Moment T_1 (s) Mean	Moment T_2 (s) Mean	Cases	P-value for T_1	P-value for T_2
1	.4	17.0	11	1.4	27.2	14	.04	N.S.
2	.4	19.0	7	1.6	27.8	12	.00	N.S.
3	.4	17.0	11	.6	12.3	9	.01	.01
4	.4	17.0	10	.7	23.2	8	N.S.	N.S.
5	.6	19.2	26	.5	11.8	5	N.S.	N.S.
6	.8	16.2	25	.5	33.1	2	N.S.	N.S.
7	.9	15.4	16	.5	18.3	2	N.S.	N.S.
8	1.1	15.2	22	-	-	-	-	-
9	.5	20.3	26	-	-	-	-	-
10	1.1	18.1	25	-	-	-	-	-
11	.6	17.7	29	1.9	15.6	15	.00	.01
12	.9	20.0	26	2.6	32.5	2	N.S.	.04
13	.6	18.0	17	1.2	20.3	6	.03	N.S.
14	.6	20.0	23	1.0	21.0	8	.00	N.S.

In tables 1-4 and 1-5 respectively the time-constants of the corresponding exponentials that were fitted to the registrations of sagittal plane (flexion/extension) and axial (torsion) moment of force are compared to those of the pressure recorded at the central location.

Table 1-5. Comparison of fast and slow time constants T_1 and T_2 of pressure registrations at the central location with those of axial (torsion) moment of force registrations, using a Kruskal-Wallis 1-way ANOVA at the 0.05 confidence level

Series	Central T_1 (s) Mean	Central T_2 (s) Mean	Cases	Moment T_1 (s) Mean	Moment T_2 (s) Mean	Cases	P-value for T_1	P-value for T_2
1	.4	17.0	11	2.6	35.1	5	N.S.	N.S.
2	.4	19.0	7	.4	11.5	3	N.S.	.02
3	.4	17.0	11	-	-	-	-	-
4	.4	17.0	10	1.9	23.7	11	.00	N.S.
5	.6	19.2	26	1.0	25.1	14	N.S.	N.S.
6	.7	16.2	25	1.0	21.2	16	.04	N.S.
7	.9	15.4	16	1.6	20.7	11	N.S.	N.S.
8	1.1	15.2	22	1.9	24.3	11	N.S.	N.S.
9	.5	20.3	26	1.1	17.1	7	.01	N.S.
10	1.1	18.1	25	1.2	20.7	4	N.S.	N.S.
11	.6	17.7	29	1.6	36.4	19	.00	.05
12	.9	20.0	26	1.3	13.3	20	.01	.00
13	.6	18.0	17	-	-	-	-	-
14	.6	20.0	23	1.3	19.9	21	.00	N.S.

In tables 1-6 and 1-7 these time-constants are compared to those of the pressure recorded at the postero-lateral location. Despite the limited number of cases of a valid fit of the bi-exponential function $g(t)$ to the recorded momentum, 32 to 42 % of the time constants of the corresponding exponentials are different. This indicates that the relaxation in the moment of force around both axes (flexion/extension and torsion) after the stepwise deformation and the pressure relaxation at the two locations are governed by different tissue properties.

Table 1-6. Comparison of fast and slow time constants T_1 and T_2 of sagittal plane (flexion/extension) moment of force registrations with those of pressure registrations at the postero-lateral location, using a Kruskal-Wallis 1-way ANOVA at the 0.05 confidence level

Series	Moment T_1 (s) Mean	Moment T_2 (s) Mean	Cases	Postero-lateral T_1 (s) Mean	Postero-lateral T_2 (s) Mean	Cases	P-value for T_1	P-value for T_2
1	1.4	27.2	14	.4	20.8	7	N.S.	N.S.
2	1.6	27.8	12	.4	15.9	10	.00	N.S.
3	.6	12.3	9	.4	22.1	24	.02	.00
4	.7	23.2	8	.4	24.3	17	N.S.	N.S.
5	.5	11.8	5	.6	17.3	24	N.S.	N.S.
6	.5	33.1	2	.4	17.9	27	N.S.	N.S.
7	.5	18.3	2	.4	16.3	20	N.S.	N.S.
8	-	-	-	1.5	25.1	21	-	-
9	-	-	-	.8	15.1	17	-	-
10	-	-	-	.7	15.3	22	-	-
11	1.9	15.6	15	.7	21.7	27	.01	.00
12	2.6	32.5	2	.8	20.2	26	.05	.05
13	1.2	20.3	6	1.5	29.2	16	N.S.	N.S.
14	1.0	21.0	8	.9	30.5	22	N.S.	N.S.

Table 1-7. Comparison of fast and slow time constants T_1 and T_2 of axial (torsion) moment of force registrations with those of pressure registrations at the postero-lateral location, using a Kruskal-Wallis 1-way ANOVA at the 0.05 confidence level

Series	Moment T_1 (s) Mean	Moment T_2 (s) Mean	Cases	Postero-lateral T_1 (s) Mean	Postero-lateral T_2 (s) Mean	Cases	P-value for T_1	P-value for T_2
1	2.2	35.1	5	.4	20.8	7	N.S.	N.S.
2	.4	11.5	3	.4	15.9	10	N.S.	.04
3	-	-	-	.4	22.1	24	-	-
4	1.9	23.7	11	.4	24.3	17	.00	N.S.
5	1.0	25.1	14	.6	17.3	24	.04	N.S.
6	1.0	21.2	16	.4	17.9	27	.00	N.S.
7	1.7	20.7	11	.4	16.3	20	.00	N.S.
8	1.9	24.3	11	1.5	25.1	21	N.S.	N.S.
9	1.1	17.1	7	.8	15.1	17	N.S.	N.S.
10	1.2	20.7	4	.7	15.3	22	.05	N.S.
11	1.6	36.4	19	.7	21.7	27	.00	N.S.
12	1.3	13.3	20	.8	20.2	26	.00	.01
13	-	-	-	1.5	29.2	16	-	-
14	1.3	19.9	21	.9	30.5	22	N.S.	.01

In table 1-8 the time-constants of the corresponding exponentials that were fitted to the registrations of sagittal plane (flexion/extension) moment of force are compared to those of the axial (torsion) moment of force.

Despite the limited number of cases of a valid fit of the bi-exponential function $g(t)$ to the recorded moment of force, 44% of the time constants of the corresponding exponentials are different. This indicates that the relaxation in the moment of force after the stepwise axial deformation (torsion) and the relaxation in the moment of force after sagittal plane deformation (flexion/extension) are governed by different tissue properties.

Table 1-8. Comparison of fast and slow time constants T_1 and T_2 of axial (torsion) moment of force registrations with those of sagittal plane (flexion/extension) moment of force registrations, using a Kruskal-Wallis 1-way ANOVA at the 0.05 confidence level

Series	Axial Moment T_1 (s) Mean	Axial Moment T_2 (s) Mean	Cases	Sagittal Moment T_1 (s) Mean	Sagittal Moment T_2 (s) Mean	Cases	P- value for T_1	P- value for T_2
1	2.2	35.1	5	1.4	27.2	14	N.S.	N.S.
2	.4	11.5	3	1.6	27.8	12	.03	N.S.
3	-	-	-	.6	12.3	9	-	-
4	1.9	23.7	11	.7	23.2	8	.03	N.S.
5	1.0	25.1	14	.5	11.8	5	N.S.	N.S.
6	1.0	21.2	16	.5	33.1	2	N.S.	N.S.
7	1.6	20.7	11	.5	18.3	2	N.S.	N.S.
8	1.9	24.3	11	-	-	-	-	-
9	1.1	17.1	7	-	-	-	-	-
10	1.2	20.7	4	-	-	-	-	-
11	1.6	36.4	19	1.9	15.6	15	N.S.	.01
12	1.3	13.3	20	2.6	32.5	2	N.S.	.04
13	-	-	-	1.2	20.3	6	-	-
14	1.3	19.9	21	1.0	21.0	8	N.S.	N.S.

For each deformation of the specimen, i.e., axial and/or sagittal plane rotation, the final value of the intradiscal pressure (C_3) can be expressed as a percentage increase or decrease of the final value (C_3) of the recuperation interval (Table 1-9).

Table 1-9. Median, minimum and maximum posterolateral and central values of C₃ (final pressures (MPa)) in pure axial loading conditions and the increase (%) of the median of C₃ under deformation. The angle of rotation while bending forward (i.e. flexion) is attributed a positive sign as is torsion (axial rotation) to the right of the upper vertebra

Series	1	2	3	4	5	6	7	8	9	10	11	12	13	14
Axial														
load (N)	500	500	500	500	1000	1000	1000	1000	1000	1000	1000	1000	1000	1000
Undeformed														
Cases	28	18	30	28	30	30	24	30	30	30	30	30	30	30
C ₃ Median	.44	.44	.48	.48	.99	.94	.93	.67	.66	.62	.99	.94	.86	.78
C ₃ Minimum	.43	.43	.46	.47	.86	.89	.88	.59	.63	.59	.95	.93	.73	.69
C ₃ Maximum	.46	.45	.50	.49	1.00	.95	.94	.77	.69	.67	1.04	.96	.90	.86
Deformation:														
Torsion	1.1°	-1.1°	1.1°	-1.1°	5.3°	-5.1°	-5.1°	3.1°	-3.1°	-3.1°	5.3°	-5.2°	3.0°	-3.0°
Cases	10	8	10	10	10	10	10	10	10	10	10	10	10	10
C ₃ Median	.44	.46	.48	.48	1.00	.95	.95	.69	.67	.64	1.01	.94	.85	.78
C ₃ Minimum	.42	.43	.45	.47	.96	.92	.92	.67	.65	.59	.96	.93	.79	.69
C ₃ Maximum	.47	.47	.49	.49	1.01	.97	.99	.72	.70	.69	1.03	.98	.89	.86
Increase	0%	4%	-1%	2%	2%	1%	3%	3%	1%	3%	3%	0%	-1%	1%
Bending	3.2°	-2.9°	2.2°	2.2°	10.3°	-7.1°	-7.2°	10.1°	-8.6°	-8.7°	10.2°	-4.9°	7.2°	-5.9°
Cases	10	6	10	10	10	10	8	10	10	10	10	10	10	10
C ₃ Median	.45	.47	.49	.48	1.08	1.10	1.08	.59	.58	.57	1.07	1.18	.99	1.07
C ₃ Minimum	.45	.46	.48	.48	1.05	1.08	1.07	.30	.41	.44	1.04	1.16	.97	1.00
C ₃ Maximum	.46	.49	.50	.49	1.13	1.12	1.11	.71	.73	.71	1.13	1.19	1.06	1.15
Increase	2%	7%	1%	1%	10%	18%	16%	-11%	-12%	-9%	9%	25%	15%	37%
Torsion	1.1°	-1.1°	1.1°	-1.1°	5.3°	-5.1°	-5.1°	3.1°	-3.1°	-3.1°	5.3°	-5.2°	3.0°	-3.0°
Bending	3.2°	-2.9°	2.2°	2.2°	10.3°	-7.1°	-7.2°	10.1°	-8.6°	-8.7°	10.2°	-4.9°	7.2°	-5.9°
Cases	8	6	10	10	10	10	8	10	10	10	10	10	10	10
C ₃ Median	.45	.48	.49	.50	1.08	1.10	1.08	.57	.51	.51	1.06	1.17	1.00	1.04
C ₃ Minimum	.44	.45	.48	.49	1.05	1.08	1.05	.28	.39	.40	1.03	1.15	.98	.99
C ₃ Maximum	.46	.50	.50	.50	1.11	1.12	1.11	.72	.59	.65	1.10	1.19	1.04	1.11
Increase	2%	8%	0%	4%	9%	17%	16%	-14%	-24%	-19%	7%	24%	17%	33%

We derived the regression line relating the final pressure change to the amount of applied deformation, i.e., axial rotation or sagittal plane rotation respectively (Table 1-10).

Table 1-10. Regression of relative final pressure (C_3) change (%) on deformation (deg.)

Deformation:	Slope (SE) (% / deg.)	Correlation	Cases
Flexion	0.8 (0.0)	1.0	20
Extension	3.0 (0.2)	0.9	24
Axial rotation	0.4 (0.1)	0.7	42

Data obtained from the first cycle were excluded since there is no preceding recuperation interval. Data from series 8, 9, 10, 13 and 14 were excluded since they showed substantial differences in final values (C_3) between the two locations (see Table 1-2).

The final pressure change appears to correlate well with deformations in the sagittal plane (flexion and extension). This influence is however limited to less than 7 and 15 percent pressure increase respectively for sagittal plane deformations that stay within the physiological ^{Roaf '60 Farfan '70 Adams '80} range of 9° flexion to 5° extension.

The correlation of the final pressure increase with axial rotations is less pronounced. The influence of axial rotations, that stay within the physiological ^{Roaf '60 Farfan '70 Adams '80} range of 3° axial rotation, on final pressure increase is limited to 1.2 percent.

During combined deformations of the FSU, a locally increased tensile strain in the annular wall and therefore an increased risk for disc damage is predicted ^{Shirazi '84} Shirazi '86 Shirazi '86(2) Shirazi '87 Shirazi '88 Shirazi '89 Shirazi '89(2). This locally increased strain, predicted under combined deformations, might be reflected by a higher pressure compared to the sum of the pressure increases caused by single deformations.

A regression line was derived to relate the pressure increase in the nucleus, caused by the combination of axial rotation and rotation in the sagittal plane, to the sum of pressure increase caused by axial rotation alone plus the pressure increase caused by rotation in the axial plane alone.

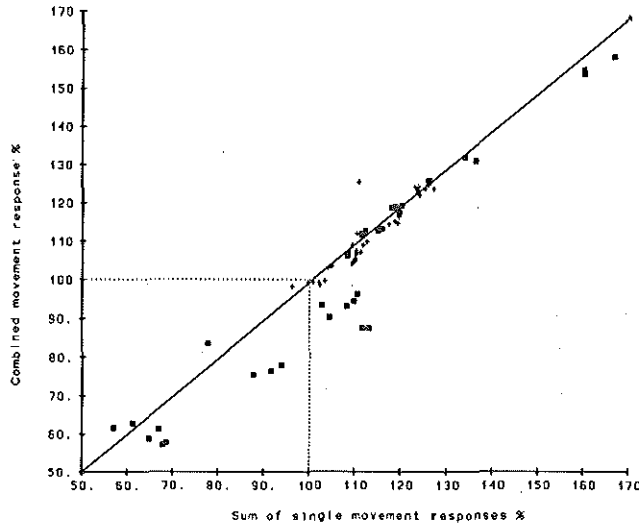


Figure 1-9.

Regression of combined movement response on the sum of single movement responses, * regression line, + used for regression, ■ excluded from regression. Slope(SE) 1.0(.01) Correlation 1.0

The final value of the intradiscal pressure(C_3) is expressed as the percentage of the final value (C_3) of the recuperation interval before the combined deformation (reference pressure) (Table 1-9). The regression line is shown in figure 1-9. The slope of the line is 1, which means that the observed pressure under combined deformation conditions is equal to the sum of the pressure increases due to the separate deformation components.

Discussion

We found that in most cases the differences in coefficients and time constants of the corresponding exponentials of the pressure relaxation are not significant. We concluded from this that the relaxation in pressure, at two locations in the nucleus is governed by common tissue properties. Remains, however, to explain some cases where the differences appeared to be significant. We will consider only those cases where the calculated median values (Table 1-2) for C_1 , C_2 and C_3 exceed $\pm 10\%$.

It is remarkable that the most extreme pressure differences are found in C_3 (final pressure), instead of the expected transient pressure differences C_1 (fast pressure change) and C_2 (slow pressure change). An explanation for the considerable pressure differences in C_3 (final pressure) found in series 8, 9 and 10 is that in these cases the sensing needles were located in different, hydrostatically isolated spaces, so called sub-nuclei ^{Andersson '79 Goobar '87}, which can be found in severely degenerated discs. In such sub-nuclei pressure relaxation will be very slow. Consequently the limited observation time of 40 seconds is too short to obtain a reliable fit of the bi-exponential model in those cases.

The pressure differences represented by C_3 in these series occur only during sagittal plane deformations. This observation provides evidence for the existence of two sub-nuclei: One, a frontal sub-nucleus which bears most of the load during flexion, containing the central pressure sensor, which explains the lower pressure at the postero-lateral located needle during flexion (Table 1-2, series 8). And two, a posterior sub-nucleus which bears most of the load under extension-deformation, containing the postero-lateral pressure sensor, which explains the higher postero-lateral pressure during extension (Table 1-2, series 9 and 10).

These pressures are, however, in contrast with our theory. The right side postero-lateral stress is expected to be highest in series 8 and lowest in series 9 and 10 under the applied deformation conditions (Table 1-2). It is however questionable whether our theory applies to a severely degenerated disc that contains sub-nuclei. We have no particular explanations concerning differences in the coefficients in other series as far as they are significant.

We generally conclude that no pressure differences, that might be attributed to local differences in annular stress, are generated in the normal nucleus when the defined deformations are applied.

Also with regard to the time constants of the corresponding exponential terms we concluded, as in most cases these time constants do not differ significantly, that the pressure relaxation at different locations in the nucleus is governed by similar tissue properties. However, here too the cases where the time constants differ significantly need particular explanation.

Comparing the fast and slow time constants T_1 and T_2 of central pressure registrations with those of postero-lateral pressure registrations (Table 1-3) shows that in series 13 and 14 T_1 (fast pressure change) was significantly slower at the postero-lateral location. In series 8, 11, 13 and 14 T_2 (slow pressure change) was significantly slower at the postero-lateral location, while in series 9 and 10 T_2 was

faster at this location. This suggests that in those series the nucleus does not have equal material properties at the postero-lateral and central locations. However, while the sensors in series 8, 9 and 10 were located in the same nucleus (i.e. the same tissue) and at the same places, the fact that the T_2 is either higher (series 8) or lower (series 9 and 10) at the same postero-lateral location needs explanation.

We note that we previously concluded from the considerable differences of the final pressure (C_3) under sagittal plane deformations, that in series 8, 9 and 10 the pressure sensors were located in two different sub-nuclei of a severely degenerated disc. Our explanation is therefore that the direction of deformation that is applied has so much influence on the solid tissue matrix and the local pressure in the respective sub-nuclei that the local permeability of the nucleus is seriously affected

Mow '80 Van Duij '84

Due to a technical malfunction, only a quarter of all moment of force recordings became available for statistical analysis. Given the accuracy of the measurements and the fitting procedure the means of the data will have to differ more extremely in order to be statistically significant. Comparing the fast and slow time constants T_1 and T_2 of central and postero-lateral pressure registrations with the registration of the moment of force in the sagittal plane and axial moment of force (Tables 1-4, 1-5, 1-6 and 1-7) shows that despite the limited data available, in 32 to 42 % of the cases the exerted moment of force, resisting rotation deformation, cannot be related to the recorded pressure changes. It is therefore not surprising that in 44% of the cases there is no clear relation between axial moment of force and sagittal plane moment of force (Table 1-8) either.

We conclude from this that the pressure relaxation, in two locations in the nucleus and in the moments of force, axial and sagittal, each are governed by different tissue properties.

No large pressure differences were found during pure axial loading (Table 1-2, recuperation periods), which is in agreement with the theoretical expectation ^{Shirazi '84 Shirazi '86(2) Shirazi '89(2)} of symmetrical stress in the annular wall. The intradiscal pressures recorded when an axial load is applied (Table 1-10) are within the expected range (of magnitude). This magnitude can be calculated from the applied axial load, intradiscal pressure (in N/m^2) being about 1.5 to 1.7 times the exerted load/ m^2 on the upper vertebra ^{Nachemson '81}. For example, with an vertebral cross-sectional area of 15 cm^2 and an axial load of 1000 N, intradiscal pressure is expected to be about 1 to 1.13 MPa ($10^6 N/m^2$) ($(load/15 \cdot 10^{-4}) \cdot 1.5$ to 1.7). In

severely degenerated discs, other structures (apart from the disc), like the facet joints, can bear a bigger percentage (up to 70%) of the applied axial load ^{Markolf '72}. This explains why the fitted final pressures found in the specimen with ID.No. S89259L4L5 (Table 1-9, series 8, 9 and 10) is $\pm 40\%$ lower. This is the same specimen that showed important pressure differences during flexion and extension. The results of this specimen show that the used classification may be erroneous, because differences in the grade of degeneration of FSU's at different levels in one subject are quite common. In our case the specimen with ID.No. S89259L4L5 was classified ^{Oakantc '67} to group 4 after the tests were performed and the specimen was split for macroscopic inspection of the nucleus. However, classification performed afterwards has to be handled with reservation, since it is possible that the classification will be lower after the experiment (i.e. more degenerated) than it would have been before.

During axial rotation (Tables 1-9 and 1-10) the rise in the fitted final intradiscal pressures (C_3), relative to the fitted final pressures in the recuperation period, was about 50 % lower than reported for similar experiments ^{Nachemson '60 Farfan '70 Nachemson '79 Adams '80 Adams '81} and than was theoretically predicted by Shirazi et al. ^{Shirazi '84 Shirazi '86(2) Shirazi '89(2)}.

This discrepancy could be ascribed to imperfections of our equipment e.g. play in the testing apparatus, in the mounting of the specimen or in the specimen themselves ^{Shirazi '89(2)}. The established rise in the final intradiscal pressure (Tables 1-9 and 1-10) in case of flexion is in agreement with the results of Adams et al. ^{Adams '80} and with the predictions of Shirazi ^{Shirazi '86 Shirazi '87}.

The pressure rises recorded after application of extension (Tables 1-9 and 1-10) are different in most series, to those reported by Nachemson ^{Nachemson '81} and to the theoretical ^{Shirazi '87 Shirazi '88} expectations: in most of our experiments the pressure rises significantly instead of slightly decreasing as reported by other investigators. The considerable decrease in the intradiscal pressures which we found after the application of combined rotations in series 9 and 10 (Table 1-9) can be attributed to increased facet-face contact due to axial rotation. In severely degenerated discs this results in an increased transmission of the axial load through the facet joints and thus a decreased axial load on the disc ^{Markolf '72 Adams '83}.

We found that the pressure increase under combined deformations is equal to the sum of the changes in pressure measured after separate application of the components of the combined deformation (Figure 1-9). This means that the change

in intradiscal pressure caused by rotation in one direction (sagittal plane or axial rotation) is independent of the existence of a rotation in the other direction.

If we would take the intradiscal pressure as a direct measure of stress in the annular wall and hence as a measure of risk of hernia nucleus pulposus in man, then from our observations presented in table 1-10 we might conclude that the annular stress anywhere around the circumference of the annular wall and consequently the risk of damage to the annular wall, is equal under the following load conditions: 1000 N axial load combined with 3 deg. axial rotation and 5 deg. flexion, or only an axial load of 1050 N, or an axial load of 1000 N combined with 6.5 deg flexion. Such a conclusion would be in flagrant contradiction to epidemiological ^{Kelsey '84 Burdorf '91}, analytical ^{Shirazi '89(2)} and experimental ^{Gordon '91} studies that predict increased stress in the annular wall under combined deformations.

Starting from a poro-elastic ^{Mow '80} view of the nucleus, pressure differences within the nucleus are possible. We experimentally verified this with the pressure needle tests. We did not find pressure differences under combined loading conditions, which would be accounted for by the weakness of the elastic matrix compared to the strength of the pressure existing in the nucleus under such loading conditions. In that case the nucleus as a whole would be displaced rather than fluid being squeezed through the pores of the matrix.

Conclusions

The results from the pressure-needle tests (Figures 1-4 and 1-5) show that the pressure in the nucleus shows a tendency to relax, and furthermore that different pressures can exist for some time in different locations in the nucleus.

No significant differences in pressure measured with the central and the posterolateral situated needle are found in normal discs when single and combined deformations are applied. Such deformations are likely to cause heterogeneously distributed stress in the annular wall. Apparently such a heterogeneous distribution of stress is not reflected in the distribution of intradiscal pressure, or else such stress differences do not exist. The latter is however unlikely considering the experimental ^{Gordon '91}, mathematical ^{Shirazi '98(2)} and epidemiological ^{Kelsey '84 Burdorf '91} evidence. This means that since high stress in some areas of the annular wall

probably determines the risk of local damage, intradiscal pressure is not a reliable measure of that risk.

Despite the relaxation phenomena we observed with the needle tests, the nucleus responds to asymmetric deformations within the physiological range, with homogeneous change in pressure, in other words the nucleus behaves hydrostatically and not visco-elastically. In our opinion the existence of different pressures in the nucleus, as measured in some cases, indicates severe disc degeneration. In those case the sensing needles may be situated in hydrostatically isolated spaces, so called sub-nuclei ^{Andersson '79 Goobar '87}.

In normal and even in light to moderately degenerated discs, the intradiscal pressure is a direct measure of the axial load on the FSU, that means that this pressure is hardly influenced by the degree of extension, flexion, axial rotation or a combination of these rotations (Tables 1-9 and 1-10). We also found that the change in the intradiscal pressure caused by rotation in one direction (sagittal plane or axial torque) is independent of the existence of a rotation in the other direction.

These findings are in harmony with the measurements and calculations published by Nachemson ^{Nachemson '81}. As there is good experimental ^{Gordon '91}, mathematical ^{Shirazi '98(2)} and epidemiological ^{Kelacy '84 Burdorf '91} evidence that (combined) rotations of the FSU (locally) increase strain and stress in the annular wall, we conclude that intradiscal pressure is not a good measure for stress and strain in the annular wall. The observations of Gordon et al. ^{Gordon '91} experimentally verified the relation between localized damage of the annular wall and combined deformations but they did not suggest a mechanism that may be responsible for the specific damage they induced, although their findings are theoretically supported by the model of Shirazi ^{Shirazi '89(2)}. To evaluate the risk of damage to the annular wall under specific deformations, we must establish another parameter than intradiscal pressure. In order to verify whether the strain load on the annular wall under simple and complex loading situations of the FSU, corresponds with the theoretical predictions of Shirazi ^{Shirazi '89(2)} we developed a technique to perform measurements directly on the annular wall (Chapter 3).

CHAPTER 2

Compression properties of the intervertebral disc

Compression properties of the intervertebral disc

2-I Confined Compression Of The Isolated Nucleus

Introduction

The relative contributions of elasticity and swelling properties of the intervertebral disc in the resistance to deformation during an axial load on the disc is not clear Inman '47 Virgin '51 Brown '57 Heady '58 Markolf '74 Sonnerup '82 Koeller '84 Kraemer '85 Urban '85 Ohshima '89. In Chapter 1 we described pressure relaxation phenomena, following stepwise deformations, with time-constants up to 30 seconds. These observed relaxation phenomena are ascribed partly to visco-elastic properties of the annular wall and partly to flow of water through the pores in the tissue of the nucleus. The structure of the nucleus is elastic and stiff enough to preserve the integrity of the isolated nucleus. The elastic matrix and the pores filled with water give the nucleus a sponge-like nature. Departing from this poro-elastic view on the nucleus, we expected to find pressure differences in an FSU under complex loading conditions (Chapter 1). We did not find any such pressure differences (under such loading conditions), which would be explained if the elastic matrix were very weak compared to the pressure existing in the nucleus under such loading conditions. Biomechanical properties of sponge-like structures have been studied by Mow and Droogendijk, concerning cartilage Mow '80 Droogendijk '84, by Oomens, concerning skin Oomens '87 and by Van Duyl concerning cervix tissue Van Duyl '84, by means of confined compression measurements. These studies yield parameters related to tissue permeability and elasticity. We performed similar studies on samples of the nucleus to assess the importance of elasticity and permeability.

Apparatus for confined compression

The confined compression measurements are performed by means of an apparatus similar to the one described by Droogendijk Droogendijk '84 which is depicted in figure 2-1; with a detail of the sample holder in figure 2-2. A cylindrical sample of the nucleus pulposus is placed in the cylindrical sample holder of stainless steel (1 in

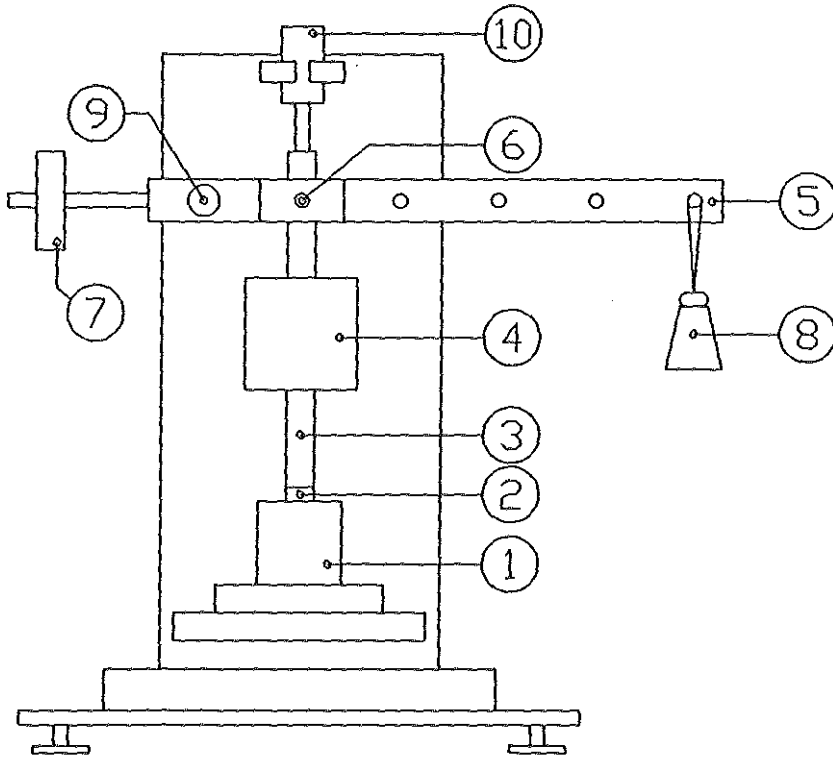


Figure 2-1. Testing apparatus according to Droogendijk (1984).

Figures 2-1 and 2-2), with a cross sectional area of 1 cm^2 . The sample can be compressed in axial direction by a bronze piston (2 in Figures 2-1 and 2-2). At the bottom of the sample holder is a draining filter (1a in Figure 2-2) of paper (Millipore) with pores of $2.0 \mu\text{m}$, which is highly permeable for water.

In order to exert a compressing force on the sample, the piston is loaded with a weight (8 in Figure 2-1) via a lever (5 in Figure 2-1) and a shaft (3 in Figure 2-1). To reduce friction the hinge of the lever (9 in Figure 2-1) is provided with

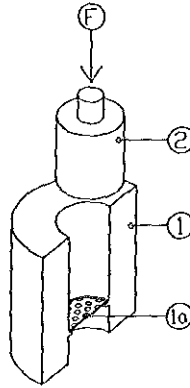


Figure 2-2. Modified pressure room.

an air lubricated bearing and the shaft is guided likewise by an air lubricated bearing (4 in Figure 2-1). Before applying the force the lever and shaft are balanced with an adjustable weight (7 in Figure 2-1). Because of the position of the hinge of the lever (9 in Figure 2-1) relative to its point of contact (6 in Figure 2-1) with the vertical shaft and the place of attachment of the weight (8 in Figure 2-1), the compressing force is two to five times the weight. The vertical displacement of the piston is measured by an electromagnetic displacement sensor ((10 in Figure 2-1) type Sangamo DF 50 STD, accuracy ± 0.025 mm). The output from the displacement sensor is low-pass filtered at a 0.25 Hz cut-off frequency, digitized with a Labmaster ADC board and fed into a PC at a sample rate of 1 Hz. Simultaneously a recording on paper was started as a back-up and, occasionally, also to cover measurements exceeding the capacity of the PC of 10.000 samples, which equals 2 hours and 45 minutes recording time.

The piston itself is not rigidly connected to the loading-shaft as a good alignment of these two parts is important to avoid resistance by jamming. The minimal load on the sample is therefore the weight of the piston, i.e., 0.248 N, which means a minimal applied pressure of 2.48 kPa (the minimal load divided by the cross sectional area of 1 cm²). The friction of the equipment is found to be less than 0.215 N, which means overestimation of the actually applied pressure of less than 2.15 kPa. As we applied loads of 25 N (Figure 2-3) or more, these values are acceptable. The permeability of the 2.0 μ m Millipore filter for water was determined by recording the loss of height of a column of water in the sample

holder under several loads, using equation (1).

$$Q = \frac{K \cdot P}{Dx} \quad (1)$$

In this equation, Q is volume flow density ($m \cdot s^{-1}$) or the speed of descent of the piston, P is pressure ($N \cdot m^{-2}$), K is the permeability modulus ($m^4 \cdot N^{-1} \cdot s^{-1}$) and Dx is the membrane thickness (m). Permeability (K/Dx) of the 2.0 μm Millipore filter was found to be $77 \pm 0.5 \cdot 10^{-6}$ ($m^3 \cdot N^{-1} \cdot s^{-1}$). This permeability appears to be high compared to the permeability of the tissue to be measured ^{Mow '80}.

Measurement and analysis of confined compression

From the onset of compression the height of the sample decreases through the expulsion of water out of the tissue sample. This compression proceeds until the applied force is in equilibrium with the stress built up in the elastic matrix of the tissue sample. Then the hydrodynamic pressure of the water phase in the sample is zero. The amount of expelled water during compression can be calculated from the decrease in height of the tissue sample. Reduction of volume of the material of the matrix is ignored. From the rate of compression and the value of final height of the tissue cylinder, both the elastic compression modulus (H) and the hydraulic permeability modulus (K) can be derived ^{Mow '80 Van Duij '84 Gomens '87}.

The decrease of height (D(t)) depends on the initial height of the tissue plug (h_0). We use a normalized measure of decreasing plug height h(t) defined as follows:

$$h(t) = \frac{h_0 - D(t)}{h_0} \quad (2)$$

Tissue samples were taken from the central area of two lumbar intervertebral discs, 15 hours after death (Specimen ID No: 89-259, male, age 58, levels L3-L4 and L5-S1, both of degeneration grade 3 ^{Galante '67}), by means of a hollow stainless steel pipe knife with an inner diameter equal to the inner diameter of the sample holder. The cylinder is filled with saline in advance. Then the sample tissue is inserted and carefully pushed to the bottom of the cylinder. The remaining space in the cylinder above the sample is filled with saline. Then the piston is inserted in the cylinder. As the tissue sample does not fit exactly in the cylinder the saline fills the voids inside the cylinder. At the start of compression the excess of saline

is expelled relatively fast. This can be observed as a fast descent of the piston that ends when the tissue sample has fully accommodated to the sample holder. The height of the plug in the cylinder at this moment is defined as the initial height h_0 in formula (2). Then the descent of the piston continues, however, much slower as it is determined from now on by compression of the sample.

Because the tissue samples were cut from the nucleus of an intact FSU, these samples were in a pre-loaded condition of at least 0.1 MPa ^{Nachemson '75}. Once placed in the cylinder, the tissue sample is in direct contact with saline for a short period and may take up some water. The sample therefore may be more relaxed and hydrated than it previously was *in-situ*. It is therefore estimated that the sample can be compressed with loads exceeding 10 N/cm² i.e. an applied pressure of 0.1 MPa.

Results

In figure 2-3 the first 2 hours and 45 minutes of compression are shown, of a sample under a compression force of 25 N. In a sample holder merely filled with water such a force would cause a pressure of 25 N/cm² or 0.25 MPa. The compression was continued for a duration of more than 18 hours. The relative height of the plug was reduced by that time to 45 % and decreased further, almost linear in time. So even after such a long period static equilibrium was not achieved.

Discussion

In the analysis of Mow ^{Mow '80} and Van Duyl ^{Van Duyl '84} is assumed that static equilibrium is almost reached exponentially during the recording period. According to the poro-elastic model the final height of the sample at equilibrium is determined by the elastic matrix, and hence an estimation of this height yields an estimation of the elastic compression modulus (H). By knowing the compression modulus the hydraulic permeability modulus (K) can be calculated according to the poro-elastic model.

The analysis of the compression of the nucleus according to this poro-elastic model is however complicated by the fact that despite the long recording period, no asymptotical approaching of the equilibrium level is seen. In other words, even

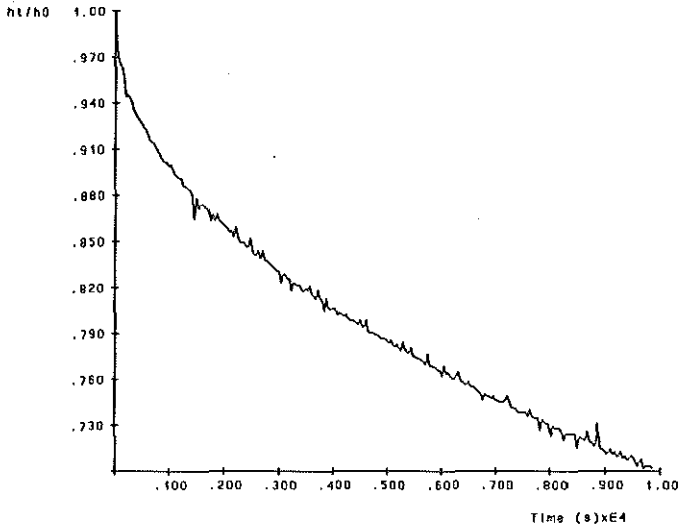


Figure 2-3. Example of the normalized load-displacement recording of a sample, loaded at an equivalent of 0.25 MPa.

after a long period of more than 18 hours, compression is not yet opposed by the elasticity of the tissue matrix, while the height of the sample may already be reduced to half its initial value. For that reason we could not apply the analysis of Van Duyl ^{Van Duyl '84} to our compression data of the nucleus. We have to conclude that, within the observed compression range, the rate of compression is not limited by elasticity of tissue matrix of the nucleus but by the resistance of the matrix to the flow of water.

These observations are in contrast with the results of experiments described in literature where equilibrium is reached with osmotic solutions as the external loading mode of nuclear tissue ^{Urban '81 Maroudas '81 Maroudas '87 Ohshima '89}. We therefore reject the poro-elastic model and focus on the swelling properties of the nucleus.

Some authors ^{Urban '81} claim that the swelling pressure is sufficient for statical carrying of physiological loads. Then swelling processes determine the declining rate and final value of compression. Evidently such a swelling equilibrium was not reached in our experiments either.

Moreover keeping the filter-membrane in an isotonic solution did not alter our finding. We wonder therefore, whether our compression experiments are

comparable with the situations *in-vivo*. Indeed decreasing intradiscal height, particularly under a load, is well known ^{Kr mer '80}, but probably not to the same degree as we find in our compression experiments. We can think of three objections to our experiments:

- 1) In our experiment fluid may be lost by evaporation at the external surface of the filter. The almost linear compression observed after a certain compression period hints at that.
- 2) In our *in-vitro* experiment a fraction of the large molecules, which are necessary for the swelling process, may pass under compression through the filter membrane. Continued loss of those molecules is accompanied by reduction of the amount of water that is kept in the sample by its swelling properties. According to this interpretation, the failure to reach an equilibrium is caused by gradual reduction of the swelling potency of the nucleus. This interpretation would be consistent with the conclusions of Urban ^{Urban '81} and others ^{Maroudas '81 Maroudas '85 Ohshima '89} that the swelling property of the nucleus is primarily responsible for opposing a statical pressure load.
- 3) *In-vivo* the extremely low hydraulic permeability of annulus and end-plates, as compared to that of the membrane in our set-up, may be the dominating factor in limiting the rate of volume decrease in the intervertebral disc under pressure.

Our attempts to use filter-membranes with a smaller pore-size, to prevent the loss of proteoglycans and still allow for swelling processes, failed. These materials proved either to be too fragile to withstand the mechanical pressures we applied, or to have too poor permeability. We modified our compression experiment in a way that swelling was not affected by the loss of molecules and water was not lost by evaporation (Chapter 2-II).

Conclusions

We did not observe stabilization of compression, not even after more than 18 hours. We conclude that the elasticity of tissue matrix of the nucleus plays an insignificant role in physiological loading conditions in the observed range of compression. The poro-elastic model given by Mow ^{Mow '80} is therefore not

applicable to nucleus tissue.

Swelling processes and hydraulic permeability are more important than tissue elasticity of the nucleus. Our experimental set-up, however, was not suitable for a separate determination of these properties.

2-II Compression Of The Isolated Disc

Introduction

Following the previously described confined compression experiments on samples of the nucleus we performed compression measurements on isolated discs. Now the nucleus is surrounded by its natural boundaries, i.e. the annulus and the end-plates, which form its "physiological" membrane. Furthermore the circumference of the nucleus is not artificially confined by a sample holder, but is free to change according to the load. In view of the discussion concerning the role of swelling pressure ^{Inman '47 Hendry '58 Maroudas '81 Urban '81 Ohshima '89}, fluid flow ^{Virgin '51 Brown '57 Markolf '74 Urban '82 Sonnerup '82 Koeller '84 Kraemer '85} and annular bulging ^{Klein '83} under long lasting axial loading conditions of the disc, the experiment was designed to be able to quantify these aspects. Compared to the previous confined compression experiments we also expect to find in these experiments a decrease of disc height and volume under constant loading conditions, but under conditions which are more representative for situations *in-vivo*. Particular provisions are made to measure expelled water while evaporation of the water is prevented.

Arrangement for the compression of an isolated disc

An isolated disc consisting of annulus (7 in Figure 2-4), nucleus (9 in Figure 2-4) and end-plates (8 in Figure 2-4) is cut out of a FSU sothat it can be fitted later on to two perspex plates, 2 in figure 2-4. The perspex plates need to be mounted in the loading apparatus described in chapter-1, figure 1-1. The disc is submersed in saline and allowed to swell. The cross-sectional area of the disc is calculated by approximating the cross-section by an ellipse with lateral the long axis and anterior-posterior the short axis. Then a thin elastic rubber tubing, 5 in figure 2-4, is placed around the contour of the disc. At both lateral sides of the disc a small hole is cut in the rubber tubing into which a draining tube is inserted, 6 in figure 2-4.

The expelled fluid is measured as follows. The disc is isolated from the FSU by sawing off the vertebral bodies parallel to the end-plates as close to the disc as possible. Then both end-plates (8 in Figure 2-4) of the disc are pressed against the thick perspex mounting plates (2 in Figure 2-4). The space between the disc in the

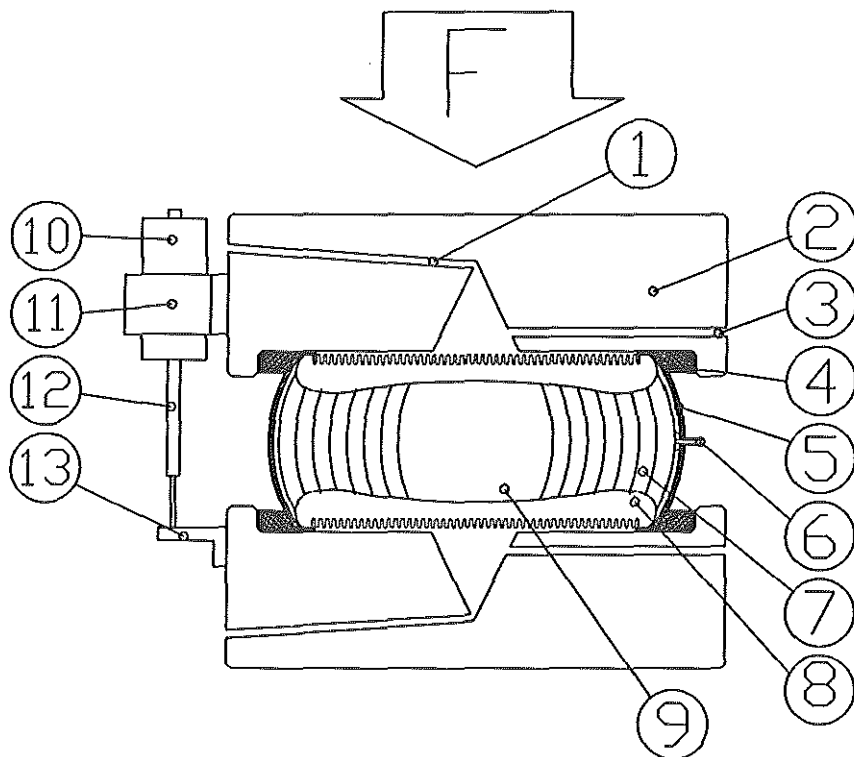


Figure 2-4. Diagram of the fixation of a specimen and draining arrangements.

rubber tube and the rim on the plate is sealed with cold-curing resin (Kulzer: Technovit® 2060) (4 in Figure 2-4). This provides sufficient attachment of the specimen to the plates and prevents leakage. In the surface of each mounting plate a cone shaped hole is made to drain the water that penetrates trough the end-plates. An opening, drilled to the base of the cone (3 in Figure 2-4), enables flushing of saline into the voids. A second opening, drilled at the top of the cone (1 in Figure 2-4), provides for the evacuation of air out of the system. The drains

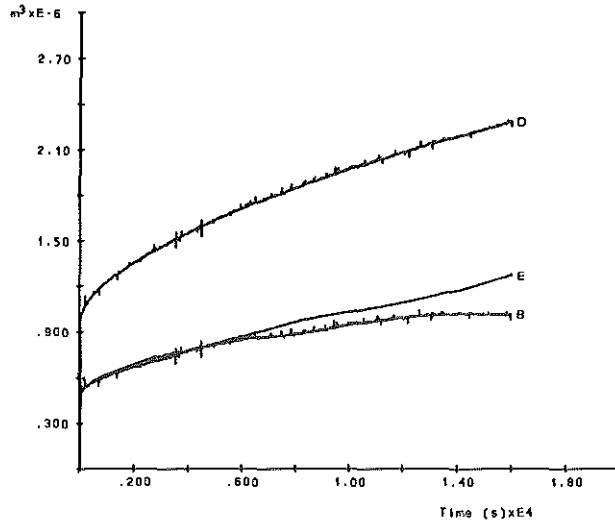


Figure 2-5. Recordings of an isolated disc compressed with an axial load of 500 N. D= Displaced volume (m³) E= Expelled volume (m³) B= Calculated bulge volume (m³).

are led to a small cup filled with saline, to the same level as the middle of the disc. All drains enter the cup just below the surface of the saline. To prevent evaporation the surface of the saline in the cup is covered with oil. The weight of the cup with saline is continuously measured by means of a Grass[®] Force-Displacement Transducer type FT03C (Grass Instrument Co. Quincy, Mass., U.S.A), with an error of less than 0.02 mN. The distance between the two perspex plates is measured continuously by means of an electro-magnetic displacement sensor (10 to 13 in Figure 2-4) type Sangamo DF 50 STD, accuracy ± 0.025 mm).

The disc, together with the perspex mounting plates, is placed in the clamps of the loading apparatus (Figures 1-1 and 1-2 in Chapter 1). The clamps of the loading apparatus are adjusted so that the mid-plane of the nucleus is exactly horizontal and thus perpendicular to the direction of the axial load that can be applied. The voids and channels of the mounted disc are then filled with saline and flushed to eliminate air bubbles. The distance between the endplates is then measured with a micrometer at the ventral and dorsal side of the disc and the mean disc height is calculated.

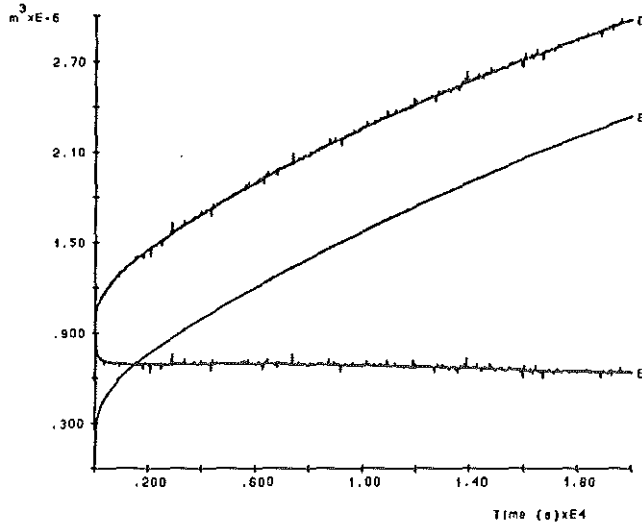


Figure 2-6. Recordings of an isolated disc compressed with an axial load of 1000 N. D= Displaced volume (m³) E= Expelled volume (m³) B= Calculated bulge volume (m³).

An axial load is applied stepwise within a tenth of a second. The signals concerning the distance between the mounting plates and the weight of expelled water are low-pass filtered at a 0.25 Hz cut-off frequency, then sampled and converted by a 12 bit ADC (Labmaster) at a rate of 0.5 per second and finally fed into a PC. The signals were also recorded on paper to cover measurements exceeding the capacity of the PC of 10,000 samples, representing 5 hours and 30 minutes recording time.

The recorded weight of expelled water is divided by the density of saline ($1.009 \cdot 10^3 \text{ kg/m}^3$) to arrive at the expelled volume.

Compression of the disc is accompanied by bulging of the circumference. So the product of recorded change of distance between the mounting plates and the cross-sectional area of the endplate of the disc, yields a measure of volume that is larger than the expelled volume of water. The difference between these volumes equals the change in volume due to bulging ^{Klein '83}.

From the confined compression experiments it was concluded that within the observed range, compression is not limited by the elastic matrix, but mainly by

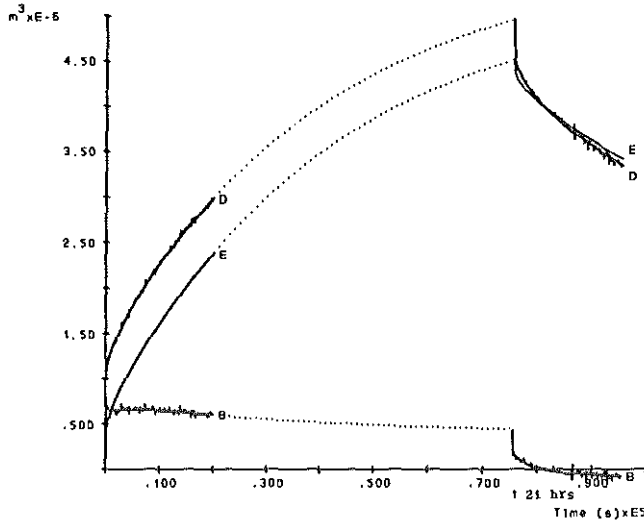


Figure 2-7. Recordings of an isolated disc compressed with 1000 N and recuperation after 21 hours of axial loading, D= Displaced volume (m^3) E= Expelled volume (m^3) B= Calculated bulge volume (m^3).

the hydrodynamics of the flow of water in tissue. Therefore during the confined compression (2-1) the intradiscal pressure must be constant. To test this we measured in one compression experiment the pressure in the intervertebral disc using the IDP-sensor described in Chapter 1.

We can also estimate the intradiscal pressure by dividing the applied force to the FSU by the largest cross-sectional area of the disc. Nachemson^{Nachemson '60} however empirically established that this estimate is wrong and needs to be multiplied with 1.5 for a better estimate of the intradiscal pressure.

Preparations of the disc

In-vivo the disc is always loaded as part of the FSU due to the ligaments attached to it. The minimum load of the disc is approximately 100 N^{Markolf '74}. Nachemson^{Nachemson '64} showed that this minimum load on the disc *in-vivo* is only achieved when the subject is fully sedated and all muscle activity is suppressed.

We submerged the disc in saline and stored it at 4 °C for 24 hours so that it

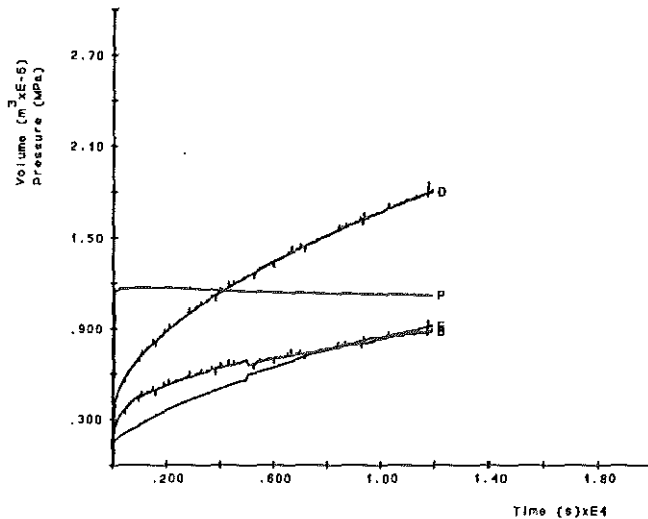


Figure 2-8. Recordings of an isolated disc compressed with an axial load of 1700 N. D= Displaced volume (m^3) E= Expelled volume (m^3) B= Bulge volume (m^3) P= Intradiscal pressure (MPa).

accommodated to an unloaded equilibrium. In order to determine the load-deformation relation of the disc we wanted to load the disc with pressures equal and higher than the reported initial pressure *in-vivo* of 0.1 MPa ^{Nachemson '75}. To prevent dehydration and deterioration of the tissue we removed it out of the testing apparatus after each test series, submerged it in saline and stored it at 4 °C for about 24 hours. By doing so we allowed for complete recuperation of the disc.

After pilot measurements with discs that were previously used in the experiments described in chapter 1, one isolated disc was used for the measurements described here; Specimen ID No: 90-249, male, 60 kg., length 178 cm, age 51, obtained 21 ours after death, degeneration grade 2, level L4-L5, cross-sectional area .0015 m^2 .

Results

In figures 2-5, 2-6, 2-7, and 2-8 the expelled fluid volume (E) and the calculated volume displaced by the descending endplate (D) (i.e. the measured change of height multiplied with cross-sectional area) are shown, obtained in four

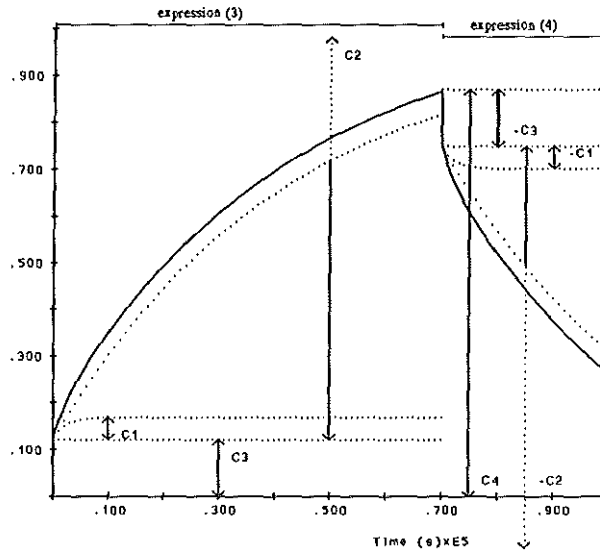


Figure 2-9. Graphical explanation of the expressions (3) and (4).

compression experiments. The change in volume due to bulging (B) is derived by subtraction of E from D. Figure 2-7 concerns the recuperation of the specimen in figure 2-6 under zero load. Previous to this recuperation it had been loaded during 21 hours with an axial load of 1000 N.

It turns out that these recordings can be fitted to a mathematical model consisting of two exponential terms and a constant (Figure 2-9) according to $m(t)$ (3):

$$m(t) = c_1 \cdot (1 - e^{-t/T_1}) + c_2 \cdot (1 - e^{-t/T_2}) + c_3 \quad (3)$$

The increase in height of the disc after removal of the axial load (Figure 2-9), in case of recuperation, is described by a similar function $n(t)$ (4) in order to compare the fitted parameters with those obtained in compression, as we expect them to be the same.

$$n(t) = -c_1 \cdot (1 - e^{-t/T_1}) - c_2 \cdot (1 - e^{-t/T_2}) - c_3 + c_4 \quad (4)$$

The initial magnitude of function (4) at the moment of unloading is now not zero but a constant term (c_4), which is not fitted but determined by the height of the

disc just before unloading.

The same functions (3) and (4) are used to describe the expelled volume under compression and recuperation respectively.

Table 2-1 gives the fitted parameter values for a series of compression and recuperation experiments. All fitted results are based on equal recording periods.

The dotted lines in figure 2-7 represent the fitted curves. Figure 2-8 shows the recordings of the same specimen as in figures 2-5, 2-6 and 2-7, but now with a pressure sensor situated in the central nucleus and axially loaded with 1700 N. Pressure (P in Figure 2-8) remained stable within $\pm 3\%$.

Table 2-1. Parameter values fitted to the first 11750 seconds of displaced and expelled volume recordings

¹ Fit without constraints
 Unloaded Displaced $c_4=4.96e-6$ (m³) ² Fit to complete recuperation
 Unloaded Expelled $c_4=4.67e-6$ (m³)

Axial load (N)	fitted volume curve	c_1 (m ³)	T_1 (sec)	c_2 (m ³)	T_2 (sec)	c_3 (m ³)
500	Displaced	0.18e-6	1147	1.85e-6	18383	1.00e-6
	Expelled	0.09e-6	442	1.18e-6	20455	0.48e-6
1000	Displaced	0.15e-6	631	2.77e-6	20827	1.06e-6
	Expelled	0.23e-6	514	3.27e-6	25727	0.33e-6
unloaded ¹	Displaced	0.16e-6	578	1.34e-6	14252	-.39e-6
	Expelled	0.11e-6	513	1.57e-6	25727	-.23e-6
unloaded ²	Displaced	0.25e-6	1661	4.28e-6	73038	-.43e-6
	Expelled	0.13e-6	1016	4.26e-6	85810	-.25e-6
1700	Displaced	0.24e-6	723	2.00e-6	13353	0.40e-6
	Expelled	0.03e-6	378	1.16e-6	11360	0.14e-6

Discussion

With the disc under a constant axial load we measured simultaneously the flow of fluid expelled out of the disc and the thickness of the disc. Furthermore we calculated the course in time of the bulging volume. A bi-exponential function (3) was fitted to the data. Because the magnitude of T_2 appears to be big compared to the recording time, its absolute value may be unreliable ^{Van Duyl '83}. Like in the

constrained compression experiments this slow exponential may be affected by a third very slow process, namely the loss of swelling potential of the disc, due to degeneration or loss of large molecules via the expelled fluid. The duration of the recording influences the magnitude of the fitted parameters. For comparison all fits were performed on the same amount of data (i.e. recording time), equal to the shortest recording (i.e. 11750 seconds).

In these compression and recuperation experiments at least two processes are involved that determine the mechanical behavior of the axially loaded disc, namely the expulsion or resorption of fluid and the visco-elastic relaxation of the annular wall.

One exponential term is ascribed to the visco-elastic relaxation of annular wall fibers ^{Galante '67} (c_1 and T_1) and the other is ascribed to the expulsion or resorption of fluid from the disc (c_2 and T_2). The constant term (c_3) is added to the model to account for the initial stepwise change in height of the disc as seen in the recordings. This initial change is ascribed to the elastic component of bulging, which occurs immediately after loading and unloading.

The same functions (3) and (4) are used to describe the expelled volume under compression and recuperation respectively. One exponential expression is ascribed to the fluid flow in (4) and out (3) of the disc (c_2 and T_2). The constant term (c_3 or c_3 and c_4) and the second (fast) exponential expression (c_1 and T_1) were needed to get an accurate description of the complete curve.

From the onset of the axial loading of the disc, or from the start of recuperation, two processes determine the change of thickness of the disc: In the initial period the fast change in thickness is caused mainly by the time dependent change of bulging, due to visco-elasticity of the annular wall (D in Figures 2-5, 2-6, 2-7, and 2-8, Table 2-1 c_3 , c_1 and T_1). Changes due to fluid flow are much slower and dominate in a later phase (D and E in Figures 2-5, 2-6, 2-7 and 2-8, Table 2-1 c_2 and T_2).

T_2 represents the time constant we found, for the time course of expelled-volume and displaced-volume, which was almost equal in all sessions. Therefore we conclude that this time constant concerns the same process (i.e., fluid flow). The stepwise change in expelled-volume, expressed by c_3 , is ascribed to the displacement of fluid that was already outside the disc before the axial load was applied. This can be caused by displacement of the specimen due to incomplete

fixation in the mounting cubes and load deformation of the endplates. Immediately after loading the disc, an important increase of bulging occurs (c_3 in the displaced-volume curve). The increased bulging causes an increased stress in the elastic tube surrounding the annular wall and some fluid will be squeezed out of the outer layers of the annulus fibrosus. As the outer annulus fibrosus has a lower resistance to fluid flow than the entire annulus or the endplates, this fluid is expelled faster. We assume that T_1 of the expelled-volume curve mainly concerns the expulsion of fluid from the outer layers of the annulus fibrosus. c_1 is about ten times smaller than c_2 , so the first exponential describes only a minor part of the expelled volume (E) when compared to the second exponential.

This experiment was designed to obtain an almost physiological confinement of nuclear material in order to prevent loss of swelling potential. We find in the results the following arguments to conclude that in these experiments swelling potential is still lost.

Firstly, because the recorded intradiscal pressure of approximately 1.2 MPa (P in Figure 2-8) was only 70 percent of the expected pressure ($1.5 \cdot 1700 \text{ N} / .0015 \text{ m}^2$ or 1.7 MPa) as calculated according to Nachemson ^{Nachemson '60}. Markolf and Panjabi ^{Markolf '72 Panjabi '88} found similar lower pressures in degenerated discs that have a lower swelling potential.

Secondly, because the fits to the data of the recuperation after an axial load of 1000 N (Figure 2-7 and calculated from table 2-1, fit without constraints) show that the volume after recuperation is significantly less than the volume before the axial load was applied.

Thirdly, because with a monotonic change in axial load on the same specimen in consecutive experiments we expect a monotonic change in displaced volume and expelled fluid volume. This is not seen however, at an axial load of 1700 N (Figure 2-8), the displaced and expelled volume is smaller than which was measured in the previous compressions with loads of 500 N (Figure 2-5) and 1000 N (Figure 2-6) which showed an increase in displaced and expelled volume after an increase of load.

Fourthly, because (for the same reason as point three) the second exponential, which is assumed to represent the process of fluid flow, is expected to be constant or change monotonically with increasing axial load. However, the values of T_2 and c_2 that were fitted to the data of the different load responses (Table 2-1 Displaced and Expelled) prove otherwise.

Our data suggest that after each compression experiment with the same specimen the disc restores to a lesser height. Eventually, when all fluid is expelled, the transmission of the load is taken over by end-plate to end-plate contact. This would imply that the intradiscal pressure becomes zero. It is quite unlikely however, that this condition is ever reached *in-vivo*. In the previously performed confined compression experiments (Chapter 2-I) we supposed that the linearly continuing compression is caused by the loss of large molecules which determine the swelling pressure. The confined compression experiment, described in chapter 2-I, was modified in order to measure the compression of the disc under conditions which more closely resemble the physiological conditions, so that the artificial loss of large molecules is reduced. Yet we conclude that in these experiments too the compression is accompanied by the loss of large molecules.

The applied axial loads are within the range of what may be called "normal work load" ^{Nachemson '81}. Even the exposure to such a load during 21 hours is not uncommon. On the other hand the recuperation time we allowed for is in fact extremely long, compared to the *in-vivo* situation.

In our opinion the discrepancy in observed *in-vitro* behavior and what we take as normal behavior *in-vivo* may be caused by a compensation mechanism for the loss of large molecules that is active *in-vivo* but not *in-vitro*, in particular a mechanism for the production of glycosaminoglycans, ^{Schnackerman '86 Bayliss '86 Bayliss '88}.

Figure 2-8 shows that the intradiscal pressure is almost constant during compression. Pressure decreases less than 3% during more than three hours of axial loading. Furthermore the recorded intradiscal pressure (Figure 2-8, curve P) under axial load is hardly influenced by the deformation of the specimen. This provides more evidence for our previously drawn conclusion that, in the range of the observed compressions, the contribution of the elastic compression of the tissue matrix in the reaction to the axial load is negligible compared to the contribution of the intradiscal pressure.

According to the literature, intradiscal pressure is linearly related to the applied external load and the cross-sectional area of the disc ^{Nachemson '60}. However, the recorded intradiscal pressure was 70 % of the pressure calculated according to Nachemson ^{Nachemson '60}. Because the discrepancy of 30% is found immediately at the onset of the load and remains constant within 3%, it cannot be ascribed to the elastic compression of the tissue matrix, this too in accordance with our previous conclusion. According to Panjabi ^{Panjabi '88} the 30% lower pressure is caused by degeneration of the specimen. Because this explanation is based on the supposition

of a significant contribution of the elastic matrix, we don't agree. In chapter 2-III we will explain this discrepancy to be consistent with our conclusion that the nucleus behaves hydrostatically.

Conclusions

Immediately after the application of an axial load, the height of the disc decreases fast due to the bulging of the annular wall. Because of the visco-elastic properties of the annular wall bulging gradually increases during a short period. The expulsion of fluid out of the disc is a much slower process and determines the further decrease of disc height and increase of bulging of the annular wall.

Even under loading conditions lasting more than 3 hours (Figure 2-8) intradiscal pressure is constant. The observed compression is not limited by the compression of the tissue matrix, but determined only by the intradiscal pressure. The resorption of water caused by the swelling properties of the disc is not sufficient to compensate for the expulsion of water, so that loss of disc height did not stop even after long periods of observation (up to 21 hours).

During compression of the disc *in-vitro*, loss of large molecules is supposed to be responsible for a slow decrease of swelling capacity. An active regeneration mechanism, missed *in-vitro* is postulated *in-vivo* to compensate the loss of proteoglycans. This would imply that results of compression studies *in vitro* are not representative for the compression of a FSU in response to a load *in-vivo*.

2-III Analytical Model of the Intervertebral Disc Subjected to Pure Axial Load

Introduction

This model was created to suit the results of the experiment described in chapter 2-II. Prior to this experiment expectations were that the loss of disc height under constant axial load would come to a halt. In which case we would have adapted the poro-elastic model ^{Mow '80} under the assumption that the solid tissue elasticity modulus H , as described in the poro-elastic model, also can be used to describe the pseudo-elastic behavior of the disc. Subsequently the permeability and pseudo-elasticity of the disc could have been calculated quite easily. Our major objection to this option was, that it would use the empirically derived load-pressure relation given by Nachemson ^{Nachemson '60} to estimate intradiscal pressure. The only refinement we could then think of was the adjustment of the cross-sectional area to the change in annular wall bulging. From our own pressure measurements, described in chapter 1, we already knew that the estimation of intradiscal pressure could be 50 % off the mark in case of unrecognized degeneration of the disc. The magnitude of the hydrostatic pressure is of vital importance to the calculation of permeability and elasticity in the poro-elastic model that we would have wanted to adapt in order to describe the poro-pseudo elastic model. The measurements described in chapter 2-II did not show an equilibration of axial load and disc deformation so an adapted poro-elastic model would not be applicable as it assumes an eventual achievement of equilibrium. At the same time however, the idea of a biomechanical mechanism that explains the load-pressure relation was born, closely resembling to the mechanism that was published by Brinckmann and Grootenboer ^{Brinckmann '91}, and the model of the intervertebral disc as it is described in this chapter was formed.

Many models of the intervertebral disc have been published, using the Finite Element Method (FEM) ^{Simon '85 Shirazi '86 (with review)} or applying an analytical approach ^{Hickey '80 Klein '83 Brinckmann '91 Broberg '93}. The powerful computers and sophisticated FEM programs available today enable us to model a complete FSU, accounting in detail for both material properties and geometry. For the analytical approach we are forced to simplify the geometry of the FSU considerably and usually only the isolated disc is regarded and the vertebral arc and the facet joints are ignored. The

necessity of a more detailed approach depends on the question to be answered. We developed a model to explain with some simple biomechanical principles the phenomena observed in axially loaded intervertebral discs. In particular we looked for a simple biomechanical explanation for the discrepancy in measured intradiscal pressure and the pressure found by simply dividing the axial force by the cross-sectional area.

We implemented the model in a computermodel to simulate the dependence of the intradiscal pressure on the applied load and on factors generally associated with the condition of the disc prior to loading. The model includes elasticity, swelling, permeability and the visco-elastic behavior of the annular wall. With this model we simulate the experimental data obtained in the *in-vitro* experiment described in chapter 2-II concerning fluid flow, disc height, annular bulging and intradiscal pressure, but also variables not measured, such as the decrease of the capacity to resorb fluid and the strain in the fibers of the annular wall. The simulation results were compared to our own experimental data and to data taken from literature. In this capacity the model elucidates the functioning of the disc according to the implemented mechanical principles. The model can also be used to predict deformation of the intervertebral disc as part of an intact spinal column under an applied axial load *in-vivo*, or reversely to calculate the applied axial load from the observed loss of height of the disc. For simulation the mathematical model has been translated into a computermodel using the simulation software PSI-e (Version 1.015 by BOZA, Delft University of Technology). In Appendix-A the theoretical derivation of the model is described. A flow diagram of the computer simulation model is given in Appendix-B.

Description of the model

Because, in the light of previous results, the elastic matrix of the nucleus can be ignored, we relate the externally applied load (F_e) only to the hydrostatic, intradiscal pressure P_h . Moreover we account for the pressure associated with swelling (P_s) and the force (F_r) exerted by the annular wall on the endplates. The intervertebral disc is considered to have the shape of a barrel with height h and a circular cross-section (Figure 2-10). The cross-sectional area is largest in the middle. The radius of the largest cross-section is expressed as the sum of the base radius r and the amount of bulging b (Figure 2-10). When there is no bulging

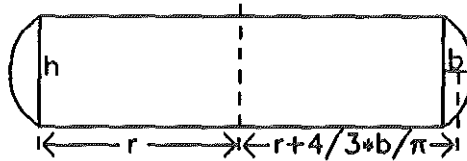


Figure 2-10. Diagram of the disc model (side view).

we assume that the distribution of fibers in the annular wall is homogeneous. In case of bulging, the density of the fibers of the annular wall and consequently also the stiffness of the annular wall decreases towards the middle of the annular wall. The curvature of the bulging is therefore approximated by a semi-elliptic course. We suppose that the angle between the inner part of the annular wall and the endplates is limited by the endplates to 90 degrees. The total disc volume is calculated according to the formulas in Appendix-A. During compression the disc volume decreases and is equal to the initial disc volume minus the expelled fluid volume.

In a first approximation we could calculate the intradiscal pressure P_h from the axial load F_e and the cross sectional area of the endplate A , but more is involved. We need to know the relation between external and internal forces and disc geometry (i.e. height h , bulging b and radius r).

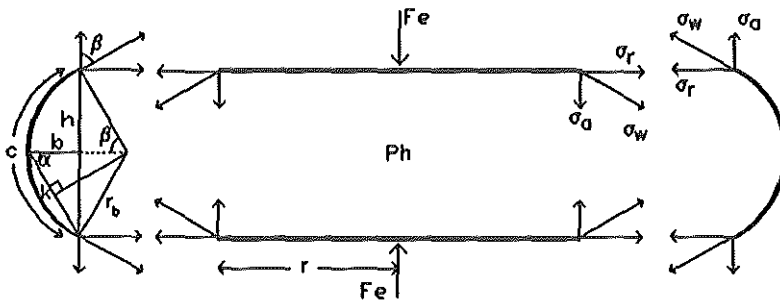


Figure 2-11. Diagram of the modelled bulging and the forces acting on the endplates and the annular wall.

Application of a load to the upper endplate of a disc changes the geometry of the disc and causes strain ϵ_w and stress σ_w in the annular wall (Figure 2-11) as well as an increase in the hydrostatic, intradiscal pressure P_h . The stress σ_w in the annular wall has a component in axial direction σ_a (i.e. acting in the same direction as the external force F_e), which pulls the endplates together. Since we assume no involvement of an elastic matrix, the external force F_e , that is applied by a load on

the upper endplate, and the axial component σ_a , of the stress σ_w in the annular wall, must be balanced by the intradiscal pressure P_h alone. When we calculate the balance of forces in axial direction between the endplate and the annular wall (Figure 2-11) ^{Briackmann '91} we get (5):

$$P_h \cdot \pi \cdot r^2 - (F_e + \sigma_a \cdot 2 \cdot \pi \cdot r \cdot d) = 0 \quad (5)$$

If we define the force exerted by the annular wall on the endplate as (6):

$$F_w = \sigma_w \cdot 2 \cdot \pi \cdot r \cdot d \quad (6)$$

with (7)

$$\sigma_a = \sigma_w \cdot \cos \beta \quad (7)$$

then (8):

$$P_h = \frac{F_e + F_w \cdot \cos \beta}{\pi \cdot r^2} \quad (8)$$

The radial component σ_r of the stress σ_w in the annular wall is also in equilibrium with the intradiscal pressure P_h . So if we calculate the balance of forces between the annular wall and the endplates in radial direction (Figure 2-11) we get (9):

$$P_h \cdot h \cdot 2 \cdot \pi \cdot r - 2 \cdot \sigma_r \cdot 2 \cdot \pi \cdot r \cdot d = 0 \quad (9)$$

with (10):

$$\sigma_r = \sigma_w \cdot \sin \beta \quad (10)$$

so (11):

$$P_h = \frac{2 \cdot F_w \cdot \sin \beta}{h \cdot 2 \cdot \pi \cdot r} \quad (11)$$

So the intradiscal pressure can be calculated following two different approaches. By substituting one expression into the other we derived an expression relating the intradiscal pressure P_h to disc geometry (height h , bulging b and radius r), annular wall stress σ_w and applied external force F_e (Appendix-A). This relation can also be used to calculate the disc-height h as a function of the external load

F_c , annular wall stress σ_w , and disc geometry. As for the unloaded situation, the disc height h is calculated from the intradiscal pressure P_i , annular wall stress σ_w , and disc geometry (Appendix-A).

The strain in the annular wall in relation to the intradiscal pressure is calculated as follows. We simplified calculations by assuming that, if the angle β is less than 90° (Figure 2-11), the curvature of the bulging is part of a circle ^{Klein '83} instead of an ellipse. The difference in calculated disc volume using the circular approach instead of the elliptic one is calculated to be less than two percent.

At a given disc volume and height, the bulging b of the disc is then determined. As shown in figure 2-11 the arc c , angle β and radius r_b can now be calculated from the bulging b and disc height h (Appendix-A).

If the angle β becomes 90° or more, a semi-elliptic bulging curvature is used to calculate the length of the arc c from b and h (Appendix-A).

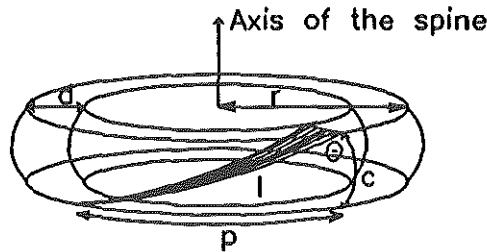


Figure 2-12. Diagram of the disc model, showing one fiber running clockwise from one endplate to the other.

With the known length of arc c of the curvature of the bulging we calculate the length of the fibers in the wall. The fibers of the annular wall, with length l , are fixed to the endplates under a certain angle θ with regard to the axis of the disc, which in the unloaded situation is approximately 60° ^{Klein '83} (Figure 2-12). We approach the annular wall by considering it as one layer with thickness d ^{Hickey '80} and with fibers running both clockwise and counterclockwise from one endplate to the other. The pitch p is defined as the distance along the circumference of the endplates between both ends of each fiber. We describe the area enclosed by fiber length l , bulging curvature c and pitch p as a rectangular triangle. This simplification can be done because the radius r of the disc is much larger than the radius r_b and arc c of bulging. Thus simplified we calculated the fiber length l and pitch p for the initial (unloaded) situation. Because during compression pitch p is

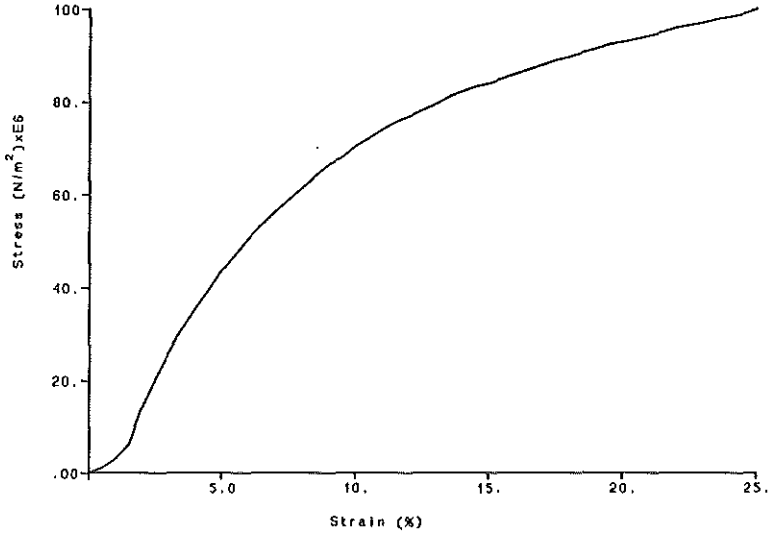


Figure 2-13. Stress-strain curve of the annular wall fibers (according to Shirazi *et al.* 1986, 1989).

constant we can calculate the fiber length l and angle Θ (Appendix-A) during compression.

The initial pressure P_0 in the unloaded isolated disc is approximately 0.1 MPa Nachemson '75. With this initial pressure the initial stress in the annular fibers can be calculated (Appendix-A). The corresponding initial strain of the annular fibers is then derived from a stress-strain relation shown in figure 2-13, which has been constructed by Shirazi Shirazi-Adl '86 Shirazi '89 from experimental data published by others Harkness '61 Haut '72 Morcin '78 Kastelic '79 Betuch '80 Sanjcevi '82 Sanjcevi '82(2) Haut '83. From the initial fiber strain at $t=0$ ϵ_0 and fiber length l_0 the unstrained fiber length l_u is then calculated (Appendix-A). For each value of the strain ($\epsilon = l/l_u$) during the simulation, the stress σ_f is estimated by using this relation. This stress in the fibers yields the stress in the annular wall σ_w and, multiplied with $2 \cdot \pi \cdot r$ and the thickness d of the annular wall, the force F_w exerted by the annular wall on the endplates. For the simulation of a response to a stepwise loading of the disc, a visco-elastic component is added to the elastic stress-strain relation of figure 2-13 (Appendix-A).

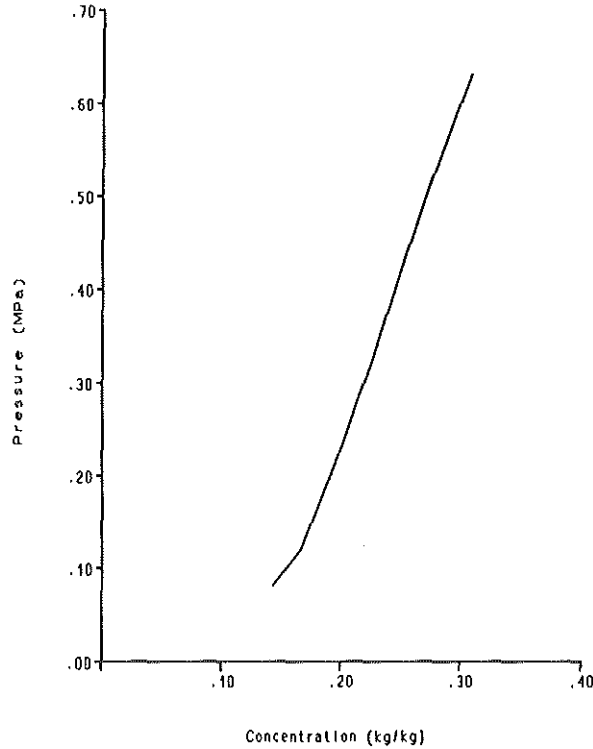


Figure 2-14. Concentration-pressure curve of the swelling pressure (according to Urban 1981).

Sofar we have only calculated the hydrostatic pressure in the disc in relation to the disc geometry and axial load. The hydrostatic pressure P_h in the disc causes a fluid flow J out of the disc that is opposed by the swelling pressure P_s caused by the glycosaminoglycans in the disc. In order to simulate fluid flow into or out of the nucleus we need to know the relation between swelling pressure P_s and the concentration C of the glycosaminoglycans in the disc. This concentration-pressure relation, shown in figure 2-14, is taken from experimental data published by Urban ^{Urban '81}. Urban measured the water content per dry weight of nucleus samples in equilibrium with different values of externally applied pressures. In our model the swelling pressure P_s is estimated for each value of the concentration C by using this relation. We derive the initial concentration C_0 from this curve using the initial swelling pressure. At the start of the simulation the model is in

equilibrium so the initial swelling pressure is equal to the initial hydrostatic pressure P_0 . The initial disc water volume V_d is assumed to be 2/3 of the initial disc volume ^{Urban '79}. By multiplying initial water volume with initial concentration we get the total amount G of glycosaminoglycans at $t=0$. Fluid flow J , in or out of the disc, is determined by the permeability K_d and the difference between the hydrostatic pressure P_h and the swelling pressure P_s according to Darcy's law (Appendix-A). The total permeability K_d of the disc has to be found by a fitting procedure of the model against the experimental data of chapter 2-II. Integration of the simulated flow J yields the expelled volume V_e and the changing total disc volume V_d (Appendix-A).

As a consequence of compression the size of the pores in the nucleus decrease and hence permeability K_d of the tissue matrix decreases. Permeability K_d is assumed to decrease according to a relation between actual disc fluid volume and initial disc fluid volume as given by Broberg ^{Broberg '93} (Appendix-A).

In order to compare the simulated results of our model to the experimental data of chapter 2-II we have to add some corrections to our model.

We have concluded previously that due to the loss of glycosaminoglycans the potential of the disc to absorb fluid decreases during long lasting loading. Glycosaminoglycans may be lost by destruction of the molecules or by expulsion suspended in fluid. In our model we considered only the loss of glycosaminoglycans via the expulsion of fluid. The concentration of glycosaminoglycans in the fluid that is expelled is assumed to be a constant fraction S of the concentration of glycosaminoglycans C in the disc (Appendix-A), which has to be found by means of a fitting procedure of the model against the experimental data of chapter 2-II.

We simulate the response of the disc model to axial loading and unloading in terms of displaced volume, expelled volume, disc height h , bulging b and the hydrostatic intradiscal pressure P_h .

Fit of the model to in-vitro data:

Table 2-2. Parameter values of the model fitted to the experimental data of Chapter 2-II

Parameter	description	value	unit
Θ_0	= initial fiber angle	1.047 ⁽¹⁾	rad
τ	= relaxation time constant of fiber	900*	s
a	= relative visco-elasticity of fiber	0.75*	-
r	= radius of the endplate	0.022*	m
c_3	= correction for height data	1.075°	-
c_h	= correction for initial height (h_0)	0.922°	-
c_k	= correction for permeability (K_d) during cold storage	0.488°	-
c_s	= correction for initial swelling pressure	1.309°	-
d	= thickness of the fiber layer	$3.69 \cdot 10^{-3(2)}$	m
h_0	= initial height	$8.6 \cdot 10^{-3(2)}$	m
K_d	= total disc hydrodynamic permeability	$1.54 \cdot 10^{-16(2)}$	$m^3 \cdot N^{-1} \cdot s^{-1}$
P_0	= initial pressure	$.1 \cdot 10^{(2)}$	pascal
S	= sieving coefficient	0.206°	-

Note: Only initial values are listed here, all other values could be calculated from these.

(°) Obtained by a fitting procedure of the model to experimental data, (*) obtained from measurements (Chapter 2-II). (1) Klein 1983, (2) Nachemson 1975.

The parameters used in our model are defined in table 2-2.

If no value is given for a parameter in table 2-2, its value follows from calculations using other parameters. The values of the parameters r , h_0 , a and τ , indicated with an asterix, are taken from our own experimental results (Chapter 2-II). As described in chapter 2-II, the initial height h_0 was measured directly and r was calculated from the approximated cross-sectional area of an ellipse with lateral the long axis and anterior-posterior the short axis. The time constant of the visco-elastic relaxation τ is considered to be equal to the mean of the values found for T_1 fitted to the displaced volume curves as described in chapter 2-II in table 2-1. The magnitude of a is derived from the experimental results as follows:

The term $(1-a)/a$ represents the elasticity of the serial (relaxation) arranged element (s in Appendix-A, Figure A-4) relative to the parallel element (p in Appendix-A, Figure A-4), or s/p . The instantaneous decrease of height (c_3 in Table 2-1 of Chapter 2-II) of the disc after application of axial load is inversely related to the elasticity of both elements ($c_3 \approx 1/(p+s)$), while the loss of height after relaxation of the visco-elastic element is inversely related to the elasticity of

the parallel element ($c_3 + c_1 \approx 1/p$). Assuming a linear relation between elasticity and change of height, which is only a rough estimate, it is possible to calculate that a equals $c_3/(c_1 + c_3)$. Total water percentage (V_w / V_d), initial intradiscal pressure (P_0), the relation between concentration and swelling pressure and the relation between stress and strain were obtained from literature ^{Nachemson '75 Urban '79 Urban '81 Shirazi-Adl '86}. The values of the parameters K_{d0} , d and S could neither be obtained from our experiments nor from literature and were obtained by fitting the model to the experimental data of chapter 2-II, however with the following modifications.

Instead of the original data, the bi-exponential function given in chapter 2-II (function 3 and 4) and the parameters fitted with it to the experimental data, were used to describe the experimental results of chapter 2-II. We disregard however the fast exponential found in the expelled-volume curve as this concerns the expulsion of fluid from the outer layers of the annulus fibrosus which is not accounted for in the model. The stepwise change in expelled-volume, expressed by c_3 , is ascribed to the displacement of fluid already outside the disc, prior to the compression of the disc. We therefore subtracted this step c_3 from the displaced-volume function and omitted it from the expelled-volume function.

As explained in chapter 2-II, errors in the estimated cross-sectional area (A) of the disc cause errors in the estimated displaced-volume. The error in A is estimated to be less than ten percent so a correction factor c_5 for the displaced-volume curve is introduced with a value between .9 and 1.1, which has to be found by a fitting procedure of the model against the experimental data of chapter 2-II.

These considerations led us to the following expression for the displaced-volume ($d(t)$) (12) to be simulated by the model (Appendix-A).

$$d(t) = (c_1 \cdot (1 - e^{-t/\tau_1}) + c_2 \cdot (1 - e^{-t/\tau_2}) + c_3 - c_{c3}) \cdot c_5 \quad (12)$$

and for the expelled-volume ($e(t)$) (13).

$$e(t) = c_2 \cdot (1 - e^{-t/\tau_1}) \quad (13)$$

For the values of the parameters used in these expressions, see chapter 2-II, table 2-1.

The fitted model should simulate a response to loads that is equal to the response

measured in the *in-vitro* experiments. When comparing the simulated results with the experimental results we need to consider the following details.

The initial intradiscal pressure prior to loading is determined by the disc geometry (defined by the disc height h , and radius r), initial fiber strain ϵ_0 and the total thickness of the fiber layer d . Together with the visco-elasticity coefficient of the fiber a , these parameters determine the response to a stepwise applied axial load. According to Nachemson^{Nachemson '75} this initial pressure is approximately .1 Mpa in a healthy disc. By cutting the vertebra just above the endplates, the disc is relieved of the axial load exerted by the ligaments of approximately 100 N^{Markolf '74}. This causes an initial imbalance between intradiscal pressure and swelling pressure P_s . At the start of the experiments described in chapter 2-II this imbalance may still exist. Therefore the initial swelling pressure, determined by the glycosaminoglycan concentration C , is less than the pressure of 0.2 MPa found in intact FSU's^{Nachemson '64}, but at least equal to and perhaps larger than the initial intradiscal pressure of 0.1 MPa. Therefore a correction factor c_s for the initial swelling pressure is introduced with a value between 1 and 2, which has to be found by a fitting procedure of the model against the experimental data of chapter 2-II.

During the recuperation periods the specimen was stored at 4 ° Celsius. Because Koeller^{Koeller '86} reports about the influence of temperature on tissue properties we suspect that cold storage may have caused a decrease of the permeability in our specimen (Chapter 2-II). We accounted for that by using a correction percentage c_k for the permeability K_d during recuperation, which has to be found in a fitting procedure of the model against the experimental data of chapter 2-II.

To store the specimen at 4° C it had to be removed from the loading apparatus and was disconnected from the height and weight transducers. When reinstalling the specimen the disc height was measured (see chapter 2-II) as a reference for the change of height to be recorded. The initial disc height h_0 was measured likewise. Measurement of disc height (h) is always an estimate as the endplates are not parallel and have no flat surface. We assume that our measurement of h_0 deviates less than 10 % from the actual height. To compensate for such an error in the estimation of h_0 we introduce a correction factor c_h for h_0 , with a value between .9 and 1.1, which has to be found by a fitting procedure of the model against the experimental data of chapter 2-II. Also the relatively big inaccuracy of approximately 0.1 mm of these measurements may cause errors in the measurement of the unrecorded recuperation of height. Furthermore no reference is available at all for the expelled fluid volume. Therefore we correct the

experimental data of chapter 2-II for the displaced volume and expelled volume simulated by the model at the time just before the loads of 1000 and 1700 N are applied.

In the experiment with 1700 newton axial load (Chapter 2-II Figure 2-8) an intradiscal pressure of 1.17 MPa \pm 3% was recorded. The simulated intradiscal pressure under a load of 1700 N, should therefore be between 1.14 and 1.21 MPa.

Results

Figure 2-15 presents the simulated response, together with the experimental response of the intervertebral disc to an axial load of successively 500 N, 1000 N and 1700 N and during recuperation, corresponding to figures 2-5, 2-6, 2-8 and 2-7 in Chapter 2-II.

A fit of the model to the data of only a single experimental response of the intervertebral disc to an axial load would give a much better result. In that case the simulated response can hardly be distinguished from the observed experimental response if plotted on the same scale as used in figure 2-15. The response to repetitive loads however yields important information concerning the recuperation of the disc. We prefer a rather sloppy fit of a model that simulates repetitive loadings of the same specimen instead of a perfect fit to a single load while ignoring the fact that for a different load different parameters will be found. Our approach provides us with information about the recuperation of a specimen subjected to long lasting and repetitive loading conditions. The courses of the variables h , b , P_s , P_h , ϵ , and G in the same simulation as figure 2-15 are shown in figure 2-16. The last part of the predicted intradiscal pressure (Figure 2-16) is comparable to the *in-vitro* measurement shown in figure 2-8. The expressions used to describe the changes in K_d and G may be disputable. At first we attempted to fit the model with constant values of K_d and G (Appendix-A). It turned out, however, that no reasonable fit could be obtained in this way.

Note: All graphs in chapter 2-II were generated by PSI-e, in an unusual format. The values of up to six parameters may be plotted in a single graph, each using a different vertical scale. The names of the parameters plotted are listed above each graph after "NAME:", together with the symbol used to discriminate them from the other parameters. The maximum and minimum value of the scale in which each parameter is plotted, is given after "MAX.:" and "MIN.:". The horizontal axis represents "TIME".

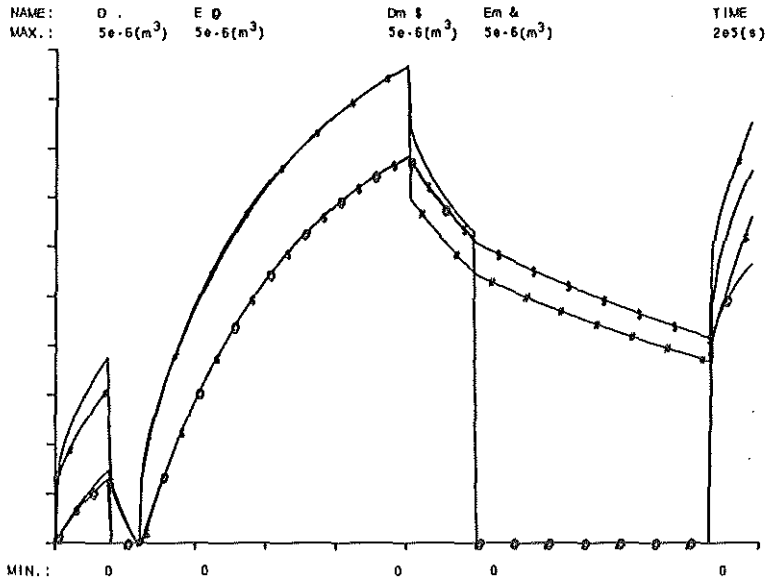


Figure 2-15. Adapted model, with changing K_d and G and permeability reduced to 48 % during cold storage. Experimentally obtained displaced- and expelled-volume (D and E) compared to simulated data (Dm and Em) at 500, 1000 and 1700 N.

Note: To reduce the size of the graphs in figures 2-15 and 2-16, we increased permeability and visco-elastic relaxation in the recuperation interval between the 500 N and 1000 N axial load with a factor 10. The recuperation interval between the 500 N and 1000 N axial load could thus be decreased with a factor 10. The time-scale in figures 2-15 and 2-16 should therefore be increased with a factor 10 for the recuperation interval between the 500 N and 1000 N axial loads.

Allowing either K_d or G to change (Appendix-A) gave rise to minor improvement only. A better fit was achieved when both K_d and G were allowed to change according to the expressions given in Appendix-A. Furthermore we used a lower permeability ($c_k \cdot K_d$) to simulate the response during the recuperation in cold storage.

The lumbar intervertebral disc is assumed to be responsible for 1/15 of the total change of body length ^{Broberg '93} under different loading conditions. So by multiplication of the simulated change in height of a disc we get the simulated change of body length. Some simulated effects which are met with *in-vitro* are not

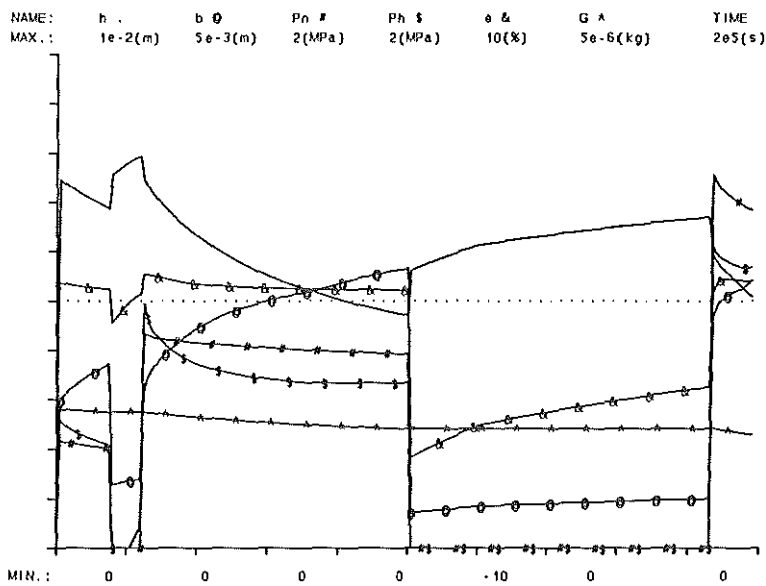


Figure 2-16. Model predictions; hydrostatic pressure P_h , height h , bulging b , fiberstrain ϵ (e in the figure), glycosaminoglycans G and calculated pressure P_a .

expected to occur in a healthy disc *in-vivo* because, *in-vivo* the loss of glycosaminoglycans is compensated by synthesis in the nucleus ^{Bayliss '86 Keller '90 Schneiderman '86}. We used our model to simulate the change in height of the disc under unknown axial load, however without the loss of glycosaminoglycans and taking the same permeability value during loading and unloading (Figure 2-17).

The model was used to determine the axial load from *in-vivo* measurements ^{Tyrrrell '85} of change of length, as shown in figure 2-17. For an optimal simulation of the body length data given by Tyrrell, our model needed a simulated axial load of 301 N during sleep and an extra 528 N (i.e. 829 N total axial load) during light activity. Permeability was simulated to be 4.8 times higher than the permeability derived from the fit to the experimental data from chapter 2-II as described above.

Discussion

With the simple model we used, we could simulate the experimental results

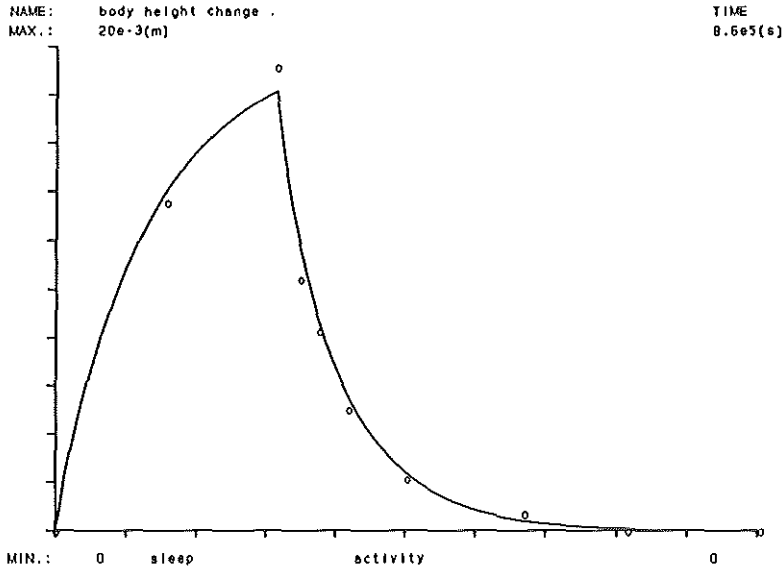


Figure 2-17. Simulation of the body length data given by Tyrrell (1985) (o), with an axial load of 301 N during sleep and 829 N during activity, K_d had to be increased with a factor 4.8

discussed in chapter 2-II, concerning displaced- expelled- and bulging- volume as well as intradiscal pressure (Figure 2-15 and 2-16). Sonnerup ^{Sonnerup '82} ascribed the pressure excess of 50% in the nucleus with respect to the externally applied axial load per cross-sectional area ^{Nachemson '60}, to the fact that only 70-80 % of the cross-sectional area of the disc is subjected to fluid pressure, while only a small part of the pressure excess is considered to be due to axial tensile stress in the fibrous structures of the annular wall.

We simulated intradiscal pressure (P_h) and calculated it according to Nachemson ^{Nachemson '60} (P_n) taking into account the change of maximum disc cross-sectional area due to the increase of bulging (Figure 2-16) (Appendix-A).

The geometry of the unloaded disc is related to it's volume (Appendix-A). The higher the swelling capacity of a disc is, the higher is the initial (unloaded) volume and the higher are the initial and loaded pressures. Initially the simulated (and *in-vitro*) hydrostatic pressure and swelling pressure are taken equivalent to the pressures found *in-vivo*. Therefore the simulated intradiscal pressure P_h immediately after the simulated application of a load of 500 N is equal to what is

predicted by Nachemson (P_n) and to what has been found both in *in-vivo* and *in-vitro* experiments ^{Nachemson '60}. We conclude from the biomechanical calculations which led to such a simulated pressure, that most, if not all, of the excess in intradiscal pressure can be ascribed to the extra force component related to annular wall stress.

The intradiscal pressure of 1.17 MPa, measured *in-vitro* under an axial load of 1700 N (Figure 2-8), can only be obtained through simulation if the angle β is about 90° during the entire loading interval. Then the bulging curvature is half a circle. Under that condition the axial component of F_w is zero and its contribution to the axial load on the endplate is negligible. In that case the intradiscal pressure is equal to the externally applied load (F_e) divided by the cross-sectional area (A) of the endplate (Appendix-A). This also explains the stability of the recorded intradiscal pressure in Chapter 2-II; with an angle β of 90° the axial component of F_w no longer decreases despite the increasing bulging and continuing loss of fluid. Even in normal discs the intradiscal pressure appears to be constant if the observation time is rather short. In the 500 N load simulation for example the pressure drops only approximately 8 percent in the first 30 minutes. In the *in-vitro* experiments described in Chapter 1 such a pressure drop could easily be masked by the fact that when a complete FSU is loaded, the actual load on the disc and consequently the intradiscal pressure, will increase a little due to visco-elastic relaxation of other load carrying structures such as the facet joints.

Only if recuperation after a load of 500 and 1000 N was severely impaired, an angle β of 90° was found with the model immediately after a stepwise load of 1700 N. This impaired recuperation was simulated by loss of glycosaminoglycans during loading and a reduced permeability during unloading of 48 % of the permeability during loading. The reduced permeability may be due to the fact that the specimen described in chapter 2-II was stored at 4° Celsius inbetween the loading intervals, while the loading tests were performed at a room temperature of 20° Celsius ^{Koeller '86}.

The pressure predicted by this artificially degenerated model is equivalent to the pressures measured in degenerated discs ^{Panjabi '88} *in-vivo* and *in-vitro*. This warrants the conclusion that the effect of decreased swelling capacity ^{Pearce '87 Bayliss '88 Urban '88} on intradiscal pressure ^{Panjabi '88} is simulated correctly by our model.

In the degenerated disc under axial load, the strain in the fibers is lower than normal, because the axial component of the fiber stress is smaller due to increased bulging and because the radial component, which causes the intradiscal pressure,

is bigger. From these mechanical considerations we conclude that a considerable (local) decrease of bulging curvature, which may be caused by rotations (flexion-extension or lateroflexion) of the disc or the FSU, combined with a significant axial load may be harmful to the annular wall. Furthermore, in case of axial rotation of the disc (torsion), two other factors endanger the fibers in the annular wall which are orientated in the same direction as the axial rotation:

1 Axial rotation increases the angle (Θ) of attachment of those fibers to the endplates. Consequently the radial component of the fiber stress that contributes to the intradiscal pressure is reduced.

2 The fibers running in the opposite direction become relaxed and contribute less to the intradiscal pressure. A bigger contribution and hence increased fiberstrain is then demanded of the fibers that are oriented in the same direction as the applied axial rotation.

With regard to strain, the optimal shape of bulging is half a circle, because any (local) flattening of the curvature that results in an angle of attachment of the fibers to the endplate of less than 90° , requires more strain in the annular wall fibers in order to cause the same intradiscal pressure. Furthermore the same intradiscal pressure then carries a lower external load because the axial component of the stress in the annular wall is larger. From this we conclude once more that there is no direct relation between intradiscal pressure and strain of fibers in the annular wall.

Furthermore we conclude that when the disc is deformed the largest strains will arise in those areas of the annulus where the bulging curvature is flattened most. This, not only for the reason previously discussed, but also because flattening of the bulging curvature due to rotation(s) also implies a (local) increase in height of the annular wall. A larger height implies an increased pressure load on that part of the annular wall, which has to be balanced by an increased stress in the annular wall (11) (Appendix-A).

This also explains the cross-sectional asymmetry of the annular wall, which is thick and strong anterior and lateral, where the bulging curvature can become flattened by extension, latero-flexion and to a lesser extent by torsion. The posterior wall may be thin, firstly, because it is closest to the instantaneous center of rotation so that the bulging curvature and disc height are less influenced by such rotations or by flexion and secondly, because the disc height is generally lower here. This explains the danger of degeneration of either the disc or the facet joints

and their capsules. Degeneration causes the flexibility of the FSU to increase. The instantaneous center of rotation is then allowed to move forward so that the bulging curvature of the postero-lateral and posterior wall will decrease more and the local disc height will increase more due to rotation(s). These changes all increase the (local) strain in the fibers.

Recently Broberg^{Broberg '93} published a model that simulates the change of body height based on the deformation of the intervertebral disc under an axial load. Broberg^{Broberg '93} concludes that running (the Stockholm marathon) increases the axial load on the spine with 75% when compared to standing and with 15% when compared to walking. This increase is explained by increased muscular action on the spine during running. In occupational epidemiology measurements of lumbar spine rotations^{Snijders '87} or observational techniques^{Burdorf '92} are used for the assessment of postural load on the back^{Eklund '84 Burdorf '92}. These methods are however unable to actually measure or even estimate the muscular action on the spine. The registration of the changes in height of the body, the lumbar spine or the lumbar intervertebral disc during rest and activity, combined with a reliable model of the intervertebral disc, enables us to calculate the actual axial load on the spine.

Broberg found a good agreement between his predictions based on his model and the intradiscal pressure measurements performed *in-vivo* by Nachemson^{Nachemson '70}. In our opinion this means that measurements of bodyheight could replace the more traumatic intradiscal pressure measurements *in-vivo*. With a reliable compression model the registration of the change of the height of the body or the lumbar spine could become an important tool in occupational epidemiology for the assessment of postural load on the back^{Eklund '84 Burdorf '92}.

Broberg's model lacks some important biomechanical mechanisms as well as experimental verification and therefore seems unsuitable for this purpose. Though quite elaborate in its description of the disc's geometric features it has some important shortcomings. An important difference with our model is that Broberg simply uses the empirically derived transformation from load to intradiscal pressure ($P = 1.5 \cdot F_e / A$) as given by Nachemson^{Nachemson '60}, while we use a biomechanical relation. Another simplification in Broberg's model is that it merely describes visco-elastic behavior (generally attributed to the annular wall fibers^{Galante '67}) in terms of the change of total disc height as a mono-exponential function of the change in axial load ($\Delta H = h \cdot \Delta F_e \cdot (1 - e^{-\Delta F_e / F_e})$). A drawback of his model is that it has been validated with data from total body length measurements taken

from Tyrrell et al. ^{Tyrrell '85} and estimated axial loads according to Nachemson ^{Nachemson '70 Nachemson '76}. These experimental results are so far removed from what may actually happen to the isolated intervertebral disc that they cannot give a solid base for experimental verification of Broberg's model. Broberg's suggestion that his model can be satisfactorily fitted to the experimental data, by using only one measured data point for the determination of his parameter k_0 , equivalent to our K_{d0} , is illusory in our opinion. In fact, the (estimated) load during daily activity in proportion to the (estimated) load during a night's rest together with the determined magnitude of k_0 and the "improved" ^{Broberg '93} proportion of visco-elasticity (h) determine the fit on the experimental data.

We simulated the experiment performed by ^{Tyrrell '85} that was used by Broberg ^{Broberg '93} to validate his model. Unlike Broberg ^{Broberg '93} who used the estimated ^{Nachemson '70 Nachemson '76} load of 440 N during the night, we calculated the axial load by using our model parameters. In this simulation the amount of glycosaminoglycans is kept constant and the permeability is put to depend solely on the hydration of the model. We found a slightly higher extra axial load during the day (528 N instead of 410 N) (Figure 2-17) than was estimated by Nachemson ^{Nachemson '70 Nachemson '76} and used by Broberg ^{Broberg '93}. Maybe this greater difference between day and night load is due to the fact that our model parameters concern the disc L4-L5 of a small, 51 year old man of 60 kg and a length of 178 cm (chapter 2-II) instead of a L3-L4 disc (11% larger in cross-section) of a well developed male aged 20-40. But because of this difference in disc size we also expected to find 11 % lower values for the loads both during night and day. The fact that we did not find any such lower values is attributed to the fact that our modeled disc height was lower than the disc height Broberg used since our man was shorter than the men from whom Tyrrell obtained his length data. To obtain the same height reduction with our model a higher load difference between night and day and/or a higher permeability is required. To obtain a reasonable fit to the registered body height we increased the permeability calculated from the experiments described in chapter 2-II with a factor 4.8. Keller ^{Keller '90} reported that after death there is a significant decrease in the speed of disc deformation as a response to axial load. We conclude from this that the difference in permeability can mainly be attributed to three factors: First, we calculated permeability from data obtained from autopsy material. Second, the experiments described in chapter 2-II were performed at 20° Celsius, instead of the 37° Celsius body-temperature in the experiment of Tyrrell ^{Tyrrell '85}. And third, we compared our model, based on a relatively small individual, to a model and to experimental data from well developed men.

Although in a simplified manner, our model incorporates all the essential biomechanical mechanisms involved in the compression of the disc and it has been validated by experimental data concerning the response of the disc under an axial load. Therefore our model seems better equipped to calculate axial load from changes of height *in-vivo* than Broberg's model. Further experimental verification of our model requires the measurement of initial swelling pressure, hydrostatical pressure and the changes in annular wall bulging. With a thoroughly validated model of the intervertebral disc the assessment of axial load under working conditions using height measurements *in-vivo* appears to be a distinct possibility in the near future. The combination of height measurements with continuous *in-vivo* measurements of lumbar spine rotations, as performed by Snijders et al. ^{Snijders '87}, and the calculation of fiber strain from those data, using the geometrically very accurate FEM model of Shirazi ^{Shirazi '89(2)}, would enable us to identify hazardous working conditions of laborers at risk.

Conclusions

A simple mechanical model of the intervertebral disc has been developed, which relates fiber visco-elasticity, fluid-flow, annular wall bulging and intradiscal pressure. The model explains the excess in intradiscal pressure compared to applied force divided by cross-sectional area. The model also gives an explanation for the lower initial and loaded intradiscal pressures in degenerated discs. The correction factor introduced by Nachemson ^{Nachemson '60} to calculate the expected intradiscal pressure in normal discs from axial load, concerns the contribution of annular wall stress and depends on the bulging of the annular wall. The intradiscal pressure appears to be constant if the observation time is short. In the first 30 minutes of our 500 N load simulation the pressure drops only 8 percent approximately. When a complete FSU is loaded such a decrease will be even less, because the actual load on the disc and consequently the intradiscal pressure will increase a little, due to visco-elastic relaxation of other load carrying structures, such as the facet joints.

The cross-sectional shape of the annular wall is explained by the model from its exposure to deformations and pressure load. In cases of low axial loads the annular wall may be damaged by combined rotations.

The model predicts a significant loss of swelling potential of the disc *in-vitro*.

Complete recuperation of the specimen is not guaranteed under *in-vitro* conditions. However, in *in-vivo* situations, loss of swelling potential is compensated by the synthesis of glycosaminoglycans ^{Schneiderman '86 Bayliss '86 Bayliss '88}. This implies that long lasting or repetitive loading experiments *in-vitro* may not reflect real life behavior of the intervertebral disc.

The model can be used to calculate axial load from changes in body length *in-vivo* and can be an essential tool in replacing registration of the intradiscal pressure to assess the axial load on the lower back.

CHAPTER 3

3-D Video registration of the strain in the annular wall

Preliminary results

3-D Video registration of the strain in the annular wall

Preliminary results

Introduction

Stress and strain in the annular wall of the intervertebral disc are generally seen as the factors causing annular wall failure ^{Galante '67}. Analytical studies ^{Shirazi '89(2)} predict that combined rotations of the spine cause extreme values of the strain on specific locations in the annular wall. These predicted locations correspond with the locations of failure seen in epidemiological studies. However these theoretical predictions have not been verified in experimental studies of the response of the annular wall to specific load conditions. Intradiscal pressure has been related to stress and strain in the annular wall and can be measured both *in-vitro* as well as *in-vivo*. In studies concerning the risk of damage of the annular wall the intradiscal pressure has been used as a measure of the load ^{Nachemson '60 '64 '70 '75 '79 '81}. As discussed before (Chapters 1 and 2), the nucleus pulposus, *in-situ* confined by the annular wall and the endplates, behaves as a hydrostatic medium. Therefore intradiscal pressure reflects the (axial) load on the intervertebral disc but does not reveal heterogeneity in the distribution of strain in the annular wall (Chapters 1 and 2).

To investigate the distribution of strain in the annular wall a more direct method of measurement is needed. Measuring the displacement of markers on the annular wall fibers is a technique that virtually achieves this goal. Stokes and Greenapple ^{Stokes '85} reported on such a method, using stereophotogrammetry to measure the surface deformation of the annular wall. They found that under physiological loads and with rotation of the FSU the strain of the annular fibers is 6% or even smaller. However they did not apply the combined rotations, which according to the theory of Shirazi ^{Shirazi '89(2)} cause extreme local values of the strain.

We developed a similar technique to record the displacement of markers on the surface of the annular wall when a FSU is loaded. The measured displacements have been interpolated along the (assumed) course of the annular wall fibers. We calculated the changes in strain of the fibers as related to the initial situation.

Basic system

The equipment for a two dimensional video registration system, based on a CCD camera (Sony AVC-D5CE) has been developed at our department ^{Kecemink '91}. The analysis of the video signals is performed by means of a VME computer system based on a 68020 data-processor. The video signals are digitized by a Datacube Digimax-7 digitizer and display module. A triple frame storage module board (Datacube Framestore-7) stores two video frames in two separate memories (512 lines 384 pixels per line). By using a FIR (fast image recognition) algorithm, this system can achieve a sampling rate of 50 frames per second, tracking six markers that may move over the whole picture.

However, the displacements of the markers on the surface of the annular wall need to be registered in three dimensions. Therefore a second camera is placed at an angle of 90° with the first camera. Both cameras operate synchronized. The frames are analyzed on-line because synchronization of frames is lost when they are stored on a videotape. Eight markers are used to map a part (20%) of the circumference of the annular wall, which appears to be the maximum area that can be covered without markers passing out of view of the two cameras. More markers in the same area could enhance resolution, however we have difficulties in the identification of the markers by the video system when the markers are placed too close to each other. The necessity to analyze on line two frames with eight markers and to calculate the three-dimensional coordinates of the markers limits the number of frames per second that can be analyzed to 2. This means that the displacements of the markers are digitized at a sampling rate of 2 per second also.

A Direct Linear Transfer (D.L.T.) analysis, described by Abdel-Aziz and Karara ^{Abdel-Aziz '71}, is used to calculate the position of the markers with respect to the cameras. DLT is based on the optical ideal camera (Camera obscura or pinhole camera). In such a camera the image of a point-object is projected on the screen in the pinhole camera lying on the line running through the hole and the point-object. Using two of such cameras gives two lines with corresponding equations. The object is situated at the point where these two lines cross each other. Errors in the calculated position of the point-object from the images in the cameras are caused by the inaccuracy in the coordinates of the camera positions.

In order to determine the inaccuracy in camera position a calibration cube is used. The calibration cube consists of a matrix of 32 infra-red LED's. The LED's are

activated one by one. Using the linear equations concerning images in each camera a matrix is constructed out of the positions of the LED's. This matrix is compared to the known positions of the LED's in the calibration cube. Thus using a least square approximation, a calibrating matrix is created, which compensates for errors in the positioning of the cameras with regard to each other.

By simple measurement of the distances with micrometer, the coordinates of each LED in the calibration cube are known with an uncertainty of 0.1 mm. For our application this uncertainty is too high. In order to reduce this uncertainty we measured the positions of the LED's in the calibration cube with the video system using two pinhole cameras. To this end the opening of each camera was equipped with a P.V.C. tube covered with a thin sheet of aluminum instead of the normal lens. In the middle of the aluminum sheet a tiny hole was stabbed. Thus two pinhole cameras were obtained. In this arrangement the positions of the LED's in the cube can be calculated with high accuracy, limited only by the errors in the reconstruction of the 3-D image of the cube, caused in turn by inaccuracies in the known positions of the cameras. By reconstructing the cube observed by the cameras from different angles, we could minimized the errors, due to the inaccuracy in the camera positions, by a least squares procedure. Following this procedure the relative positions of the LED's in the calibration cube could be measured with an accuracy of 0.01 mm.

The pinhole camera has a very poor light intensity and it cannot zoom-in or focus on an object. Hence the use of the cameras with lenses for our experiments. These lenses introduce distortions of the image, but we can now use a reference matrix with known positions of the LED's with the uncertainty of only 0.01 mm to calculate the calibrating matrix. To finally evaluate our system we used a rigid metal plate with three markers placed in a triangle at distances of roughly 20 mm. The distance between the markers was then calculated from the 3-D image. Observing the markers from different view angles yielded calculated differences in distance between the markers, which differed less than 0.02 mm (0.1 %).

The center of the images of the markers in the two cameras is used to calculate the position of the center of each marker. To this end spherical markers are used sothat the center of the marker coincides with the center of its image in each camera and remains visible at different view angles.

The image of the marker has irregularities on the perimeter, because it is composed of pixels. These irregularities affect the accuracy of the calculated center of the marker. To reduce this effect a large diameter of the marker was chosen. Simplest would be the use of light reflecting markers. However, since the

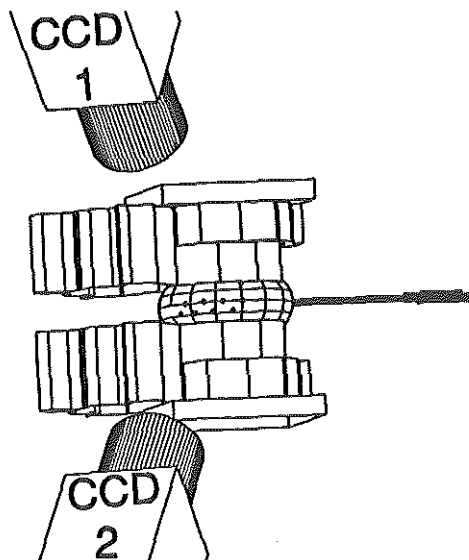


Figure 3-1. Schematic representation of an FSU mounted in fixation blocks and equipped with intradiscal pressure sensing needles and infrared LED markers.

FSU is moistened, it produces unwanted reflexions. As markers we used LED's with a diameter of 2.5 mm which emit infra-red light (850 nm). A spherically shaped marker with a diameter of 5 mm, which emits homogeneously, is obtained by embedding the LED in a mixture of epoxy resin and infra-red diffusing glass pearls. The intensity of the LED's is sufficient to penetrate the epoxy resin and the water covering the marker. The LED's are connected in series so that the current and therefore the intensity of the light emitted by all markers is equal. The markers are fixed to the annular wall with thin stainless-steel needles (ϕ 0.5 mm, length 10 mm), glued perpendicularly to the back of the LED.

Stokes and Greenapple ^{Stokes '85 Stokes '87} placed their cameras in the same (horizontal) plane as the intervertebral disc. They removed the posterior elements of the FSU's to have a better view on the posterolateral part of the annulus fibrosus. The posterior elements however significantly affect the instantaneous center of rotation of the FSU ^{Gertzbein '84 Shirazi '86 Shirazi '86(2)}. As we discussed in chapter 2-III, this may seriously affect the deformation of the annular wall. We placed the cameras at an angle of 45° to the plane of the disc (Figure 3-1). Furthermore we measured on an intact human lumbar FSU (Specimen ID No. S-90-249 level L2-L3). In future experiments can be done to determine the influence of the posterior elements on deformations of the annular wall.

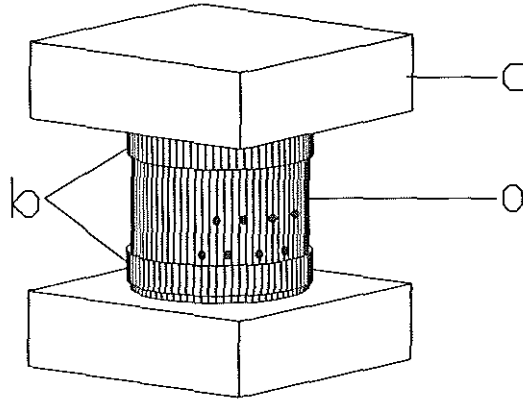


Figure 3-2. Schematic representation of the physical model equipped with infra-red LED markers.

Physical model

In analogy to Stokes ^{Stokes '87} we tested our technique by using a physical dummy model of the intervertebral disc (Figure 3-2). We developed this physical model for three reasons;

1. To test the system without using valuable human autopsy material.
2. The data obtained from measurements on the well defined model can be used for the interpretation of measurements on human FSU's, which are not symmetrical and not composed of homogeneous material.
3. On the dry surface of the model, both the light emitting LED markers and disc shaped infrared light reflecting stickers can be used as markers and compared to each other to determine the influence of the fixation of the LED markers by means of the needles.

The model, depicted in figure 3-2, consists of a rubber cylinder (a in Figure 3-2) (outer diameter 45 mm inner diameter approximately 20 mm) fixed with hose clamps (b in Figure 3-2) to two PVC dowels (c in Figure 3-2) (distance between the clamps 20 mm). Small canals in the dowels enable us to fill the model with water, to evacuate air, to measure the pressure in the model and to allow for fluid loss. The model was filled with water until a pressure of between 0.05 and 0.15 MPa was reached. The wall size was adjusted until the bulging (b in Figure 2-10 of Chapter 2-III) amounted 1.5 to 2.5 millimeters.

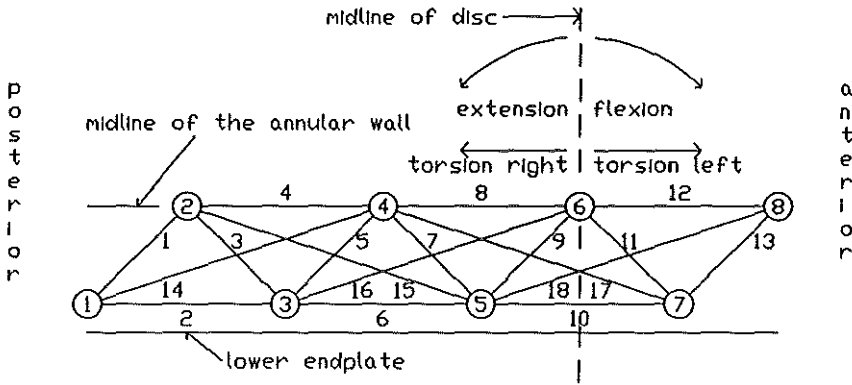


Figure 3-3. Diagram showing the numbers assigned to the markers and to the distances between them.

An axial load of 500 newton was applied. Then the pressure was between 0.4 and 0.6 MPa and the bulging was between 5 and 7 mm, which is comparable to what is found in human intervertebral discs (see Chapter 1). The same movements were then applied as we did with the human FSU specimen (see Chapter 1). Differences in deformation patterns between the model and the human FSU, observed on the surface by means of the markers, are ascribed to non-homogeneous properties of the disc and to the influence of the posterior elements of the FSU.

Calculations of the strain in the annular wall.

We arranged eight markers in a matrix of two rows of four markers (Figure 3-3). One row of markers is placed just above the lower endplate of the specimen, distributed from posterolateral to lateral. The second row is placed on the midline between the two endplates and shifted a little to anterior with respect to the first row. Thus the markers are arranged in triangles (Figure 3-3).

To calculate the strain in the wall accurately, the curvature of the wall between two markers needs to be known. The largest curvature is the annular bulging. The calculated strain will be underestimated if we ignore the bulging curvature. If for example the wall curvature between two markers describes a quarter of a circle, the distance between the markers is $\sqrt{2}$ times the radius of the circle and the length of the curvature is $\frac{1}{2} \pi$ times the radius of the circle. The distance between

the markers is then a factor $1.412 / 1.570$ or 90 percent of the actual length following the surface of the wall. Because a bulging curvature of half a circle rarely occurs, this underestimation will be smaller in practice. We also calculate the length of lines running at an angle of about 45 and 67° with the axis of the specimen instead of parallel to it, which decreases the underestimation of length by about a half. (Ignorance of the circumference of the annular wall causes even less error). When we completely ignore the curvature of the annular wall, the largest error in the calculated distance between two fibers is estimated to be less than 5 %. However, we are not interested in the exact distances between the markers but in the relative changes in distance, or, simply called, strain. The change in distance between the markers as compared to their distance prior to the application of an axial load, (i.e. the strain), is quite inaccurate. We are however particularly interested in the distribution of strain during different rotations of the FSU under a constant physiological axial load. Therefore we use the distances between the markers when the FSU is axially loaded, as a reference for the distances between the markers when single or combined rotations are applied under constant axial load. We ignore the change in annular wall curvature during such rotations of the FSU.

We expect that combined rotations of the FSU as discussed in chapter 1, cause a deformation that is different to the sum of deformations caused by the same rotations applied separately.

In order to verify this hypothesis we add the displacement vector of each marker, due to axial rotation, to the relative position of each marker during flexion-extension. In order to calculate this displacement vector, we subtract the position of the marker during axial loading from its position during axial loading combined with axial rotation. Because of small movements of the specimen, for example caused by vibrations of the testing apparatus, the measured data are very noisy. In order to reduce the effect of noise we translate and rotate the matrix of marker positions to a standard situation. The matrix is translated so that marker nr. 3 (Figure 3-3) is situated in the origin of the x-y-z coordinates. The matrix is then rotated around the origin so that marker nr. 5 is on the positive x-axis and marker nr. 4 is in the plane defined by the x- and y-axis. Displacement vectors due to axial rotation are calculated to this position and added to the position of the markers measured during flexion- or extension-rotation. These cumulative marker positions are used to calculate the distance between the markers.

Deformation of the annular wall is expressed in percents of increase or decrease

of the distance between the markers. The initial distances in the unloaded situation are set to equal 100 %, which means that we ignore the strain in the annular wall caused by the initial intradiscal pressure. As we concluded previously the accuracy of the calculated strain caused by axial loading is low. Hence all strains are considered with respect to the strain, due to an axial load, by subtracting the strain due to axial loading from the strain due to rotations. We focus our attention on the effects of single and combined rotations only. Figure 3-4 shows an example of the relative deformation of the model, derived from the positions of light-reflecting markers and according to our definitions (Figure 3-3). The strain due to the application of an axial load of 500 N is given in the first row. Vertically the percentage of strain (1 division = 10 % strain) is given as related to the initial unloaded situation, with the strain due to axial loading (first row, indicated with the amount of applied axial load) subtracted (to get the total strain add the first row to the other rows). Each horizontal division refers to sixty consecutive recordings (which equals approximately 30 seconds recording time) of the strain between two markers, starting immediately after a change in loading conditions. The strains can be inferred from the distances between the markers as they are numbered in Figure 3-3. They are grouped for easier interpretation.

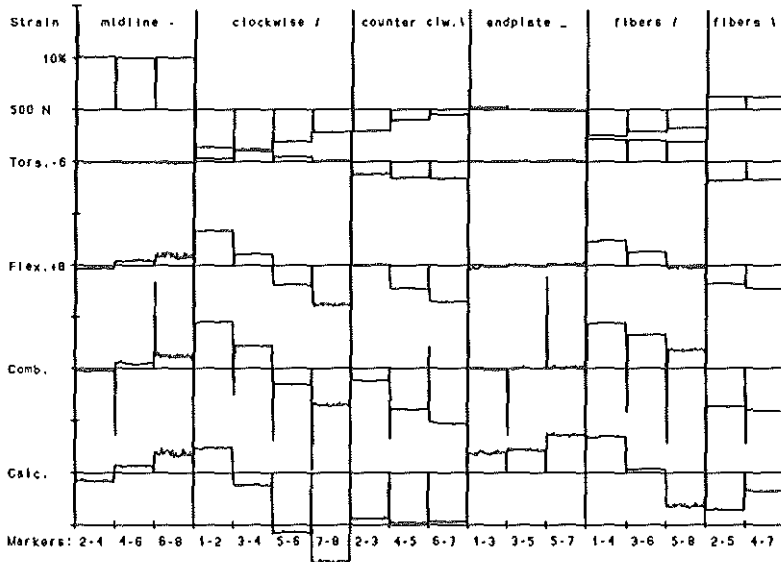


Figure 3-4. Changes in relative distance between the light-reflecting sticker markers on the physical model, due to compression and the changes due to rotations (Tors., Flex., Comb., Calc.) compared to compression alone.

Results

At the moment we can report only about results obtained in a pilot experiment with one FSU.

The figures 3-5, 3-6, and 3-8 show the relative changes in distance between the LED markers due to axial loading and the changes with respect to axial loading due to rotations of the physical model. In figure 3-4 the model is subjected to the same axial load and rotations as in figure 3-5 but the relative deformations are now derived from the positions of light reflecting markers. This enables us to study the influence of the needle fixation of the LED markers compared to light reflecting sticker markers. In figure 3-7 and 3-9 a human lumbar FSU is subjected to the same axial load and rotations as the model in figure 3-6 and 3-8 respectively, in order to compare the response to rotations and axial loading of the homogenous model with that of the heterogenous FSU.

It turned out that the markers need to be a little smaller because, depending on the point of view of the cameras, the images of separate markers sometimes fused.

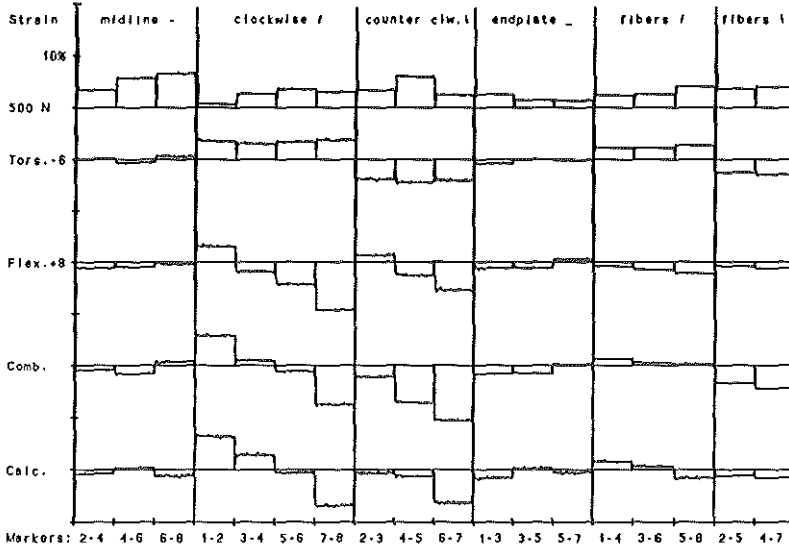


Figure 3-5. Changes in relative distance between the LED markers on the physical model, due to compression and the changes due to rotations (Tors., Flex., Comb., Calc.) compared to compression alone.

Therefore we tried to use glass fiber tips with a diameter of one millimeter as markers. Glass fiber markers can be stuck through the annular wall with their tip placed just above the surface. They are also less rigid than the needles used for the fixation of the LED markers. The light output appeared to be sufficient.

Discussion

We expect that the strain in the surface of the rubber model under axial load is distributed homogeneously in each group of distances between the markers. Our results however show that this is not the case (Figures 3-4, 3-5, 3-6 and 3-8). Our explanation for this discrepancy is as follows.

Detailed measurement of the model revealed slight asymmetries. The upper "endplate" is rotated 3 ° around the longitudinal axis toward the left ("torsion" to the left), tilted 2 ° around the sagittal axis toward the left ("latero-flexion") and 4 ° around the transversal axis toward the back ("extension"). When the model was fixed in the loading apparatus we assumed perfect symmetry, however the

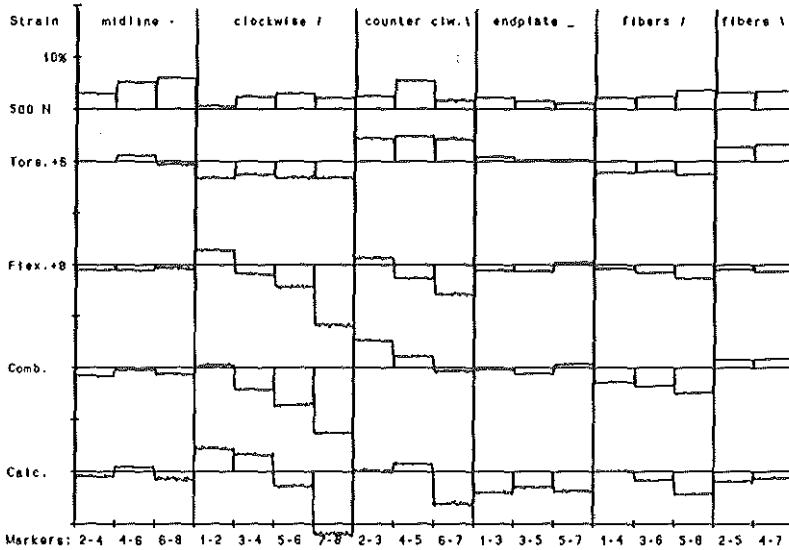


Figure 3-6. Changes in relative distance between the LED markers on the physical model, due to compression and the changes due to rotations (Tors., Flex., Comb., Calc.) compared to compression alone.

geometrical irregularities cause an asymmetrically strained state of the model previous to the application of the axial load. Once axially loaded, the pre-strain contributes to a non-homogeneous distribution of the increase of strain. Measurements, using infrared reflecting stickers as markers on the surface of the model, did indeed show a decrease of strain caused by the axial load going from the least pre-strained part to the most pre-strained part of the surface of the model (Figure 3-4). Attempts to fix the model without straining it anywhere failed. This is a serious drawback of the model. On the other hand the results with it show how sensitive our method is to measure deformations.

These effects of the heterogeneously distributed pre-strained state are less visible when LED-markers on needles are used in stead of stickers under the same load and rotations, as appears in figure 3-5 (compared with figure 3-4). Because the center of a marker is situated some millimeters above the surface, it can be tilted by the needle and may not follow exactly the displacement of the material on the surface.

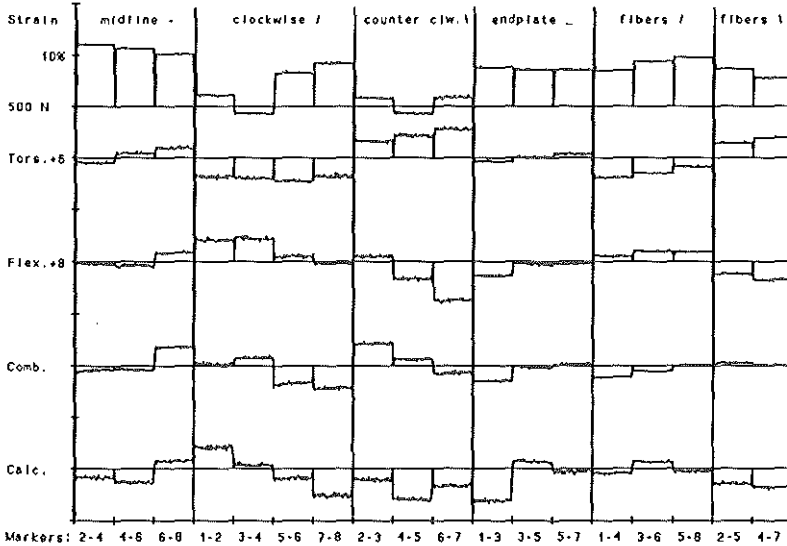


Figure 3-7. Changes in relative distance between the LED markers on the FSU, due to compression and the changes due to rotations (Tors., Flex., Comb., Calc.) compared to compression alone.

In the experiment with the light-reflecting stickers on the rubber model (Figure 3-4), the calculated strain under axial load alone decreased in all tilted directions except in the direction determined by the angle of 67 ° with the axis of the model (counterclockwise). Probably, this can be ascribed to the error in the calculation introduced by not taking the bulging curvature into account, as discussed before, maybe combined with the fact that the stickers on the "endplate" were attached to the hoseclamp, i.e. in a more outward position. Due to the outward bulging of the "annular" wall the distance between these markers and the markers on the midline then decreases so much that negative strains (shortenings) are recorded, although the strain of 10 % around the midline of the model is evident. The positioning of the markers on the hoseclamp also explains why the strain around the "endplate" is zero (Figure 3-4).

That these effects were less in the recording under the same conditions on the rubber model when LED-markers on needles were used (Figure 3-5) in stead of stickers can be explained as follows:

Firstly, because of the needle fixation the markers were all fixed on the "annular"

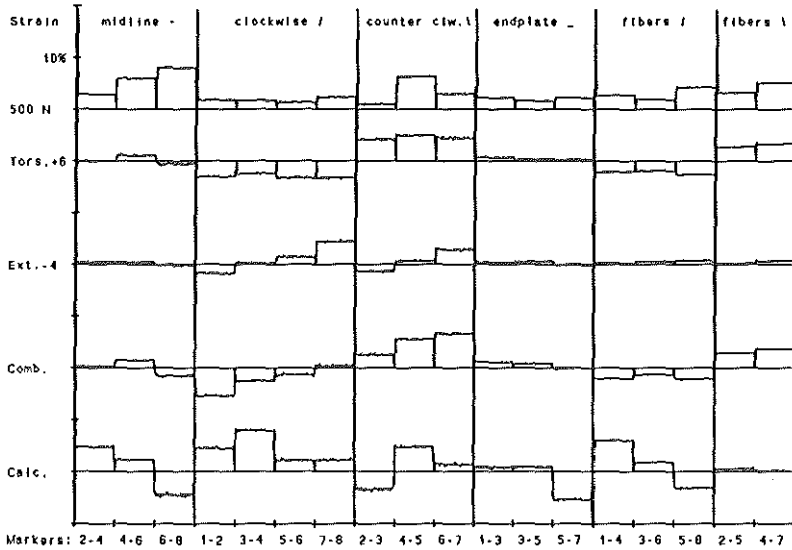


Figure 3-8. Changes in relative distance between the LED markers on the physical model, due to compression and the changes due to rotations (Tors., Ext., Comb., Calc.) compared to compression alone.

wall. The markers on the midline are then already in a relative outward position compared to those on the "endplate". Secondly, because the hoseclamp around the "endplate" hindered the positioning of the markers they were fixed closer to the midline than the stickers. As this decreases the distance between the markers at the "midline" and those at the "endplate", the error in the relation between measured distance and actual strain between the markers also decreases. This is also why a strain of 2 to 3 % around the theoretically rigid "endplate" is observed in figure 3-5.

The stainless steel needles, used for fixation of the LED's, exhibited electrolytic corrosion when used on a human FSU. Unfortunately, only the measurements on the human FSU in which axial rotation (torsion) to the right is combined with flexion and extension could be performed before the corroded needles broke. According to the analysis of Shirazi ^{Shirazi '89(2)}, these combined rotations are quite harmless to the fibers on the right posterolateral side of the annular wall, which we observed. Our results (Figures 3-7 and 3-8) are in agreement with his conclusions. We found that the most strained fibers are the ones running counter

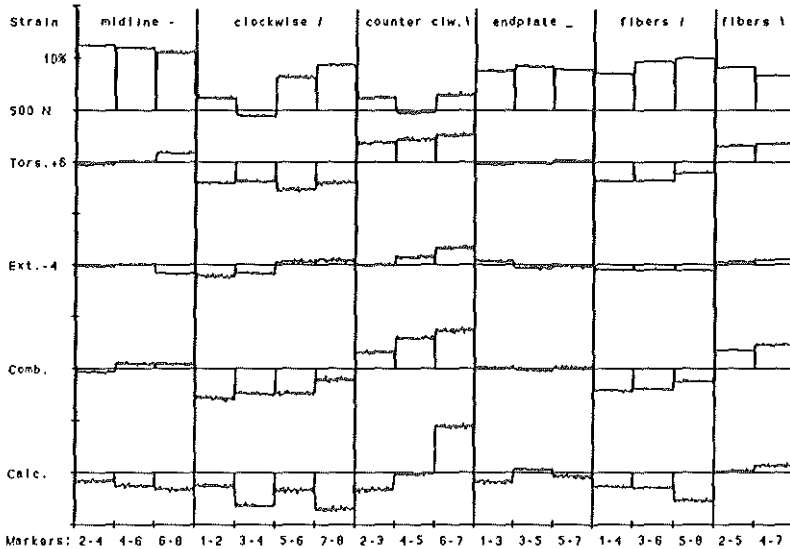


Figure 3-9. Changes in relative distance between the LED markers on the FSU, due to compression and the changes due to rotations (Tors., Ext., Comb., Calc.) compared to compression alone.

clockwise (as defined by Figure 3-3) under axial rotation to the right combined with extension (Figure 3-8).

We did not directly calculate the strain in the annular wall fibers, but the strain of the annular wall at an angle of about 67° with the axis of the specimen, which is roughly along the course of the fibers. As we neglected the curvature of the annular wall, the error in the calculated strains is approximately 5 % or less, depending on the direction of the strain.

Increasing the number of markers in the area would enable us to estimate the curvature but then smaller markers would be required because otherwise the marker images could become fused.

Our data showed little or no change in strain during each interval after a stepwise applied deformation of the FSU. This means that a lower sampling rate than 2 per second can be chosen, for instance 0.2 per second, in which case the markers can be illuminated one at a time and their position calculated. This simplifies the identification of the markers and gives us more freedom in choosing the locations

of the markers. In future experiments measurements can be performed with markers of glassfiber (placed in three rows of four) which are illuminated one at a time (sequentially).

Conclusions

The presented method to measure deformations on the surface of the annular wall is usable, yet a number of improvements are suggested.

An initial inhomogeneous pre-strained condition of the physical model causes deviations from the expected homogeneous strain pattern under pure axial loading conditions. It might be useful to look for a better way to fix the model to avoid this heterogeneous pre-strained state, because this complicates the interpretation of deformations seen on the specimen.

Our data obtained from combined rotations of the axially loaded FSU display the same trend in deformation as concluded in the analytical studies of Shirazi^{Shirazi '89(2)}. This provides experimental evidence for the theory that combined rotations in the physiological range (especially flexion with lateroflexion and axial rotation) create an increased risk of failure of the annular wall, even when the axial load is relatively low. To specify the risky loading conditions more precisely, more measurements need to be done and more specimen need to be tested.

General conclusions

General conclusions

Epidemiological studies attribute an important role to complex spinal loading situations in the multi-factorial pathogenesis of intervertebral disc herniation. Biomechanical analysis of such loading conditions using the Finite Element Method, predicts severely increased strains under these conditions. Though the nucleus has visco-elastic properties (Chapters 1 and 2), (and important pressure differences existing between two sensing needles, located in the same nucleus are possible) no significant pressure differences between the central and the posterolateral nucleus are found in normal discs under complex loading conditions. We conclude that no pressure differences are generated in the normal nucleus (Chapter 1). However in case of severe disc degeneration pressure differences may exist, which do not equilibrate (Chapter 1) as the nucleus can be divided in several hydrostatically isolated spaces, so called sub-nuclei.

The nucleus of the normal intervertebral disc behaves hydrostatically (Chapters 1 and 2). The nucleus can be described as a gel like structure, its matrix ensures its integrity when isolated from the disc (Chapter 2-I and 2-II). The matrix can be deformed quite easily, so that the nucleus is actually a visco-elastic structure, but it behaves hydrostatically under physiological loading conditions (Chapter 2-I).

The magnitude of the intradiscal pressures in normal, and even in light to moderately degenerated discs, under "normal" working conditions, depends merely on the applied axial load and is hardly influenced by extension, flexion, axial rotation or a combination of these rotations (Chapter 1). Furthermore, we concluded that the change in the intradiscal pressure caused by rotation in one direction (sagittal plane or axial rotation) is independent of the existence of a rotation in the other direction (Chapter 1). If intradiscal pressure is interpreted as a measure of the stress and strain load on the annular wall, then our findings would be in contrast with epidemiological ^{Kelsey '84 Burdorf '91}, analytical ^{Shirazi '89(2)} and experimental ^{Gordon '91} studies that predict an increased load on the annular wall under combined deformations. We therefore conclude that the intradiscal pressure is not a reliable measure of the stress and strain in the annular wall (Chapter 1).

Observations of shortening of the spine in the course of the day ^{Krämer '80} suggest that *in-vivo* the intervertebral disc is not fully capable of opposing pressure load. We did not observe stabilization of the compression of the nucleus *in-vitro*, not even after more than 18 hours (Chapter 2-I). We conclude that the elasticity of the

tissue matrix of the nucleus plays an insignificant role in the observed range of compression in physiological loading conditions. Swelling processes and hydraulic permeability are more important than tissue elasticity of the nucleus. The poro-elastic model given by Mow ^{Mow '80} is therefore not applicable to nucleic tissue.

Under unconfined compression, immediately after applying an axial load, the bulging of the annular wall determines the decrease of the height of the disc. Bulging then gradually increases a little, due to visco-elastic relaxation of the annular wall. Fluid flow out of the disc is a much slower process and more dominant in a later phase. Finally fluid flow is primarily responsible for the rate of decrease in disc height and the deformation of the annular wall (Chapters 2-II and 2-III). Because no equilibrium was observed during our tests (lasting up to 21 hours), we conclude that the hydraulic permeability is at least as important as the swelling pressure of the nucleus in limiting the compression rate under a constant axial load (Chapter 2-II). The observation *in-vitro* that compression under a constant axial load continues so long, may not be completely representative for the *in-vivo* situation because recuperation, dependent on an active process, is disturbed in the *in-vitro* situation (Chapter 2-III). Hence great care should be exercised when transposing data from *in-vitro* experiments to *in-vivo* conditions.

A simple mechanical model of the intervertebral disc is developed that relates visco-elasticity of the fibers in the annular wall, fluid-flow and bulging of the annular wall to the intradiscal pressure (Chapter 2-III). The model has been verified with experimental data (Chapter 2-III) and it explains the excess of pressure in normal discs, and the lower pressure in degenerated discs in accordance with the work of Brinckmann and Grootenboer ^{Brinckmann '91}. In normal discs the intradiscal pressure appears to be constant if the observation time is relatively short. In our 500 N load simulation the pressure drops only 8 percent approximately in the first 30 minutes. When a complete FSU is loaded such a decrease will be even less, because the actual load on the disc and therefore the intradiscal pressure will increase a little, due to visco-elastic relaxation of other load carrying structures, such as the facet joints.

Based on the biomechanical mechanisms used in this model we predict increased fiberstrain in the flattened annular wall (Chapter 2-III). We conclude that there is no direct and constant relation between intradiscal pressure and annular wall

strain, not even when disregarding the fact that local differences in strain in the annular wall do not translate into differences in intradiscal pressure (Chapter 1), hence intradiscal pressure disqualifies as a measure of strain in the annular wall (Chapter 2-III).

We find in this mechanism an explanation for the asymmetric shape of the annular wall (Chapter 2-III).

The model indicates that there is a significant loss of swelling potential in the disc *in-vitro*. Complete recuperation of the specimen as manifested *in-vivo* is not guaranteed under *in-vitro* conditions. Hence long lasting or repetitive loading experiments *in-vitro* may not reflect behavior of the intervertebral disc *in-vivo*.

The model can be used to estimate axial load *in-vivo*, simply from changes in body length instead of traumatic measurements of intradiscal pressure.

A 3-D video registration method is presented, which registers marker displacements of less than 0.02 mm. Measurements on a rubber dummy of the intervertebral disc reveal that an initial inhomogeneously strained condition of the dummy causes deviations (in strain) from the expected homogeneous strain pattern under axial loading conditions.

In-vitro measurements under single and combined rotations of an axially loaded FSU (Chapter 3) show the same trend in deformation as concluded in the analytical studies of Shirazi ^{Shirazi '89(2)}. This provides experimental evidence for the theory that combined rotations can create an increased risk of failure in the annular wall, even in cases of a relatively small axial load.

Recommendations for future experiments

The continuous measurement of changes in body length combined with an accurate and valid model of the intervertebral disc can be used in the future to assess the axial load on the back in occupational health studies. To achieve such an important and clinically relevant goal the following recommendations for improvement need to be implemented first.

- The merging of the biomechanical principles of our model with the geometrically more refined model of Broberg ^{Broberg '93}.
- The validation of such an improved model with measurements on human lumbar FSU's as described in Chapter 2-II under continuous registration of

intradiscal pressure.

- The tools that are currently used in our department to continuously measure lumbar spine rotations and form ^{Snijders '87 Goossens '94} need to be used to measure the change of length of the lumbar spine (estimated to be 6 mm a day) as well. The data that may thus be obtained can be used in the FEM model of Shirazi ^{Shirazi '89(2)} to calculate the maximum strain in the annular wall.
- Once a reliable method to continuously measure the length of the lumbar spine is available the (improved) model can be validated with *in-vivo* measurements.
- As the predictions of the model strongly depend on the geometry of the disc, non-invasive and harmless methods, such as MRI, need to be used or developed to acquire as much data as possible concerning the geometry of the intervertebral disc in the subject.

In order to specify the risky loading conditions more precisely, more measurements need to be done and more specimen need to be tested. The application of the 3-D video registration technique we developed is not yet optimal. The use of passive markers has its drawbacks as we discussed in Chapter 3. The potentialities of this video technique can be improved if the following recommendations for improvement are implemented:

- The use of smaller markers, which yield a more detailed registration of local deformations.
- The presentation and interpretation of data from a matrix composed of eight markers as we described in Chapter 3 is satisfactory. The use of more markers will be far more complicated. When complex matrixes are used, a semi 3-D reconstruction of the matrix is more suited for the interpretation of the acquired data.
- The one by one activation and registration of active markers, a technique already used in our calibration procedure, implemented in the measurements on the specimen, enables us to use complex matrices with a large number of markers in order to get detailed information covering a larger area.

Appendices

Appendices

Appendix A: Composition of the analytical model.

In order to calculate the deformation of a disc exposed to an axial load we need to relate disc volume, intradiscal pressure, disc geometry and annular wall strain to each other and to the axial load. It should be noted that the sequence followed here is not necessarily the sequence of calculation.

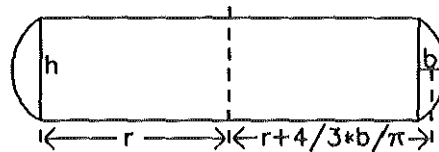


Figure A-1. Diagram of the disc model.

First we relate disc volume to disc geometry. The volume of a barrel shaped disc V_d (Figure A-1), with a semi-elliptic bulging curvature is calculated as follows: The disc is separated in a cylindrical part with volume $\pi \cdot r^2 \cdot h$ and a torus of the bulging with a volume calculated by rotating the center of mass ($r + 4/3 \cdot b/\pi$) of the semi-elliptic bulging surface ($\pi \cdot b \cdot h/4$) around the axis of the disc ^{Dubbel '74}. The volume of the torus is added to the volume of the cylindrical part sothat:

$$V_d = h \cdot \pi \cdot r^2 + 2 \cdot \pi \cdot \left(r + \frac{4}{3} \cdot \frac{b}{\pi} \right) \cdot \pi \cdot b \cdot \frac{h}{4} \quad (1)$$

We will now derive a relation between disc geometry and both external load and intradiscal pressure. In order to simplify calculations from now on the bulging curvature is considered to be semi-circular.

The stress σ_w in the annular wall with thickness d causes a force F_w on the endplate. The hydrostatic intradiscal pressure P_h has to balance the forces F_e and F_w acting on the endplate (Figure A-2) ^{Dubbel '74 Brinckmann '91}.

$$P_h \cdot \pi \cdot r^2 - (F_e + \sigma_w \cdot 2 \cdot \pi \cdot r \cdot d) = 0$$

The force F_w is related to the stress σ_w in the annular wall as follows:

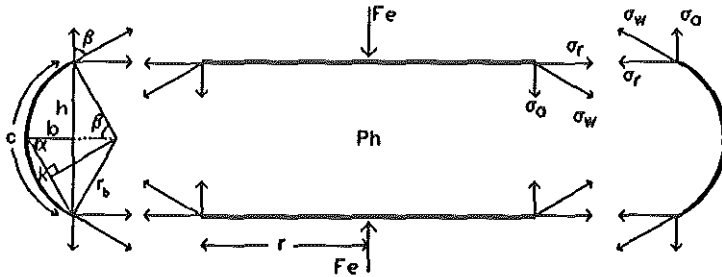


Figure A-2. Diagram of the modelled bulging and the forces acting on the endplates and the annular wall.

$$F_w = \sigma_w \cdot 2 \cdot \pi \cdot r \cdot d \quad (2)$$

The axial component σ_a (Figure A-2) of σ_w is:

$$\sigma_a = \sigma_w \cdot \cos \beta$$

where β is the angle between the annular wall and the axis of the disc at the point of contact with the endplate (Figure A-2). In addition β is half the angle described by the bulging curvature c (Figure A-2). Then:

$$P_h = \frac{F_e + \sigma_a \cdot 2 \cdot \pi \cdot r \cdot d}{\pi \cdot r^2}$$

or

$$P_h = \frac{F_e + F_w \cdot \cos \beta}{\pi \cdot r^2} \quad (3)$$

The hydrostatic, intradiscal pressure P_h is also in equilibrium with the radial component σ_r of the stress (Figure A-2) in the annular wall ^{Dubbel '74}:

$$P_h \cdot h \cdot 2 \cdot \pi \cdot r - 2 \cdot \sigma_r \cdot 2 \cdot \pi \cdot r \cdot d = 0$$

where

$$\sigma_r = \sigma_w \cdot \sin \beta$$

hence,

$$P_h = \frac{2 \cdot F_w \cdot \sin \beta}{h \cdot 2 \cdot \pi \cdot r} \quad (4)$$

or

$$F_w = \frac{P_h \cdot h \cdot 2 \cdot \pi \cdot r}{2 \cdot \sin \beta} \quad (5)$$

By combining expressions (3) and (5) we find:

$$P_h = \frac{F_e + \frac{P_h \cdot h \cdot 2 \cdot \pi \cdot r}{2 \cdot \sin \beta} \cdot \cos \beta}{\pi \cdot r^2}$$

or

$$P_h = \frac{F_e}{\pi \cdot r^2 - h \cdot \pi \cdot r \cdot \operatorname{ctg} \beta} \quad (6)$$

We use this relation between P_h and both disc geometry and external load to derive the disc height h under an axial load when P_h holds ((4) and (6)):

$$\frac{2 \cdot F_w \cdot \sin \beta}{h \cdot 2 \cdot \pi \cdot r} = \frac{F_e}{\pi \cdot r^2 - h \cdot \pi \cdot r \cdot \operatorname{ctg} \beta}$$

sothat

$$h = \frac{r \cdot F_w \cdot \sin \beta}{F_e + F_w \cdot \cos \beta} \quad (7)$$

In the unloaded situation F_e is equal to zero, so

$$h = r \cdot \tan \beta \quad (8)$$

It appears in formula (8) that h is independent of the stress in the annular wall. This is not true however, both in the loaded (formula 7) and in the unloaded situation the wall stress causes an intradiscal pressure P_h , which has to be balanced by the swelling pressure P_s . Until these pressures are in equilibrium the disc volume V_d will change and so will σ_w , b , β and h .

So far we have related disc geometry to disc volume, pressure, and external load. We now derive some important geometric features from the relation between disc volume and disc geometry.

When disc volume (V_d) and disc height (h) are known, the bulging (b) can be calculated using (1):

$$b = -\frac{3}{8} \cdot \pi \cdot r \pm \frac{3}{4 \cdot \pi \cdot h} \cdot \sqrt{\left[\frac{\pi^2 \cdot h \cdot r}{2}\right]^2 - \frac{8 \cdot \pi \cdot h}{3} \cdot (h \cdot \pi \cdot r^2 - V_d)} \quad (9)$$

We previously used the angle β that we now derive from the disc geometry. We also derive the length of curvature (c), which is needed to calculate the strain and tension in the annular wall.

The curvature (c) (Figure A-2) can be approximated by a part of a circle ^{Klein '83} with angle 2β and radius r_b (Figure A-2) sothat:

$$c = r_b \cdot 2 \cdot \beta \quad (10)$$

To calculate r_b we use cord k and angle α as defined in figure A-2, where

$$k = \frac{h}{2 \cdot \sin \alpha} \quad (11)$$

sothat

$$r_b = \frac{k}{2 \cdot \cos \alpha} = \frac{h}{4 \cdot \sin \alpha \cdot \cos \alpha} \quad (12)$$

with

$$\alpha = \arctan \frac{h}{2 \cdot b} \quad (13)$$

and

$$\beta = 2 \cdot \arcsin \cos \alpha = 2 \cdot \arcsin \frac{k}{2 \cdot r_b} \quad (14)$$

However, when β is 90° and bulging increases then the curvature is considered to be semi-elliptic. The length of the curvature (c) can then be calculated using the description of the circumference of half an ellipse ^{Dubbel '74} with β equal to 90° :

$$c = \pi \cdot \left[\frac{b + \frac{h}{2}}{2} \right] \quad (15)$$

We will now relate disc geometry to the length l and strain ϵ of the fibers in the annular wall.

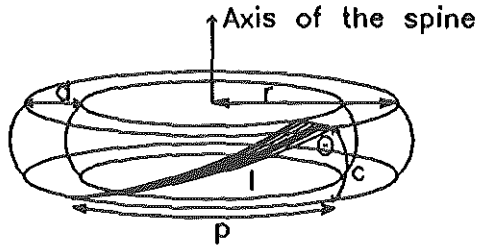


Figure A-3. Diagram of the disc model, showing one fiber running clockwise from one endplate to the other.

We assume that a fiber in the annular wall can be taken as the long side of a rectangular triangle with sides l , c and p around the annular bulge (Figure A-3), hence:

$$l = \frac{c}{\cos \theta} \quad (16)$$

As the disc is only axially loaded, the pitch p is continuously described as the horizontal distance between the connection of a fiber to one endplate and the connection to the other endplate on the circumference of the endplates. As Θ is given for the initial unloaded situation ($t=0$), l_0 can be calculated and so can p_0 :

$$p_0 = c_0 \cdot \tan \theta_0 \quad (17)$$

During loading and unloading l and Θ are functions of time and can be calculated using (16) and the value of p calculated from the initial situation.

$$\theta_t = \text{atan} \left[\frac{p_t}{c_t} \right] \quad (18)$$

and

$$l_t = \frac{P_0}{\sin \theta_t} = \frac{c_t}{\cos \theta_t} \tag{19}$$

To calculate strain (ϵ) we need to know the unstrained fiber length l_u .
As

$$\epsilon_t = \frac{l_t}{l_u} - 1 \tag{20}$$

at $t=0$, the unstrained fiber length l_u follows from:

$$l_u = \frac{l_0}{\epsilon_0 + 1} \tag{21}$$

In the initial situation ($t=0$) h at $t=0$ (h_0) can be measured, β_0 and therefore b_0 and l_0 can then be calculated using (8), (12), (13), (14), (10) and (16).

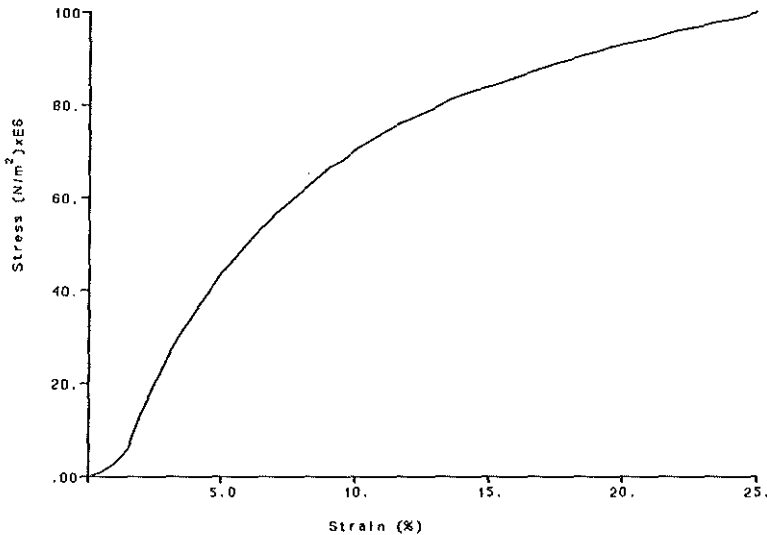


Figure A-4. Stress-strain curve of the annular wall fibers (according to Shirazi *et al.* 1986, 1989).

The fiber strain at $t=0$ ϵ_0 can then be derived from the disc geometry and initial pressure using (5), (2), (24) and the stress-strain relation given in figure A-4.

Hence fiber strain in time ϵ_t is described as:

$$\epsilon_t = \frac{l_t \cdot \epsilon_0 + l_t}{l_0} - 1 \quad (22)$$

The annular wall behaves visco-elastic ^{Galante '67}. The visco-elastic properties of the annular wall fibers are represented by the mechanical model of figure A-5.

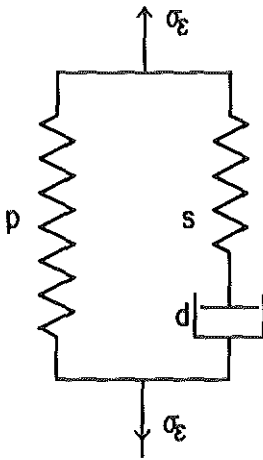


Figure A-5. Mechanical model of viscoelastic fiber.

In the initial situation, i.e., prior to loading, the visco-elastic element is relaxed. Fiber stress is now caused only by the parallel elastic element p . The instant the specimen is axially loaded, the annular fibers become more strained. Because of viscosity (dashpot d in the model) the parallel (p) and the serial (s) elastic element are strained. In the time following this step, the visco-elastic element relaxes. The exponential term in (23) simulates the relaxation. The term $(1-a)/a$ represents the elasticity of the serial arranged element relative to the parallel element.

We thus describe stress after a stepwise elongation by the expression:

$$\sigma_f(t) = \sigma_f(v)$$

with

$$v = \epsilon + \Delta \epsilon \cdot H(t) \cdot \left[\frac{1-a}{a} \cdot e^{-t/\tau} \right] \tag{23}$$

The stress σ_f in the fibers is derived from ϵ_f using the stress-strain curve of figure A-4 Shirazi-Adl '86 Shirazi '89.

Fibers run around the annular wall in two directions (Figure A-3), so the stress in the annular wall perpendicular to the endplate σ_w is:

$$\sigma_w = 2 \cdot \sigma_f \cdot \cos \theta \tag{24}$$

We assume that the initial pressure (at $t=0$) in the disc (caused by swelling of the nucleus prior to loading) is approximately 0.1 MPa Nachemson '75. Expressions (2) and (3) then yield the stress σ_w in the annular wall that accompanies the initial pressure at the measured disc height h_0 and the calculated bulging b_0 ((12), (13), (14)), β_0 (8) as well as l_0 ((10) and (16)). From equation (24) and the stress-strain relation given in figure A-4 the initial fiberstrain ϵ_0 can now be calculated (assuming that no visco-elastic relaxation is involved here) and used in expression (22).

We can now calculate the intradiscal, hydrostatic pressure P_h from the axial load and the initial (measured) disc geometry. This hydrostatic pressure P_h causes a fluid flow through the annular wall and the endplates, which is opposed by the concentration-dependent swelling pressure P_s of the nucleus.

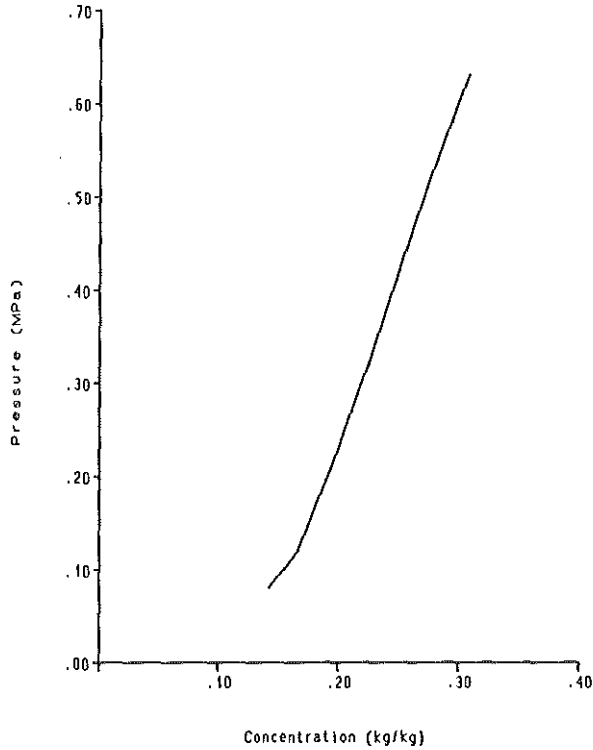


Figure A-6. Concentration-pressure curve of the swelling pressure (according to Urban 1981).

Figure A-6 gives the concentration-pressure relation considered for the swelling pressure P_s .

Fluid-flow (J) in and out of the disc depends on the difference between the swelling pressure P_s and the hydrostatic pressure P_h and the hydrodynamic permeability constant K_d of the complete disc ^{Comper '87} (flow out is negative, flow in is positive):

$$J = K_d \cdot (P_s - P_h) \quad (25)$$

Integration of fluid-flow in time gives the flow volume in time:

$$V_f(t) = \int_0^t [K_d(t) \cdot (P_s(t) - P_h(t))] dt \quad (26)$$

Initial water volume is considered to be 2/3 of the initial total disc volume ^{Urban '81}:

$$V_w(0) = V_d(0) \cdot \frac{2}{3} \quad (27)$$

The assumed initial pressure of approximately 0.1 MPa ^{Nachemson '75} is then used (Figure A-6) to find the initial concentration (C_0) of glycosaminoglycan molecules. This concentration is then multiplied with the initial water volume to find the initial amount of glycosaminoglycan molecules (G_0).

Water volume in the disc as a function of time is then

$$V_w(t) = V_w(0) + V_f(t) \quad (28)$$

Total disc volume in time is then

$$V_d(t) = V_d(0) + V_f(t) \quad (29)$$

We have now derived all the equations needed to simulate compression and recuperation of an axially loaded disc. Some refinements and other equations are discussed next.

Under compression the size of the pores in the annular wall and the endplates decreases due to the expulsion of fluid. An expression for K_d , that was derived from a review article by Levick ^{Levick '87}, is given by Broberg ^{Broberg '93}:

$$K_d(t) = 1/2 \cdot K_d(0) \cdot \left[1 + \left[\frac{FCD(0)}{FCD(t)} \right]^{3/4} \right] dt$$

In this expression FCD is the fixed charge density that is inversely related to the amount of available water. We can substitute this FCD for the amount G of glycosaminoglycans divided by the amount $V_w(t)$ of available water:

$$K_d(t) = 1/2 \cdot K_d(0) \cdot \left[1 + \left[\frac{G(0)/V_w(0)}{G(t)/V_w(t)} \right]^{3/4} \right] dt \quad (30)$$

We incorporate the possibility of loss of swelling potential. We express this loss of swelling potential, due to the loss of glycosaminoglycan molecules (G), with the expelled fluid by:

$$G(t) = G(0) - \int_0^t [S \cdot C(t) \cdot J(t)] dt \quad (31)$$

where S is the sieving coefficient that determines the fraction of the concentration C of glycosaminoglycans that is expelled via the fluid flow J .

For comparison we will also calculate intradiscal pressure according to the transformation of Nachemson ^{Nachemson '60}. This transformation correlates very well with in-vivo and in-vitro measurements and uses only the externally applied load (F_e), the cross-sectional surface of the disc and an empirically derived correction factor to calculate intradiscal pressure P_n with:

$$P = \frac{1.5 \cdot F_e}{\pi \cdot (r + b)^2}$$

To make a fair comparison this expression needs to be corrected to accommodate the change of maximum disc cross-sectional area due to the increase of bulging, so:

$$P_n = \frac{1.5 \cdot F_e}{\pi \cdot (r + b(t))^2} \quad (32)$$

Appendix B: Flow diagram of the PSI-e model.

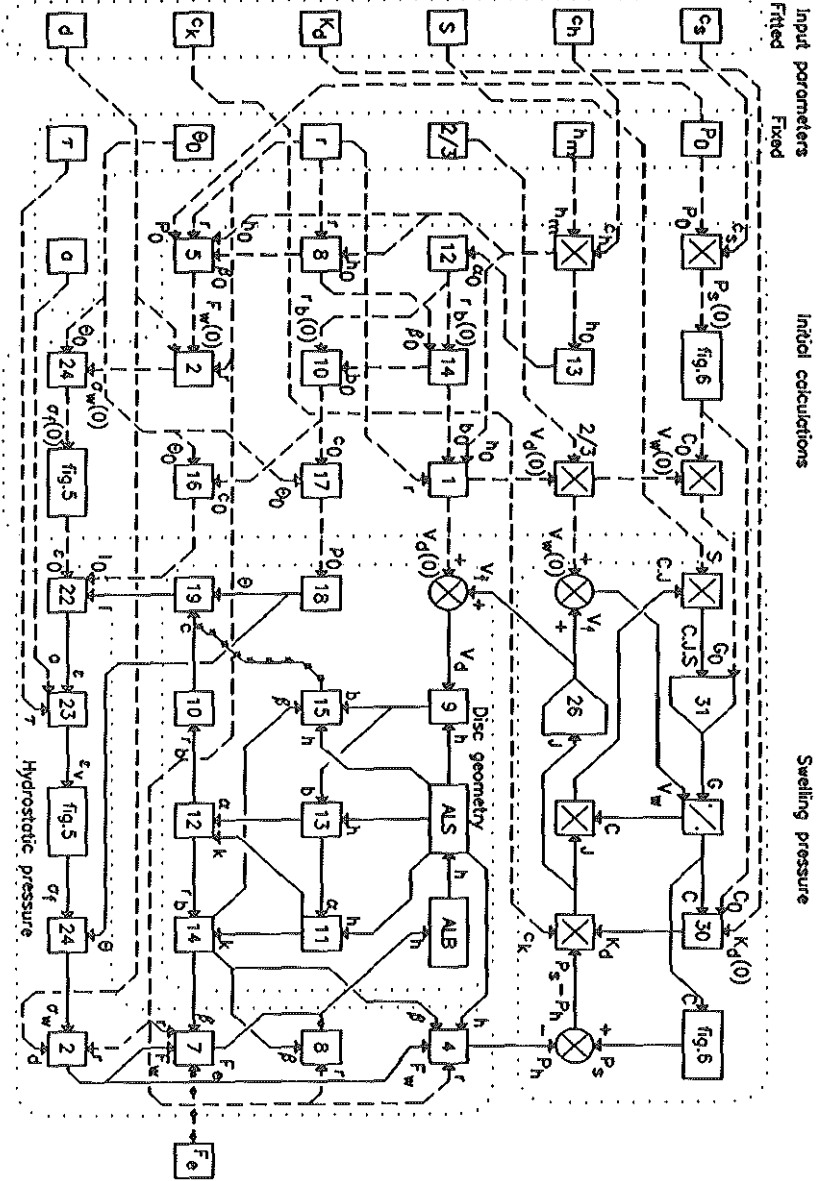


Figure B-1. Flow diagram of the intervertebral disc model, alternative pathways are marked with an asterisk (*).



References

References

- Abdel-Aziz YI, Karara HM: Direct Linear Transformation from comperator coordinates into object space coordinates in close range photogrammetry. *Proceedings of the ASP/UI Symposium on close-range photogrammetry*, Urbana, Illinois, January 1971
- Adams MA, Hutton WC, Stott JRR: The resistance to flexion of the lumbar intervertebral joint. *Spine* 1980 Vol 5 Nr 3:245-253
- Adams MA, Hutton WC: The relevance of torsion to the derangement of the lumbar spine. *Spine* 1981 7:184-191
- Adams MA, Hutton WC: Prolapsed intervertebral disc; a hyperflexion injury. *Spine* 1982 Vol 7 Nr 3:184-191
- Adams MA, Hutton WC: The effect of posture on the fluid content of lumbar intervertebral discs. *Spine* 8 1983 665-671
- Adams MA, Hutton WC: The mechanical function of the lumbar apophyseal joints. *Spine* 1983 Apr 8(3): P 327-30
- Adams MA, Hutton WC: Has the lumbar spine a margin of safety in forward bending? *Clin Biomech* 1:3-6, 1986
- Andersson GB, Schultz AB: Effects of fluid injection on mechanical properties of intervertebral discs. *J Biomech* 1979 Vol 12 (6), P: 453-8
- Bayliss MT, Urban JP, Johnstone B, Holm S: In vitro method for measuring synthesis rates in the intervertebral disc. *J Orthop Res* 1986 4(1): P 10-7
- Bayliss MT, Johnstone B, O'Brien JP: 1988 Volvo award in basic science. Proteoglycan synthesis in the human intervertebral disc. Variation with age, region and pathology. *Spine* 1988 Sep 13(9): p 972-81
- Beadle OA: *The intervertebral discs*. Special report series no. 161 H.M.Stationary Office London 1931
- Betsch DF, Baer E: Structure and mechanical properties of rat tail tendon. *Biorheology* 1980 17 p 83-94

- Brinckmann P, Grootenboer H: Change of disc height, radial disc bulge, and intradiscal pressure from discectomy. An in vitro investigation on human lumbar discs. *Spine* 1991 16(6) 641-6
- Broberg KB: Slow deformation of intervertebral discs. *J Biomechanics* 26 4/5 1993 501-512
- Brown T, Hansen RJ, Yorra AJ: Some mechanical tests on the lumbosacral spine with particular reference to the intervertebral disc. *J Bone Joint Surg* 1957 39A:1135-1165
- Burdorf A, Govaert G, Elders L: Postural load and back pain of workers in the manufacturing of prefabricated concrete elements. *Ergonomics* 1991 1;34:909-18
- Burdorf A: *Assessment of postural load on the back in occupational epidemiology*. Thesis, Rotterdam The Netherlands 1992
- Comper WD, Williams RP: Hydrodynamics of concentrated proteoglycan solutions. *J Biol Chem* 1987 Oct 5 262(28): p 13464-71
- Droogendijk L: *On the lubrication of synovial joints*. Thesis 1984 TH Twente The Netherlands
- Dubbel: *Taschenbuch für den Maschinenbau*. Berichtigter Neudruck der 13. Auflage 1974. Herausgegeben von: Sass F, Bouché Ch, Leitner A; Springer-Verlag Berlin Heidelberg New York.
- Dunlop RB, Adams MA, Hutton WC: Disc space narrowing and the lumbar facet joints. *J Bone Joint Surg* 1984 66-B
- Eie N: Load capacity of the low back. *J Oslo City Hosp* 1966 Apr Vol 16 (4) p 73-98 ISSN: 0030-6207
- Eklund JAE, Corlett EN: Shrinkage as a measure of the effect of load on the spine. *Spine* 9 1984 189-194
- Farfan HF, Cossette JW, Robertson GH, Wells RV, Kraus H: The effects of torsion in the production of disc degeneration. *J Bone and Joint Surg* 1970 Vol 52A:468-497
- Galante JO: Tensile properties of the human lumbar annulus fibrosus. *Acta Orthop Scand Suppl* 100 p 1-91 1967
- Gertzbein SD, Kapasouri A, Cruickshank B: Determination of a locus of instantaneous rotation of the lumbar disc by Moiré Fringes: *Spine* 1984 9 4:409-413
- Goobar JE, Pate D, Resnick D, Sartoris DJ: Radiography of the hyperextended lumbar spine: an effective technique for the demonstration of discal vacuum phenomena. *J Can Assoc Radiol* 1987 Dec 38(4): P 271-4

Goossens RHM: *Biomechanics of body support*. Thesis, Rotterdam The Netherlands 1994

Gordon SJ, Yang KH, Mayer PJ, Mace AH, Kish VL, Radin BL: Mechanism of disk rupture: A preliminary report. *Spine* 1991 Vol 16 4:450-456

Harkness RD: Biological functions of collagen. *Biol Rev* 1961 36 p 399-463

Haut RC, Little RW: A constitutive equation for collagen fibers. *J Biomechanics* 5 p 423-430 1972

Haut RC: Age-dependent influence of strain rate on the tensile failure of rat-tail tendon. *J Biomech Engng* 105 p 296-299 1983

Hendry NGC: The hydration of the nucleus pulposus and its relation to intervertebral disc derangement. *J Bone & Joint Surg* 40 B:132, 1958

Hickey DS, Hukins DWL: 1979 Volvo Award for Bioengineering: Relation between the structure of the annulus fibrosus and the function and failure of the intervertebral disc. *Spine* Vol 5:2 march/april 1980 p 106-116.

Inman VT, Saunders JBdeCM: Anatomicophysiological aspects of injuries to the intervertebral disc. *J Bone Joint Surg* 29:461 1947

Kastelic JR: *Structure and mechanical deformation of tendon collagen*. Thesis 1979 Case Western Reserve University

Keemink CJ, Hoek van Dijke GA, Snijders CJ: Upgrading of efficiency in the tracking of body markers with video techniques. *Medical & Biological Engineering & Computing* Jan 1991 70-74

Keller TS, Holm SH, Hansson TH, Spengler DM: 1990 Volvo Award in experimental studies. The dependence of intervertebral disc mechanical properties on physiologic conditions. *Spine* 1990 Aug 15(8) p 751-61

Kelsey JL, Githens PB, White AA, Holford TR, Walter SD, O'Conner T, Ostfeld MO, Weil U, Southwick WO, Calogero JA: An epidemiologic study of lifting and twisting on the job and risk for acute prolapsed intervertebral disc. *Journal of Orthopaedic Research* 2:61-66 1984

Klein JA, Hickey DS, Hukins DW: Radial bulging of the annulus fibrosus during compression of the intervertebral disc. *J Biomech* 1983 16(3) p 211-7

Koeller W, Funke F, Hartmann F: Biomechanical behavior of human intervertebral discs subjected to long lasting axial loading. *Biorheology* 1984 21(5) p 675-86

- Koeller W, Muehlhaus S, Meier W, Hartmann F: Biomechanical properties of human intervertebral discs subjected to axial dynamic compression, influence of age and degeneration. *J Biomech* 1986 19(10): P 807-16
- Koreska J, Robertson D, Mills RH, Gibson DA, Albisser AM: Biomechanics of the lumbar spine and its clinical significance. *Orthop Clin of North Am* 1977 Vol 8 Nr 1:121-133
- Kraemer J: Pressure dependent fluid shifts in the intervertebral disc. *Orthop Clin North Am* 1977 Jan Vol 8 (1) P: 211-6, ISSN: 0030-5898
- Kraemer J, Gritz A: Körperlängenänderungen durch druckabhängige Flüssigkeitsverschiebungen im Zwischenwirbelabschnitt. *Z Orthop* 1980 118:161-164
- Kraemer J, Kolditz D, Gowin R: Water and electrolyte content of the human intervertebral discs under variable load. *Spine* 1985 Vol 10 Nr 1:69-71
- Kulak RF, Schultz AB, Belytschko T, Galante J: Biomechanical characteristics of vertebral motion segments and intervertebral discs. *Orthop Clin North Am* 1975 Jan Vol 6 (1) P: 121-33 ISSN:0030-5898
- Kulak RF, Belytschko TB, Schultz AB, Galante JO: Nonlinear behaviour of the human intervertebral disc under axial load. *J Biomechanics* 9:377-386 1976
- Levick JR: Flow through interstitium and other fibrous matrices. *Q J Exp Physiol* 1987 Oct 72(4) P 409-37
- Markolf KL: Deformation of the thoracolumbar intervertebral joints in response to external loads: a biomechanical study using autopsy material. *J Bone Joint Surg (Am)* 1972 Apr Vol 54 (3), P: 511-33, ISSN:0021-9355
- Markolf KL, Morris JM: The structural components of the intervertebral disc. (a study to the contribution of the ability of the disc to withstand compressive forces). *J Bone Joint Surg* 56A p 675-687 1974
- Maroudas A, Bannan C: Measurement of swelling pressure in cartilage and comparison with the osmotic pressure of constituent proteoglycans. *Biorheology* 1981 18(3-6) p 619-32
- Maroudas A, Ziv I, Weisman N, Venn M: Studies of hydration and swelling pressure in normal and osteoarthritic cartilage. *Biorheology* 1985 22(2) p 159-69
- Maroudas A, Schneiderman R: "Free" and "exchangeable" or "trapped" and "non-exchangeable" water in cartilage. *J Orthop Res* 1987 5(1) p 133-8

- Morein G, Goldgefter L, Kobylansky E, Goldschmidt-Nathan M, Nathan H: Changes in the mechanical properties of rat tail tendon during postnatal ontogenesis. *Anat Embryol* 154 p 121-124 1978
- Mow VC, Kuei SC, Lai WM, Armstrong CG: Biphasic creep and stress relaxation of articular cartilage in compression: theory and experiments. *J Biomech Eng* 1980 102 p 73-84
- Nachemson A: Lumbar Intradiscal Pressure. *Acta Orthop Scand* (suppl) 43 p 1-104 1960 (Thesis)
- Nachemson A: The influence of spinal movements on the lumbar intradiscal pressure and on the tensile stresses in the annulus fibrosus. *Acta Orthopedica Scandinavia* 33 p 183-207 1963
- Nachemson AL, Morris JM: In vivo measurements of intradiscal pressure. *J Bone and Joint Surg* 1964 46-a 5:1077-1092
- Nachemson A, Elfstrom G: Intravital dynamic pressure measurements in lumbar discs. A study of common movements, maneuvers and exercises. *Scand J Rehabil Med* 1970 Vol 2 (1) Suppl 1:1-40, ISSN: 0036-5505
- Nachemson A: Towards a better understanding of low-back pain: a review of the mechanics of the lumbar disc. *Rheumatol Rehabil* 1975 Aug Vol 14 (3) p 129-43 ISSN: 0300-3396
- Nachemson AL: The lumbar spine. An orthopaedic challenge. *Spine* 1 1976 59-71
- Nachemson AL, Schultz AB, Berkson MH: Mechanical properties of human lumbar spine motion segments. Influence of age, sex, disc level, and degeneration. *Spine* 1979 Jan-Feb Vol 4 (1) p 1-8 ISSN: 0362-2436
- Nachemson AL: Disc pressure measurements. *Spine* 1981 Jan-Feb Vol 6 (1) p 93-97 ISSN: 0362-2436
- Nixon J: Intervertebral disc mechanics: a review. *J R Soc Med* 1986 Feb Vol 79 (2), P: 100-4, ISSN: 0141-0768 50 Refs
- Ohshima H, Tsuji H, Hirano N, Ishihara H, Kato Y, Yamada H: Water diffusion pathway, swelling pressure, and biomechanical properties of the intervertebral disc during compression load. *Spine* 1989 Nov 14(11) p 1234-44
- Oomens CW, Van Campen DH, Grootenboer HJ: A mixture approach to the mechanics of skin. *J Biomech* 1987 20(9) 877-85
- Panjabi MM, Krag MH, White AA: Effects of preload on load displacements curves of the lumbar spine. *Orth Clin N AM* 8:181-192 1977 (jan)

- Panjabi M, Brown M, Lindahl S, Irstam L, Hermens M: Intrinsic disc pressure as a measure of integrity of the lumbar spine. *Spine* Vol 13:8 p 913-917 1988
- Pearce RH, Grimmer BJ, Adams ME: Degeneration and the chemical composition of the human lumbar intervertebral disc. *J Orthop Res* 1987 5(2) p 198-205
- Pelker RR, Friedlaender GE, Markham TC, Panjabi MM, Moen CJ: Effects of freezing and freeze-drying on the biomechanical properties of rat bone. *J Orthop Res* 1984 1(4): P 405-11
- Rabischong P, Louis R, Vignaud J, Massare C: The intervertebral disc. *Anatomica Clinica* 1 p 55-64 1978
- Roaf R: A study of the mechanics of spinal injuries. *J Bone Joint Surg* 42B:810-823, 1960
- Sanjeevi R, Somanathan N, Ramaswamy D: A viscoelastic model for collagen fibres. *J Biomech* 1982 15(3) p 181-3
- Sanjeevi R: A viscoelastic model for the mechanical properties of biological materials. *J Biomech* 1982 15(2) p 107-9
- Schneiderman R, Keret D, Maroudas A: Effects of mechanical and osmotic pressure on the rate of glycosaminoglycan synthesis in the human adult femoral head cartilage: an in vitro study. *J Orthop Res* 1986 4(4) p 393-408
- Shirazi SA, Ahmed AM, Shrivastava SC: Stress analysis of the lumbar disc body unit in compression; a three dimensional non-linear finite element study. *Spine* 1984 9 2:120-134
- Shirazi SA, Ahmed AM, Shrivastava SC: A finite element study of a lumbar motion segment subjected to pure sagittal plane moments. *J Biomech* 1986 19 4:331-350
- Shirazi AdIA, Drouin G: Load-bearing role of facets in a lumbar segment under sagittal plane loadings. *J Biomech* 1987 20 6 P 601-13
- Shirazi AdIA, Drouin G: Nonlinear gross response analysis of a lumbar motion segment in combined sagittal loadings. *J Biomech Eng* Vol 110 aug 1988 216-222
- Shirazi AdIA: On the fibre composite material models of disc annulus - Comparison of predicted stresses. *J Biomech* Vol 22 No 4 pp 357-365 1989
- Shirazi SA, Ahmed AM, Shrivastava SC: Mechanical response of a lumbar motion segment in axial torque alone and combined with compression. *Spine* 1986 11 9:914-927
- Shirazi AdIA: Strain in fibers of a lumbar disc, analysis of the role of lifting in producing disc prolapse. *Spine* 1989 1 14:96-103

Simon BR, Wu JS, Carlton MW, Evans JH, Kazarian LE: Structural models for human spinal motion segments based on a poroelastic view of the intervertebral disk. *J Biomech Eng* 1985 Nov VOL 107 (4) P:327-35, ISSN: 0148-0731

Snijders CJ: On the form of the human spine and some aspects of its mechanical behaviour. *Acta Orth Belgica* 1969, 35

Snijders CJ: *On the form of the human thoracolumbar spine and some aspects of its mechanical behaviour*. Thesis Eindhoven 1970

Snijders CJ, van Riel MP, Nordin M: Continuous measurements of spine movements in normal working situations over periods of 8 hours or more. *Ergonomics* 1987 Apr 30(4): P 639-53

Sonnerup L: Stress and strain in the intervertebral disk in relation to spinal disorders. *Osteoarthromechanics*, McGraw-Hill Book Company, Ghista Dhanjo-N Ed., 1982 Chapter 8 p 315-351

Stokes I, Greenapple DM: Measurement of surface deformation of soft tissue. *J Biomechanics* Vol 18:1 p 1-7 1985

Stokes IAF: Surface strain on human intervertebral discs. *J Orthop Res* Vol 5:3 p 348-355 1987

Troup JDG: Causes, prediction and prevention of back pain at work. *Scan J Environ Health* 1984 10:419-428

Tyrrell AR, Reilly T, Troup JDG: Circadian variation in stature and the effects of spinal loading. *Spine* 10 1985 161-164

Urban JPG, Maroudas A, Bayliss MT, Dillon J: Swelling pressures of proteoglycans at the concentrations found in cartilaginous tissues. *Biorheology* vol 16 p 447-464 1979

Urban JP, Maroudas A: Swelling of the intervertebral disc in vitro. *Connect Tissue Res* 1981 Vol 9 (1), P: 1-10, ISSN: 0091-1690

Urban JP, Holm S, Maroudas A, Nachemson A: Nutrition of the intervertebral disc: effect of fluid flow on solute transport. *Clin Orthop* 1982 Oct(170) p 296-302

Urban JP, McMullin JF: Swelling pressure of the intervertebral disc: influence of proteoglycan and collagen contents. *Biorheology* 1985 Vol 22 (2), P: 145-57, ISSN: 0006-355X

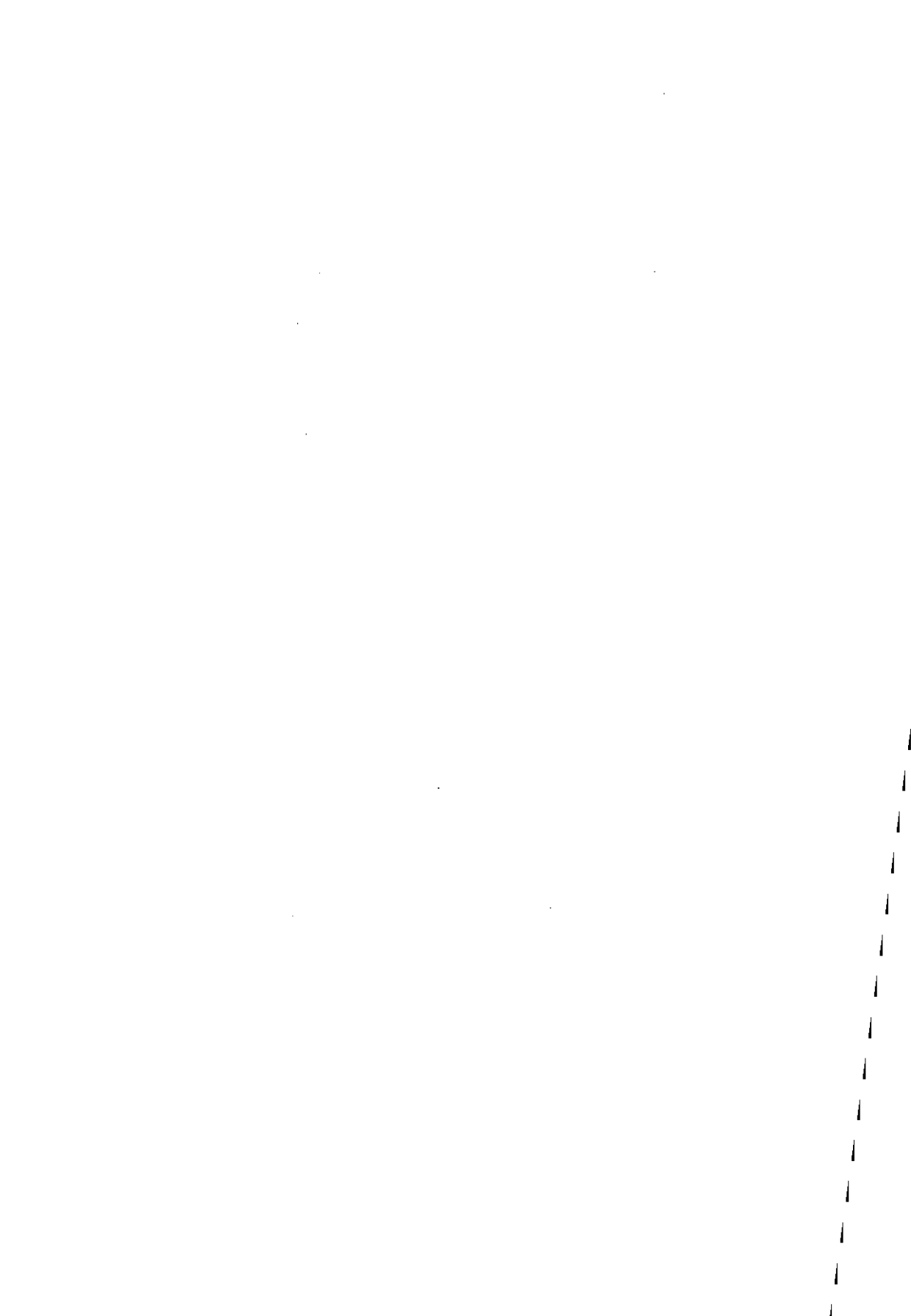
Urban JP, McMullin JF: Swelling pressure of the lumbar intervertebral discs: influence of age, spinal level, composition, and degeneration. *Spine* 1988 Feb 13(2) p 179-87

Valkenburg HA, Haanen HCM: The epidemiology of low back pain. *Idiopathic Low back pain*. 1980 Edited by AA White and SL Gordon, SV Mosby Company 1982

Van Duyl WA: Measurement of cerebral Circulation: Physical and mathematical Aspects in using Radioactive clearance methods. *Adv Cardiovasc Phys* vol 5 (PartII) p 67-89 (Karger, Basel 1983)

Van Duyl WA, Van der Zon AT, Drogendijk AC: Stress relaxation of the human cervix: a new tool for diagnosis of cervical incompetence. *Clin Phys Physiol Meas* 1984 Aug; 5(3): 207-18

Virgin WJ: Experimental investigations into the physical properties of the intervertebral disc. *J Bone Joint Surg* 33B p 607-611 1951



Summary

Summary

The primary target of this PhD project was the assessment of biomechanical factors responsible for rupture of the annular wall of the intervertebral disc. We concentrated our research on the biomechanical properties of the structures and materials of the intervertebral disc. We developed the hypothesis that rupture of the annular wall is a result of the non-homogeneous distribution of strain in the fibers of the annular wall. A strain, which is caused by combined rotations and therefore non-homogeneous deformations of the intervertebral disc. Though supported by recent publications of experimental ^{Gordon '91}, mathematical ^{Shirazi '89(2)} and epidemiological ^{Kelsey '84 Burdorf '91} research, direct experimental verification of this hypothesis lacked so far. For the assessment of this presumed non-homogeneous distribution of strain in the annular wall a method was chosen, which would be applicable *in-vitro* as well as *in-vivo*; the measurement of intervertebral disc pressure.

The intervertebral disc pressure, or more accurately, the pressure in the nucleus pulposus has been measured *in-vitro* as well as *in-vivo* under many conditions by many authors. When measuring the intervertebral disc pressure these authors assume that the nucleus pulposus behaves hydrostatically, i.e. the pressure is instantaneously equal anywhere in the nucleus. However, the nucleus is also described in several studies ^{Kramer '77 Krcamer '80 Urban '81 Kramer '85 Urban '85} as a visco-, or poro-elastic structure with a solid matrix that offers resistance to fluid flow ^{Mow '80}. In that case temporary pressure differences within the nucleus are possible.

Departing from the poro-elastic ^{Mow '80} view of the nucleus, where solid tissue in the nucleus is responsible for both the elastic and the viscotic behavior, we designed our first experiment, described in chapter 1.

Experimentally induced volume changes of the nucleus did indeed lead to detectable differences in (and subsequent equilibration of) pressure, between two pressure sensitive needles inserted in the nucleus, thus substantiating the poro-elastic view of the nucleus.

Four human Functional Spinal Units (FSU's), levels L2-L3 and L4-L5, were mounted in a specially designed loading apparatus and subjected to axial load alone and to axial load combined with axial rotation, sagittal plane rotation and combined rotations, simulating a light to moderate workload. Intradiscal pressure

was recorded, at two locations in the nucleus simultaneously, with specially developed pressure sensitive needles, to detect possible pressure differences. Based on FEM analysis, Shirazi ^{Shirazi '89(2)} predicted local differences in annular wall stress during combined rotations. In the experiment, described in chapter 1, local differences in annular wall strain and stress were expected to coincide with local pressure differences, which could be measured before they would equilibrate as a result of fluid flow through the solid matrix. However, we did not find any significant transient pressure differences inside the nucleus, which could be related to those predicted local stress differences in the annular wall. These results are in harmony with the hydrostatic concept generally used, rather than the poro-elastic ^{Mow '80} model of the nucleus. Our conclusion is, that in physiological loading conditions, intradiscal pressure does not reflect local differences in annular wall stress, or else that those stress differences do not exist. However, the latter is unlikely considering the experimental ^{Gordon '91}, mathematical ^{Shirazi '93(2)} and epidemiological ^{Kelsey '84 Burdorf '91} evidence, that combined rotations cause an in-homogeneous distribution of stress and strain in the annular wall. Under constant axial load we found only an insignificant influence of rotations of the FSU, both single and combined, on the recorded intradiscal pressure. We also found that the change in the intradiscal pressure caused by rotation in one direction (sagittal plane or axial rotation) is independent of the existence of a rotation in the other direction. Therefore we conclude, that the magnitude of the recorded intradiscal pressure depends mainly on the applied axial load and that it is not a good measure of stress and strain in the annular wall.

An explanation for the fact that we did not find pressure differences under loading conditions where local differences in wall stress and strain are predicted ^{Shirazi '89(2)}, could be that the elastic matrix is very weak compared to the pressure existing in the nucleus under such loading conditions. In that case the nucleus as a whole will be displaced and deformed and the equilibrating pressure difference, caused by the reorganization of the matrix, is too small to be recognized. The *in-vitro* experiment described in chapter 2-I was consequently designed to assess the elasticity and permeability of the solid matrix in the light of the poro-elastic model. Plugs of nucleus tissue were subjected to confined compression in a modified version of the testing apparatus, as described by Drogendijk ^{Drogendijk '84}. According to the poro-elastic model ^{Mow '80}, matrix permeability and elasticity can be calculated from the rate of decrease of plug height and from the height of the plug when equilibrium between the applied compressive force and the elasticity of

the plug is reached.

Even under a minor axial load, amounting to a hydrostatic pressure of 0.25 MPa, equilibrium was still not established after more than 18 hours of compression. It is therefore concluded that the poro-elastic model is not applicable to the nucleus pulposus and that the load-bearing capacity of the solid tissue of the nucleus is negligible under such a load.

In the visco-elastic model of the nucleus, elastic behavior is attributed ^{Kramer '77} to the water imbibing properties of the glycosaminoglycans. The time dependent equilibration of the hydrostatic pressure with the swelling pressure, associated with imbibition, causes the viscotoc behavior. In Chapter 2-I it was concluded that permeability and swelling properties of the nucleus are more important than solid tissue elasticity, but the experimental set-up did not allow their quantification. In order to assess the contribution of swelling pressure ^{Inman '47 Hoody '58 Maroudas '81 Urban '81 Ohshima '89}, permeability and fluid flow ^{Virgin '51 Brown '57 Markolf '74 Urban '82 Sommerup '82 Koeller '84 Kraemer '85} as well as annular bulging ^{Klein '83} under conditions of long lasting axial loading of the disc, the experiment described in Chapter 2-II was designed.

An isolated disc was subjected to axial loads for considerable time (up to 21 hours), while expelled fluid volume and decrease of height were measured. Between different loads the specimen was allowed to recuperate. In this experiment special provisions were made to measure expelled water, while evaporation of the water was prevented. Now the nucleus was surrounded by its natural boundaries, i.e., the annulus and the end-plates, which form its "physiological" membrane, to which its viscotoc behavior is ascribed. Furthermore, the circumference of the disc was not artificially confined by a sample holder, but was free to change according to the load. Compared to the previous, confined compression experiments we expected to find in this experiment too a decrease of disc height and volume under a constant load, but now the conditions were more representative for situations encountered *in-vivo*.

We observed that after the application of an axial load, the height of the disc decreased abruptly, due to bulging of the annular wall. Because of the visco-elastic relaxation of the annular wall, the bulging gradually increased during a short period. The expulsion of fluid from the disc is a much slower process and determined the further decrease of disc height and increase of bulging of the annular wall. We measured the intradiscal pressure under an axial load of 1700 N for more than 3 hours and found it to decrease less than 3 %, while a substantial

decrease of disc height and volume was recorded. This again led us to the conclusion that the observed compression is not limited by the compression of the tissue matrix, but determined only by the intradiscal fluid pressure. The swelling properties of the disc are not sufficient to compensate for the expulsion of water, so that compression did not even stop after long (up to 21 hours) periods of observation. The response to repetitive loadings indicated that recuperation inbetween the loading intervals was not complete. This led to the conclusion that *in-vitro* loss of large molecules is responsible for a slow decrease of swelling capacity. This decrease of swelling capacity is held responsible for both the continuing loss of disc height under axial load and the incomplete recuperation after a loading interval. An active regeneration mechanism, which is absent *in-vitro*, is postulated *in-vivo* to compensate the loss of glycosaminoglycans. This would imply that results of compression studies *in-vitro* are not representative for the compression of a disc in response to a load *in-vivo*.

In chapter 2-III an analytical model is described, which was developed to quantify, through simulation of the observed experimental results, the disc properties described in chapter 2-II.

The model assumes hydrostatic behavior of the nucleus in the light of our experimental results (Chapters 1, 2-I and 2-II). A simple biomechanical theory ^{Brinckmann '91} is used which relates fiber visco-elasticity, fluid-flow and annular wall bulging to intradiscal pressure. The model explains the correction factor introduced by Nachemson ^{Nachemson '60} to calculate the expected intradiscal pressure in normal discs from the axial load and the cross-sectional area is explained by the model. This excess in intradiscal, pressure compared to applied force divided by cross-sectional area, concerns the contribution of annular wall stress to the forces in axial direction and depends on the amount of bulging of the annular wall. The model also gives an explanation for the lower initial and loaded intradiscal pressures in degenerated discs.

The intradiscal pressure appears to be constant, if the observation time is only a few minutes (which it is in most *in-vivo* and *in-vitro* experiments). The model predicts a significant loss of swelling potential in the axially loaded disc *in-vitro*. Complete recuperation of the specimen after axial loading is not guaranteed under *in-vitro* conditions. In *in-vivo* situations, however, loss of swelling potential is compensated by the synthesis of glycosaminoglycans ^{Schneiderman '86 Bayliss '86 Bayliss '88}. This implies that long lasting or repetitive loading experiments *in-vitro* do not reflect the *in-vivo* behavior of the intervertebral disc.

The model can be used to calculate axial load from changes in body length *in-vivo*. It can thus be an essential tool to replace registration of the intradiscal pressure as a means of assessing the axial load on the lower back.

From the biomechanical theory implemented in the model we conclude that combined rotations of the FSU may damage the annular wall. The asymmetric shape of the annular wall can also be explained by this theory.

In Chapters 1 and 2 we showed that intradiscal pressure cannot be used as a measure of (local differences in) annular wall strain. Since the theory, that combined rotations of the FSU cause locally increased strain and increase the risk of rupture of the annular wall, still wanted experimental verification, we looked for other ways to measure strain in the fibers of the annular wall.

Chapter 3 gives the description of a 3-D video registration system is that was developed in order to measure the deformations of the annular wall of the intervertebral disc of intact FSU's. Under axial loads in the physiological range, combined with rotations of the FSU, differences in strain in the annular wall could be measured with an accuracy of a half percent.

We presented the measuring technique, calibration and analysis of some preliminary results. According to what is predicted ^{Shirazi '89(2)}, non-homogeneous distributions of stress in the annular wall were found. These preliminary results support the theory, that the combined rotation of the FSU under physiological axial loads, causes a severe strain in the annular wall particularly in areas that are prone to rupture *in-vivo*.

Our final conclusion is that the risk of damage to the annular wall, (as far as it is related to strain of fibers in the annular wall), cannot be derived from intradiscal pressure, nor from intradiscal pressure differences. This risk can only be derived from direct assessment of the strain in the annular wall. However, the technique to measure strain as presented in Chapter 3, can only be used *in-vitro*. To assess the risk for annular wall damage, (due to excessive strain *in-vivo*), the FEM model developed by Shirazi ^{Shirazi '89}, which has proved to be correct so far, could be used. To calculate the strain in the annular wall this model then needs rotation and axial load data from *in-vivo* measurements. The necessary data concerning rotations of the lumbar spine *in-vivo* can be provided by an existing technique ^{Snijders '87}, while axial load *in-vivo* no longer needs to be estimated by traumatic intradiscal pressure measurements, but can be calculated from continuous measurements of the changing of height of the lumbar spine. Therefore the

realization of continuous height measurement, using the techniques ^{Suijders '87} ^{Goossens '94} that are already in use to measure the form and rotations of the lumbar spine, calls for continued research.

Samenvatting

Samenvatting

Het primaire doel van dit promotie-onderzoek is het vaststellen van biomechanische factoren die verantwoordelijk zijn voor het ontstaan van scheuren in de wand van de tussenwervelschijf. Daarbij werd het accent vooral gelegd op de biomechanische eigenschappen van de materialen en structuren in de tussenwervelschijf. De geformuleerde hypothese daarbij luidt, dat het scheuren van de wand van de tussenwervelschijf een gevolg is van de niet-homogeen verdeelde rek in de vezels van de wand. Gecombineerde rotaties en dientengevolge niet-homogene vervormingen van de tussenwervelschijf veroorzaken deze rek. Recente publikaties van experimenteel ^{Gordon '91}, analytisch ^{Shirazi '89(2)} en epidemiologisch ^{Kelsey '84 Burdorf '91} onderzoek ondersteunen deze hypothese. Tot dusver ontbrak echter direct experimenteel bewijs. Voor het vaststellen van deze veronderstelde niet-homogene verdeling van de rek in de wand kozen wij een methode die zowel *in-vitro* als *in-vivo* toepasbaar zou zijn, namelijk het meten van de intradisciale druk.

Menig onderzoeker heeft de intradisciale druk - of correcter, de druk in de nucleus pulposus - onder verschillende omstandigheden zowel *in-vivo* als *in-vitro* gemeten. In het algemeen neemt men daarbij aan, dat de nucleus pulposus zich hydrostatisch gedraagt, waardoor de druk in de tussenwervelschijf direct en overal in de nucleus gelijk is. Echter, een aantal onderzoekers ^{Kramer '77 Kramer '80 Urban '81 Urban '85 Kramer '85} beschrijft de nucleus pulposus als een visco-elastische of poro-elastische structuur met een vaste matrix, die weerstand biedt aan vloeistofstromen ^{Mow '80}. In dat geval zijn tijdelijke drukverschillen in de nucleus mogelijk.

Ons eerste experiment, beschreven in hoofdstuk 1, gaat uit van een poro-elastische visie op de nucleus ^{Mow '80}, waarin vast weefsel verantwoordelijk is voor zowel het elastische als het visceuze gedrag. Experimenteel opgewekte volumeveranderingen van de nucleus leidden inderdaad tot meetbare verschillen in (en vereffening van) de druk tussen twee drukgevoelige naalden in de nucleus, waarmee de poro-elastische theorie over het gedrag van de nucleus werd bevestigd.

Vervolgens werden vier functionele eenheden (Functional Spinal Unit of FSU) van de niveaus L2-L3 en L4-L5 van de menselijke wervelkolom in een speciaal ontwikkelde belastingsopstelling gemonteerd om een lichte tot matige werkbelasting te simuleren. Deze simulatie bestaat uit een zuiver axiale belasting, en een axiale belasting in combinatie met rotaties rond de axiale as, rotaties in het

sagittale vlak of een combinatie van deze rotaties. Teneinde eventuele drukverschillen te kunnen waarnemen, hebben wij simultaan op twee lokaties in de nucleus de intradiscale druk geregistreerd met speciaal daartoe ontwikkelde drukgevoelige naalden.

Shirazi ^{Shirazi '89(2)} voorspelt lokale spanningsverschillen in de annuluswand gedurende gecombineerde rotaties, waarbij hij zich baseert op analyses met behulp van een eindige elementenmethode. Wij verwachtten met het experiment - beschreven in hoofdstuk 1 - lokale drukverschillen op te wekken ten gevolge van lokale verschillen in de rek en spanning in de annuluswand. Wij hoopten deze lokale drukverschillen waar te kunnen nemen voordat deze vereffenden ten gevolge van een vloeistofstroom door de vaste matrix. Wij vonden echter geen significante voorbijgaande drukverschillen in de nucleus die zouden kunnen worden gerelateerd aan de voorspelde lokale spanningsverschillen in de annuluswand. Deze resultaten stemmen meer overeen met het algemeen gebruikelijke hydrostatische beeld van de nucleus dan met het poro-elastische ^{Mow '80} model van de nucleus. Wij trekken hieruit de conclusie dat gedurende fysiologische belastingscondities lokale verschillen in wandspanning òf niet leiden tot lokale drukverschillen, òf in het geheel niet optreden. Dit laatste is echter onwaarschijnlijk gezien het experimenteel ^{Gordon '91}, analytisch ^{Shirazi '89(2)} en epidemiologisch ^{Kelsey '84 Burdorf '91} bewijs dat gecombineerde rotaties leiden tot een niet-homogeen verdeelde rek en spanning in de annuluswand. Daarnaast bleek dat de geregistreerde intradiscale druk onder constante axiale belasting nauwelijks wordt beïnvloed door enkelvoudige of gecombineerde rotaties van de FSU. Bovendien werd gemeten dat de druktoename veroorzaakt door een rotatie in de ene richting (dus in het sagittale vlak of om de axiale as) onafhankelijk is van de aanwezigheid van een rotatie in de andere richting. Wij concluderen daarom dat de grootte van de intradiscale druk voornamelijk afhangt van de aangebrachte axiale belasting en geen goede maat is voor de rek en de spanning in de annulus fibrosus.

Er werden geen drukverschillen gevonden gedurende belastingscondities waarin rek- en spanningsverschillen in de wand worden voorspeld ^{Shirazi '89(2)}. Een verklaring hiervoor zou kunnen zijn dat de elastische matrix van de nucleus erg zwak is in verhouding tot de druk in de nucleus onder dergelijke belastingscondities. In dat geval zal de gehele nucleus zich laten vervormen en verplaatsen. De herschikking van de elastische matrix veroorzaakt dan slechts een zo klein vereffendend drukverschil dat het zich aan onze waarneming onttrekt. Wij ontwierpen daarom

het in hoofdstuk 2-I beschreven *in-vitro* experiment. Uitgaande van het poro-elastisch model ^{Mow '80} wilden wij de elasticiteit en permeabiliteit van de vaste matrix van de nucleus bepalen. In een aangepaste versie van het test-apparaat, zoals beschreven door Drogendijk ^{Drogendijk '84}, werden stansen van nucleus weefsel in een besloten ruimte onderworpen aan compressie. Volgens het poro-elastisch model ^{Mow '80} kan de permeabiliteit en elasticiteit van de vaste matrix worden berekend aan de hand van de snelheid waarmee de hoogte van de weefselstans afneemt, en de hoogte van de weefselstans wanneer evenwicht is bereikt tussen de elasticiteit van de stans en de aangebrachte compressiekracht. Zelfs onder een relatief lage belasting, overeenkomend met een hydrostatische druk van 0,25 MPa, werd na 18 uur belasten nog geen evenwicht bereikt. Wij trekken daaruit de conclusies dat het poro-elastische model niet kan worden toegepast op de nucleus en dat het dragend vermogen van de vaste matrix van de nucleus onder dergelijke belastingen kan worden verwaarloosd.

Het visco-elastische model schrijft elastisch gedrag van de nucleus toe aan de wateropnemende eigenschappen van glycosaminoglycanen ^{Kramer '77 Kraemer '80 Urban '81 Urban '85 Kramer '85}. De zwellingsdruk, veroorzaakt door deze wateropnemende eigenschappen van de nucleus, veroorzaakt dan door een tijdsafhankelijke vereffening met de hydrostatische druk het visceuze gedrag. In hoofdstuk 2-I trokken wij de conclusie, dat de permeabiliteit en de zwellingeigenschappen van de nucleus belangrijker zijn dan de elasticiteit. De proefopzet stond echter geen nadere specificatie toe.

Het experiment beschreven in hoofdstuk 2-II ontwikkelden wij om de afzonderlijke bijdragen van de zwellingsdruk ^{Inman '47 Hendry '58 Maroudas '81 Urban '81 Ohshima '89}, de permeabiliteit, de vloeistofstromen ^{Virgin '51 Brown '57 Markolf '74 Urban '82 Sonnerup '82 Koeller '84 Kraemer '85} en de annulusuitstulping ^{Klein '83} onder langdurige axiale belastingscondities vast te stellen.

Een geïsoleerde tussenwervelschijf werd daartoe langdurig (tot 21 uur) axiaal belast, terwijl het uitgedreven vloeistofvolume en de hoogte-afname werden geregistreerd. Tussen de verschillende axiale belastingen in werd het specimen de gelegenheid gegeven zich te herstellen. Gedurende dit experiment werden speciale voorzieningen getroffen ter voorkoming van verdamping van vloeistof. De nucleus was in dit experiment omgeven door haar natuurlijke grenzen, de annulus en de eindplaten. Deze was daarmee voorzien van haar fysiologische membraan, welke verantwoordelijk wordt geacht voor het visceuze gedrag. Bovendien werd ervoor gezorgd, dat de omvang van de tussenwervelschijf niet werd beperkt door een

besloten ruimte maar kon vervormen onder invloed van de belasting. Het vorige compressie experiment vond plaats in een besloten ruimte waardoor geen vervorming mogelijk was. Tijdens dit experiment verwachtten wij ook een verkleining van hoogte en volume te vinden, doch onder omstandigheden die representatiever zijn voor de omstandigheden *in-vivo*.

Wij stelden vast dat direct na het aanbrengen van een axiale belasting de hoogte van de tussenwervelschijf zeer snel afnam ten gevolge van het uitpuilen van de annuluswand. Dit uitpuilen nam nog enige tijd geleidelijk toe door de visco-elastische relaxatie van de annuluswand. De uitdrijving van vloeistof uit de tussenwervelschijf verliep veel trager en bepaalde de verdere afname van de hoogte en de toename van de uitpuiling van de annuluswand. De intradiscale druk gaf gedurende een registratie van meer dan 3 uur onder een axiale belasting van 1700 N een afname te zien van minder dan 3 procent, terwijl een belangrijke afname van hoogte en volume optrad. Andermaal trekken wij daarom de conclusie, dat de waargenomen compressie wordt beperkt door de intradiscale vloeistofdruk en niet door compressie van de vaste stof.

De zwellings eigenschappen van de nucleus zijn niet in staat om het uitdrijven van vloeistof onder belasting volledig te compenseren, waardoor de afname van de hoogte en de vloeistofuitdrijving zelfs na een zeer langdurige belasting (tot 21 uur) niet tot stilstand kwamen. De respons op herhaalde belastingen suggereerde dat het herstel tussen de belastingen onvolledig was. Dit leidde tot de conclusie dat onder *in-vitro* omstandigheden een verlies van grote moleculen (glycosaminoglycanen) verantwoordelijk is voor een langzame afname van de zwellingscapaciteit van de nucleus. Deze afnemende zwellingscapaciteit kan dus worden gezien als de oorzaak van de voortschrijdende afname van de hoogte onder belasting en tevens van het onvolledige herstel na belasting. Wij veronderstellen dat een actief mechanisme dat *in-vivo* het verlies van glycosaminoglycanen compenseert *in-vitro* afwezig is. Dit houdt in dat de resultaten van compressieproeven *in-vitro* niet representatief hoeven te zijn voor de compressie van een tussenwervelschijf *in-vivo*.

In hoofdstuk 2-III wordt een model beschreven dat is ontwikkeld om de verschillende eigenschappen van de tussenwervelschijf door middel van simulatie van de experimentele waarnemingen, zoals beschreven in hoofdstuk 2-II, te kunnen kwantificeren.

Het model gaat uit van een zich hydrostatisch gedragende nucleus, omdat onze experimentele resultaten (hoofdstukken 1, 2-I en 2-II) deze visie ondersteunen.

Wij maken gebruik van een eenvoudige biomechanische theorie ^{Brinckman '91} die de visco-elasticiteit van de annulusvezels, de vloeistofstroming en het uitstulpen van de annuluswand relateert aan de intradiscale druk. Ons model verklaart de correctiefactor die Nachemson ^{Nachemson '60} introduceerde om de intradiscale druk in normale tussenwervelschijven te kunnen berekenen uit de axiale belasting en het oppervlak van de dwarsdoorsnede. De intradiscale druk kent een overmaat in vergelijking tot de druk berekend uit de uitgeoefende belasting gedeeld door het oppervlak van de dwarsdoorsnede. Deze overmaat betreft de bijdrage van de spanning in de annuluswand aan de krachten in axiale richting, en is afhankelijk van de uitstulping van de annuluswand. Het model verklaart ook de lagere initiële druk en de lagere druk onder axiale belasting in gedegenereerde tussenwervelschijven.

De intradiscale druk lijkt constant te zijn wanneer de observatietijd slechts enkele minuten bedraagt (zoals in de meeste *in-vivo* en *in-vitro* experimenten het geval is). Het model voorspelt een belangrijk verlies van zwellingscapaciteit van de tussenwervelschijf onder axiale belasting *in-vitro*. Een compleet herstel van het preparaat na axiale belasting *in-vitro* is daardoor niet gegarandeerd. *In-vivo* wordt dit verlies van zwellingscapaciteit echter gecompenseerd door de synthese van glycosaminoglycanen. Dit houdt in dat langdurige of herhaalde belastingsexperimenten *in-vitro* niet het *in-vivo* gedrag van de tussenwervelschijf weerspiegelen.

Het model kan worden gebruikt om, uitgaande van veranderingen van lichaamslengte, de axiale belasting *in-vivo* te berekenen. Het model kan zodoende een belangrijk instrument zijn en de registratie van de intradiscale druk als methode ter bepaling van de axiale belasting vervangen.

Uit de in het model toegepaste biomechanische theorie werd geconcludeerd, dat gecombineerde rotaties van een FSU de annuluswand kunnen beschadigen. Vanuit dezelfde theorie kan ook de asymmetrische vorm van de annuluswand worden verklaard.

In de hoofdstukken 1 en 2 toonden wij aan, dat de intradiscale druk niet kan worden gebruikt als een maat voor (lokale verschillen in) de rek in de annuluswand. Daarom werd gezocht naar andere methoden om deze rek te meten, omdat de theorie dat gecombineerde rotaties van een FSU de oorzaak zijn van lokaal verhoogde rek in en een verhoogde kans op scheuren van de annuluswand nog steeds proefondervindelijk moet worden onderbouwd.

Hoofdstuk 3 geeft de beschrijving van een 3-D video-registratiesysteem dat werd

ontwikkeld voor de meting van vervormingen van de annuluswand van intacte FSU's. Onder axiale belastingen binnen het fysiologische bereik, gecombineerd met rotaties van het FSU, konden hiermee verschillen in de rek in de annuluswand worden gemeten met een nauwkeurigheid van een half procent.

Beschreven worden de meettechniek, de ijking en de analyse van onze voorlopige resultaten. Overeenkomstig de voorspellingen ^{Shirazi '89(2)} werden niet-homogene verdelingen van de rek in de annuluswand aangetoond. Deze voorlopige resultaten ondersteunen de theorie, dat gecombineerde rotaties van een FSU onder fysiologische axiale belasting een grote rek in de annuluswand veroorzaken, met name op die lokaties waar *in-vivo* de kans op scheuren groot is.

Eindconclusie van dit onderzoek is, dat het risico voor beschadigingen van de annuluswand, voor zover dit gerelateerd is aan de rek van vezels in de annuluswand, niet kan worden afgeleid uit de intradiscale druk noch uit intradiscale drukverschillen. Een dergelijk risico kan slechts worden afgeleid uit een directe bepaling van de rek in de annuluswand. De techniek om rek te meten zoals we die in hoofdstuk 3 presenteerden kan echter alleen *in-vitro* worden toegepast. Om het risico voor beschadiging van de annuluswand *in-vivo* te bepalen zou het eindige elementen-model van Shirazi ^{Shirazi '89}, dat tot dusverre correct bleek te zijn, kunnen worden gebruikt. Om de rek in de annuluswand *in-vivo* te kunnen berekenen, moet dit model worden voorzien van gegevens over rotaties en axiale belastingen uit *in-vivo* metingen. De noodzakelijke gegevens betreffende rotaties van de wervelkolom *in-vivo* kunnen worden verkregen door middel van een reeds bestaande techniek ^{Snijders '87}, terwijl de axiale belasting *in-vivo* niet langer hoeft te worden geschat met behulp van de invasieve intradiscale drukmeting, maar kan worden berekend uit continue meting van de verandering van lengte van de lumbale wervelkolom. Daarom bevelen wij nader onderzoek aan naar een methode voor continue lengteregistratie van de lumbale wervelkolom, uitgaande van reeds bekende technieken ^{Snijders '87 Goossens '94} om de vorm en rotaties van de lumbale wervelkolom te meten.

Nawoord

Tot slot dit stukje, het laatste dat ik nog schrijf voor dit boekje. Met gemengde gevoelens laat ik de afgelopen zeven (!) jaren nog eens aan me voorbij gaan.

Eigenlijk zou een toekomstig promovendus eerst de tijd voor dit soort bespiegelingen moeten nemen alvorens een promotieonderzoek te starten. Gedegen wetenschappelijk onderzoek laat zich nu eenmaal slecht combineren met het stichten van een gezin met tenslotte vier kinderen en het volledig verbouwen van een huis. En elke dag schitterde het water van de Maas aan de voet van de universiteit mij verleidelijk toe, het laat zich raden waardoor het allemaal wat langer heeft geduurd. Uiteindelijk is alles en iedereen toch nog wel iets te kort gekomen. Laat het een les zijn voor toekomstige promovendi; streef naar perfectie, maar realiseer je op tijd dat je dit doel nooit zult bereiken.

Dit is het definitieve einde van een belangrijke fase in mijn leven. Wetenschappelijk onderzoek is een zaak van discipline en een lange adem, maar ook van creativiteit en inventiviteit en vooral daarom zal ik dit werk missen. Want *"creativiteit is niet zozeer het vinden van nieuwe dingen als wel het anders samenbrengen van bestaande kennis"* (Umberto Eco) en dat betekende lezen, veel nadenken en vooral veel, heel veel praten met collega's. Niet alleen over de problemen die ik in mijn eigen onderzoek tegenkwam, maar ook over de problemen van anderen want dat houdt de geest scherp, het levert soms ideeën op voor je eigen onderzoek en het is gewoon leuk. Zodoende heeft eigenlijk iedereen die ik de afgelopen jaren heb leren kennen wel een steentje bijgedragen aan dit proefschrift en ik ben hen daar zeer dankbaar voor. Laat een ding vooral duidelijk zijn, wetenschappelijk onderzoek is boeiend en leuk. Ik hoop dan ook in de toekomst opnieuw met wetenschappelijk onderzoek bezig te kunnen zijn, want zoals ik in de conclusies al heb aangegeven, dit boekje vraagt om een vervolg.

"This is the end my friend,
my only friend the end."
(The Doors)

Curriculum vitae

De schrijver van dit proefschrift werd op 28 januari 1959 te Schipluiden geboren. Na het doorlopen van de middelbare school (Atheneum-B) te Delft studeerde hij van 1978 tot 1979 civiele techniek aan de Technische Universiteit te Delft. Van 1979 tot 1988 studeerde hij geneeskunde aan de Erasmus Universiteit te Rotterdam. Na het behalen van zijn arts-examen was hij van 1988 tot 1992 als assistent in opleiding (AIO) in dienst bij de vakgroep Biomedische Natuurkunde en Technologie van de Erasmus Universiteit Rotterdam. Na het einde van zijn aanstelling als AIO is hij aan deze afdeling verbonden gebleven als gastonderzoeker. Sinds 1 februari 1994 is hij daarnaast in deeltijd-dienstverband werkzaam als keuringsarts voor de Stichting Rode Kruis Bloedbank Leidsenhage.